Swiss Federal Institute of Technology, Lausanne
Center for Research in Plasma Physics

AC losses computations for ITER magnets

EFDA Ref. TW5-TPO-ACLOS / Contract no. 05-1307
Deliverable no. 2 and 3

Claudio Marinucci[a], Luca Bottura[b]

[a] *EPFL, CRPP, 5232 Villigen PSI, Switzerland*
[b] *CERN, AT–MAS, 1211 Geneva 23, Switzerland*

CRPP/SC/CM/2006/02

30 September 2006

Abstract

The calculation of AC losses due to the control currents in ITER is a cumbersome task. The reason is that control transients require small field changes (0.1 T or less) at moderate frequency (up to 10 Hz), where effects of partial penetration of the filaments and shielding are important and need to be taken into account to produce sound AC loss estimates. Models were developed for AC loss calculation, in particular hysteresis and coupling current losses, that are suitable for the above regime (Deliverable no. 2). Both hysteresis and coupling loss models are adapted to the conductor analyzed through few parameters (the effective filament diameter and time constants) that can be derived from measurement of loss on short samples. An example of calculations of AC loss in the ITER TF and PF coils for two vertical control scenarios (VS1 and VS2) during high beta operation at flattop is described in detail in this report (Deliverable no. 3).

This page left intentionally blank.

Contents

1 Introduction

The calculation of AC losses due to the control currents in ITER is a cumbersome task. The reason is that control transients require small field changes (0.1 T or less) at moderate frequency (up to 10 Hz), where effects of partial penetration of the filaments and shielding are important and need to be taken into account to produce sound AC loss estimates.

Goals of the EFDA Task TW5-TPO-ACLOS are:

- To develop models for AC loss calculation, in particular hysteresis and coupling current losses, that are suitable for the above regime. This work is summarized in the Deliverable no. 2 (Appendix A).
- To perform, as an example, calculations of AC loss in the ITER TF, CS and PF coils during the operation Scenario 2 and during two vertical control scenarios (VS1 and VS2) applied to (a) noise during high beta operation at flattop and (b) minor disruption at the end-of-cycle (Deliverable no. 3).

This Report includes Deliverable no. 2 and 3.

The main goal of this study is not a detailed analysis of the AC losses in the ITER coils but a robust check of the feasibility of the new computational tool in a complex coil environment. After integration of the new tool, the CryoSoft code M'C is tested – based on the EFDA inputs – to verify its overall functionality and ability to be integrated in the plasma controller. M'C is a computer program for the calculation of magnetic field, vector potential, AC losses, AC and DC cable magnetization, operating point, volume and resultant forces, inductance and energy of superconducting magnetic system of arbitrary shape. If offers high level modeling capabilities and plotting facilities for post–processing the results.The algorithm used in M'C is described in Appendix A [1, 2]. A command language is used for the data input and options selection [3].

The results shown in this report are only a minor fraction of the large amount of data which have been used to perform a careful check of the code. The CD with the electronic documentation, described below, integrates this Report.

2 Model

The input data used for the simulations with the code M'C are taken from the ITER Design Description Document [4] unless otherwise noted.

2.1 Coil geometry

The ITER magnet system consists of axis-symmetric and non axis symmetric coils. A 3-D rendering of the magnetic model is shown in Fig. 1. The plasma is described in Section 2.4

2.1.1 Axis symmetric coils

The axis symmetric coils are:

- 6 modules of the central solenoid (CS), i.e. CS3U, CS2U, CS1U, CS1L, CS2L, and CS3L (Fig. 2);
- 6 poloidal field (PF) coils, i.e. PF1, PF2, PF3, PF4, PF5 and PF6 (Fig. 3).

These coils are generated in the model with the M'C command LOOP. Some of the data required by this command, i.e. the origin of the local reference frame (X_c, Y_c, Z_c), the average radius (R), the thickness in the radial direction (ΔR) and in height (ΔZ), the number of subdivisions (N_{GCE}), the number of pancakes (N_p), the number of turns (N_t) and the number of in–hand lengths (N_{inhand}), are listed in Table 1. These data are taken from the EFDA documentation [5] and are slightly different from the values in [4].

In our model the number of pancakes of the CS coils is 39 (instead of 40 in [4]) in order to match the actual total number of turns (546 in the model, 548 in [4]): this approximation is within the scope of this study.

2.1.2 Non axis symmetric coils

The non axis symmetric coils are the 18 toroidal field (TF) coils. The TF1 coil is generated with the M'C commands ARC and SEGMENT. Some of the data required by the command ARC, i.e. the origin of the local reference frame (X_c, Y_c, Z_c), the average radius (R), the angle (ϕ), the thickness in the radial direction (ΔR) and in height (ΔZ), the number of subdivisions (N_{GCE}), are listed in Table 2 [4]. The remaining TF coils are generated by rotation of TF1. In this study the TF coils are assumed to have a rectangular cross section, i.e 12 pancakes, 11 turns and 1 in–hand lengths, whereas the ITER TF coils have a tapered cross section. This simplification is within the scope of our study, in particular as the total number of turns is very close in the two cases, i.e. 132 in this model and 134 in [4]. Details of the TF coils are shown in Fig. 4.

2.1.3 Passive coils

The magnetic model includes also 60 axis symmetric passive circuits (PA) that represent the conductive wall of the vacuum vessel vessel (Fig. 5). The full geometric description of these virtual, axis symmetric coils [5] is part of the electronic documentation and is omitted here for simplicity.

A check of the geometric compatibility of all components of the M'C model is shown in Fig. 6 and 7.

2.2 Current scenarios

2.2.1 Operation scenario

The whole operation *Scenario 2*, referred to as S2 in this Report, (duration 1800 s) is considered for the evaluation of the AC losses. Currents during this operation scenario in the PF and CS coils, as well as in the static plasma, are shown in Fig. 8 [4]. S2 is the most critical scenario for vertical stabilization using the VS1 and VS2 stabilization circuits during the flat top phase.

2.2.2 Control scenarios

A total of 4 control scenarios have been considered [6]:

- Noise during high beta operation at the start-of-burn (SOB) with the vertical stabilization VS1, referred to as SOBVS1 in this Report. This 'fast' control scenario starts at time t=130s and lasts 10s. The time history of current variation in the ITER coils, i.e. to be added to the S2 current, are shown in Fig. 9. In order to reduce the computational time, the number of points during the control scenario are reduced by a factor 15. The resulting loss of information is minimal and within the scope of this study (compare Fig. 9 with Fig. 10). The same data decimation has been applied to all control scenarios investigated. The currents in the passive coils are shown in Fig. 11. The same currents after integration in S2 are shown in Fig. 12 and 13 in the CS and PF coils, respectively.
- Noise during high beta operation at the start-of-burn (SOB) with the vertical stabilization VS2, referred to as SOBVS2. As in SOBVS1, this scenario starts at t=130s and lasts 10s. The currents in the passive coils are shown in Fig. 14. The same currents after integration in S2 are shown in Fig. 15 and 16 in the CS and PF coils, respectively. The plasma current and the offset of the plasma centroid coordinates with respect to S2 are shown in Fig. 26.
- Minor disruption at the end-of-cycle (EOC) with the vertical stabilization VS1, referred to as EOCVS1. This 'slow' control scenario starts at t=590s and lasts 10s. The currents in the passive coils are shown in Fig. 17. The same currents after integration in S2 are shown in Fig. 18 and 18 in the CS and PF coils, respectively.

- Minor disruption at the end-of-cycle (EOC) with the vertical stabilization VS2, referred to as EOCVS2. As in scenario EOCVS1, this scenario starts at t=590s and lasts 10s. The currents in the passive coils are shown in Fig. 20. The same currents after integration in S2 are shown in Fig. 21 and 21 in the CS and PF coils, respectively. The plasma current and the offset of the plasma centroid coordinates with respect to S2 are shown in Fig. 29.

2.2.3 TF current

The current in the TF coils is constant with time, i.e. 9.112 MA. This corresponds to a nominal current of 68 kA.

2.3 Conductor data

The conductor data used in the model are listed in Table 3 and 4. The input to M'C are the superconductor cross section (A_{Sc}), the copper cross section (A_{Cu}), the effective filament diameter (d_{eff}), the operating temperature (T_{op}), the longitudinal strain (ϵ), the cable coupling currents time constants (τ) and the magnetization shape factors (n). The last two parameters are assumed to be the same along the 3 coordinate of the local cartesian reference frame ξ, η and ζ. The data are derived from [4][1].

2.4 Plasma

During the control scenarios the plasma is not static. However, as the code M'C allows only static coils, i.e. the geometry of the coil cannot be changed during the time evolution. To simulate nonetheless a moving plasma the following approach is followed. Three coils are defined around the radius and height region spanned by the plasma center coordinate, placed at coordinates R_i, z_i, with $i = 1 \ldots 3$. The current of these three (static) coils is defined as follows:

$$I_1 + I_2 + I_3 = I_P \quad (1)$$

$$R_1 I_1 + R_2 I_2 + R_3 I_3 = R_P I_P \quad (2)$$

$$z_1 I_1 + z_2 I_2 + z_3 I_3 = z_P I_P \quad (3)$$

where the I_i indicate the current in the three coils, while I_P is the plasma current and R_P, z_P are the plasma center coordinates. The above set of equations forms a system that provides the coil currents Ii at each instant when I_P, R_P and z_P are defined. The above approach conserves the moments of order zero (total current) and order one of the plasma current.

In the control scenario SOBVS1 the plasma current variation and the offset of the plasma centroid coordinates with respect to S2 are shown in Fig. 23. Also in this case a decimation

[1] Some discrepancy have been observed between the information in drawings and text of [4], e.g. the cabling pattern of the TF conductor, the number of strands in the CS conductor, etc.

of the data set by a factor 15 is acceptable (compare Fig. 23 with Fig. 24). The interpolation of the moving plasma is not a function of the vertical stabilization, i.e. the moving plasma is the same in SOBVS1 and SOBVS2 (Fig. 25).

In the control scenario EOCVS1 the plasma current and the offset of the plasma centroid coordinates with respect to S2 are shown in Fig. 27. The currents resulting from the interpolation of the moving plasma are shown in Fig. 28, and are the same in the control scenario EOCVS2.

Table 1: Central solenoid and poloidal field coil geometric data.

Coil	X_c (s) [m]	Y_c [m]	Z_c [m]	R [m]	ΔR [m]	ΔZ [m]	N_{GCE} [-]	N_p [-]	N_t [-]	N_{inhand} [-]
CS3U	0.0	0.0	5.313	1.722	0.719	2.075	20	39	14	1
CS2U	0.0	0.0	3.188	1.722	0.719	2.075	20	39	14	1
CS1U	0.0	0.0	1.063	1.722	0.719	2.075	20	39	14	1
CS1L	0.0	0.0	-1.063	1.722	0.719	2.075	20	39	14	1
CS2L	0.0	0.0	-3.188	1.722	0.719	2.075	20	39	14	1
CS3L	0.0	0.0	-5.313	1.722	0.719	2.075	20	39	14	1
PF1	0.0	0.0	7.557	3.943	0.968	0.976	20	16	16	2
PF2	0.0	0.0	6.530	8.319	0.649	0.595	20	10	11	2
PF3	0.0	0.0	3.265	11.997	0.708	1.125	20	16	12	2
PF4	0.0	0.0	-2.243	11.967	0.649	1.125	20	16	11	2
PF5	0.0	0.0	-6.730	8.395	0.820	0.945	20	16	14	2
PF6	0.0	0.0	-7.557	4.263	1.633	0.976	20	16	27	2

Table 2: Toroidal field coil geometric data.

Arc	X_c (s) [m]	Y_c [m]	Z_c [m]	R [deg]	ϕ [m]	ΔR [m]	ΔZ [-]	N_{GCE}
1	0.0	4.240	0.0	6.510	69.70	0.6334	0.835	10
2	0.0	5.334	2.954	3.360	40.00	0.6334	0.835	6
3	0.0	4.967	3.980	2.270	70.30	0.6334	0.835	6
4	0.0	4.967	-3.980	2.270	64.50	0.6334	0.835	6
5	0.0	5.367	-3.140	3.200	45.80	0.6334	0.835	6
6	0.0	4.200	0.0	6.550	69.70	0.6334	0.835	10

Segment	X_c (s) [m]	Y_c [m]	Z_c [m]	ΔX [m]	ΔY [m]	ΔZ [m]	N_{GCE} [-]
1	0.0	2.697	0.0	0.853	0.6334	7.960	10

Table 3: Superconductor data.

lala	Unit	PF1-PF6	PF2-PF3-PF4	PF5	CS	TF
Superconductor		NbTi	NbTi	NbTi	Nb3Sn	Nb3Sn
A_{Sc}	[mm2]	244.0	48.19	85.72	246.0	250.1
A_{Cu}	[mm2]	390.4	457.5	449.1	246.0	500.3
d_{eff}	[mm]	0.006	0.006	0.006	0.030	0.030
T_{op}	[K]	4.7	4.7	4.7	4.7	5.0
ϵ	[%]	0.0	0.0	0.0	-0.69	-0.77
τ	[s]	0.025	0.025	0.025	0.025	0.025
n	[-]	2.0	2.0	2.0	2.0	2.0
d_{st}	[mm]	0.073	0.073	0.072	0.083	0.082
n_{st}	[-]	1440	864	1080	864	900
$cos\theta$	[-]	0.95	0.95	0.95	0.95	0.95
Cu/NCu	[-]	1.6	6.9	4.4	1.0	1.0

Table 4: Cabling pattern.

Coil	Cabling pattern	Cu core diam. at stage 1/2/3/4 [mm]
PF1-PF6	3x4x4x5x6	
PF3-PF4-PF5	((3x3x4+1)x4+1)x6	– / – /1.8/3.5
PF5	((3x3x4+1)x5+1)x6	– / – /1.2/2.7
CS	3x3x4x4x6	
TF	((2+1)x3x5x5+core*)x6	0.82/ – / – / –
* Core TF	3x4	0.82

Table 5: Operation Scenario 2. Currents [MA] in the ITER Central Solenoid coils and in the plasma [4]). The operation are: SOD = Start of Discharge, XPF = X Point Formation, SOF = Start of Flat-top, SOB = Start of Burn, EOB = End of Burn, EOC = End of Control, EOP = End of Plasma.

Operation	Time (s)	Plasma	CS3U	CS2U	CS1U	CS1L	CS2L	CS3L
SOD	0.00	0.00	21.91	21.91	21.91	21.91	21.91	21.91
	1.60	0.40	19.69	19.06	19.58	19.58	17.77	19.73
	4.61	1.50	18.25	17.00	14.19	14.19	15.99	18.98
	7.82	2.50	16.93	15.14	11.40	11.40	14.37	18.29
	11.38	3.50	15.61	13.27	8.81	8.81	12.75	17.61
	15.24	4.50	14.30	11.40	6.40	6.40	11.13	16.93
	19.52	5.50	12.98	9.53	4.06	4.06	9.50	16.24
	24.17	6.50	11.66	7.67	1.79	1.79	7.88	15.56
XPF	29.37	7.50	10.35	5.80	-0.64	-0.64	6.26	14.88
	35.25	8.50	7.47	4.87	-3.49	-3.49	4.63	13.65
	42.12	9.50	4.59	3.94	-6.21	-6.21	2.57	12.42
	49.26	10.50	3.67	3.00	-9.39	-9.39	1.60	11.19
	56.21	11.50	2.52	1.40	-12.13	-12.13	0.25	10.00
	63.22	12.50	1.93	-1.00	-14.57	-14.57	-1.79	9.50
	72.55	13.50	0.91	-3.33	-17.28	-17.28	-3.74	8.43
SOF	100.00	15.00	-1.16	-8.80	-22.17	-22.17	-8.57	5.66
	105.00	15.00	-1.24	-9.04	-21.39	-21.39	-8.63	4.94
	110.00	15.00	-1.30	-9.21	-20.90	-20.90	-8.68	4.44
	115.00	15.00	-1.34	-9.33	-20.57	-20.57	-8.75	4.06
	120.00	15.00	-1.37	-9.42	-20.38	-20.38	-8.83	3.79
	125.00	15.00	-1.39	-9.47	-20.34	-20.34	-8.92	3.64
SOB	130.00	15.00	-1.40	-9.50	-20.39	-20.39	-9.00	3.56
EOB	530.00	15.00	-1.66	-19.20	-24.66	-24.66	-17.60	0.56
	546.00	14.20	-0.43	-20.22	-24.04	-24.04	-17.82	0.31
	564.00	13.30	1.33	-21.38	-23.23	-23.23	-18.08	0.15
	580.00	12.50	3.17	-22.40	-22.40	-22.40	-18.30	0.09
EOC	590.00	12.50	3.71	-23.40	-23.71	-23.71	-19.02	1.10
	616.10	10.00	0.88	-22.71	-21.68	-21.68	-18.44	-0.76
	647.40	7.00	-2.53	-20.72	-18.07	-18.07	-16.88	-2.99
	668.30	5.00	-4.79	-18.62	-15.03	-15.03	-15.61	-4.47
	689.10	3.00	-7.06	-14.60	-12.95	-12.95	-13.35	-5.96
	710.00	1.00	-9.33	-9.77	-9.77	-9.77	-9.77	-7.45
EOP	720.00	0.00	-10.50	-10.00	-10.00	-10.00	-10.00	-9.00
	900.00	0.00	0.00	0.00	0.00	0.00	0.00	0.00
	1490.00	0.00	0.00	0.00	0.00	0.00	0.00	0.00
	1790.00	0.00	21.91	21.91	21.91	21.91	21.91	21.91
SOD	1800.00	0.00	21.91	21.91	21.91	21.91	21.91	21.91

Table 6: Operation Scenario 2. Currents [MA] in the ITER Poloidal Field coils[4]).

Operation	time	PF1	PF2	PF3	PF4	PF5	PF6
SOD	0.00	9.63	0.63	0.49	0.38	0.77	8.50
	1.60	8.26	0.27	0.33	0.20	0.08	8.26
	4.61	8.58	-1.06	0.28	0.31	-1.85	9.31
	7.82	8.87	-1.92	0.76	-0.87	-1.64	10.26
	11.38	9.17	-2.18	0.56	-1.45	-1.92	11.21
	15.24	9.46	-2.34	0.23	-1.88	-2.40	12.15
	19.52	9.75	-2.25	-0.53	-1.78	-3.31	13.10
	24.17	10.05	-2.33	-1.11	-1.78	-4.24	14.05
XPF	29.37	10.34	-2.28	-1.85	-1.86	-5.09	15.00
	35.25	10.03	-2.28	-2.35	-2.15	-5.59	15.64
	42.12	9.73	-2.37	-2.85	-2.36	-6.12	16.28
	49.26	8.81	-2.41	-3.32	-2.68	-6.40	16.51
	56.21	8.39	-2.60	-3.67	-3.07	-6.64	16.74
	63.22	7.94	-2.73	-4.09	-3.40	-6.96	16.98
	72.55	7.31	-2.82	-4.54	-3.71	-7.27	17.15
SOF	100.00	5.45	-2.73	-5.50	-3.92	-8.15	17.53
	105.00	5.45	-2.51	-5.83	-4.26	-7.90	17.43
	110.00	5.46	-2.38	-6.05	-4.48	-7.73	17.36
	115.00	5.46	-2.28	-6.23	-4.64	-7.61	17.31
	120.00	5.47	-2.24	-6.34	-4.75	-7.53	17.27
	125.00	5.47	-2.24	-6.41	-4.79	-7.51	17.25
SOB	130.00	5.47	-2.27	-6.43	-4.82	-7.50	17.24
EOB	530.00	1.74	-1.98	-6.75	-4.91	-7.61	14.93
	546.00	1.75	-2.12	-6.16	-4.83	-7.45	14.37
	564.00	1.76	-2.42	-5.37	-4.77	-7.26	13.75
	580.00	1.77	-2.77	-4.60	-4.73	-7.09	13.20
EOC	590.00	2.43	-3.52	-3.79	-4.48	-7.30	13.06
	616.10	0.73	-2.90	-3.16	-3.86	-5.49	8.77
	647.40	-1.31	-2.15	-2.25	-3.05	-3.45	3.63
	668.30	-2.67	-1.83	-1.65	-1.97	-2.84	0.20
	689.10	-4.03	-1.24	-1.08	-1.20	-1.56	-3.22
	710.00	-5.39	-0.40	-0.50	-0.46	-0.12	-6.65
EOP	720.00	-6.00	-0.40	-0.40	-0.40	0.00	-7.00
	900.00	0.00	0.00	0.00	0.00	0.00	0.00
	1490.00	0.00	0.00	0.00	0.00	0.00	0.00
	1790.00	9.63	0.63	0.49	0.38	0.77	8.50
SOD	1800.00	9.63	0.63	0.49	0.38	0.77	8.50

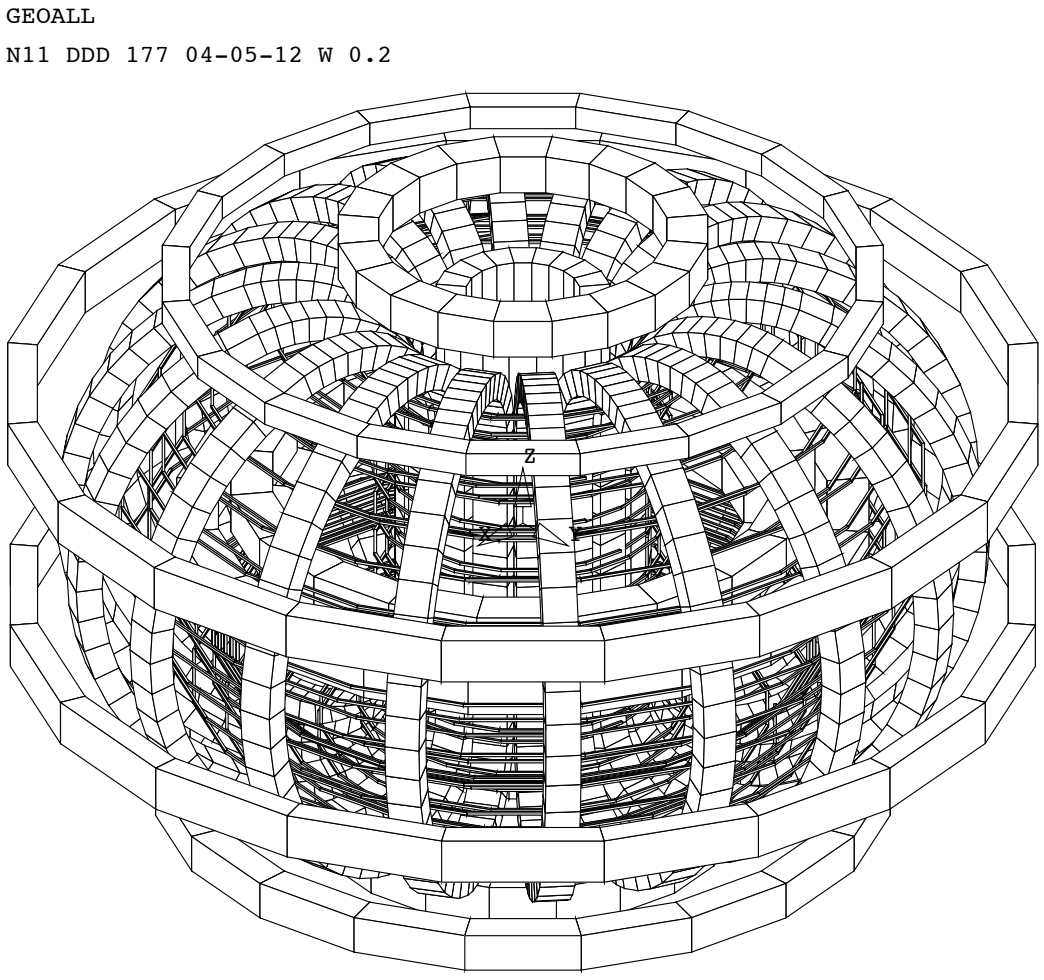

Figure 1: M'C model with all ITER coils included in the simulations.

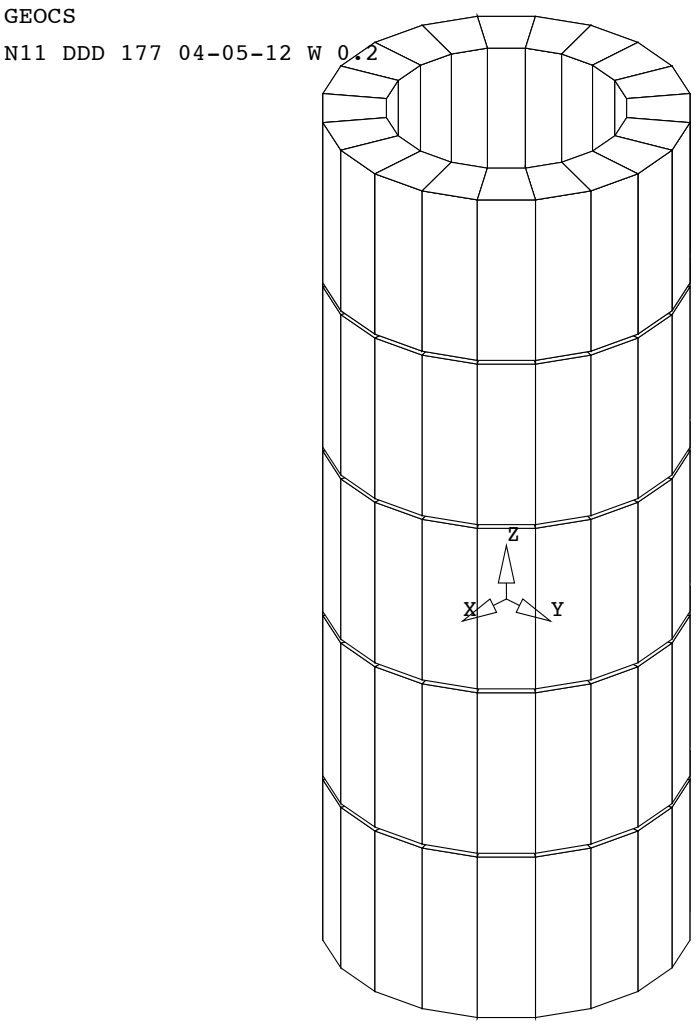

Figure 2: Details of the 6 coils of the ITER central solenoid. From top to bottom: CS3U, CS2U, CS1U, CS1L, CS2L and CS3L.

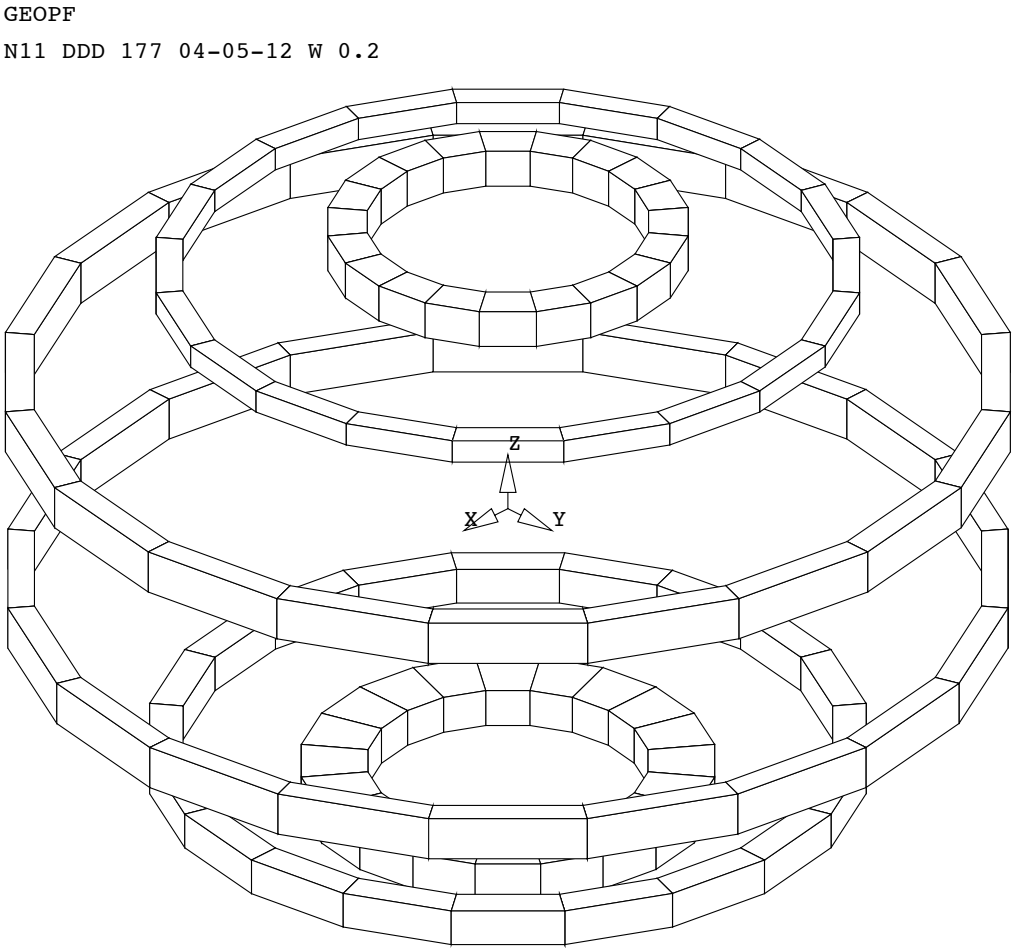

Figure 3: Details of the 6 ITER Polodial Field coils. From top to bottom: PF1, PF2 PF3, PF4, PF5 and PF6.

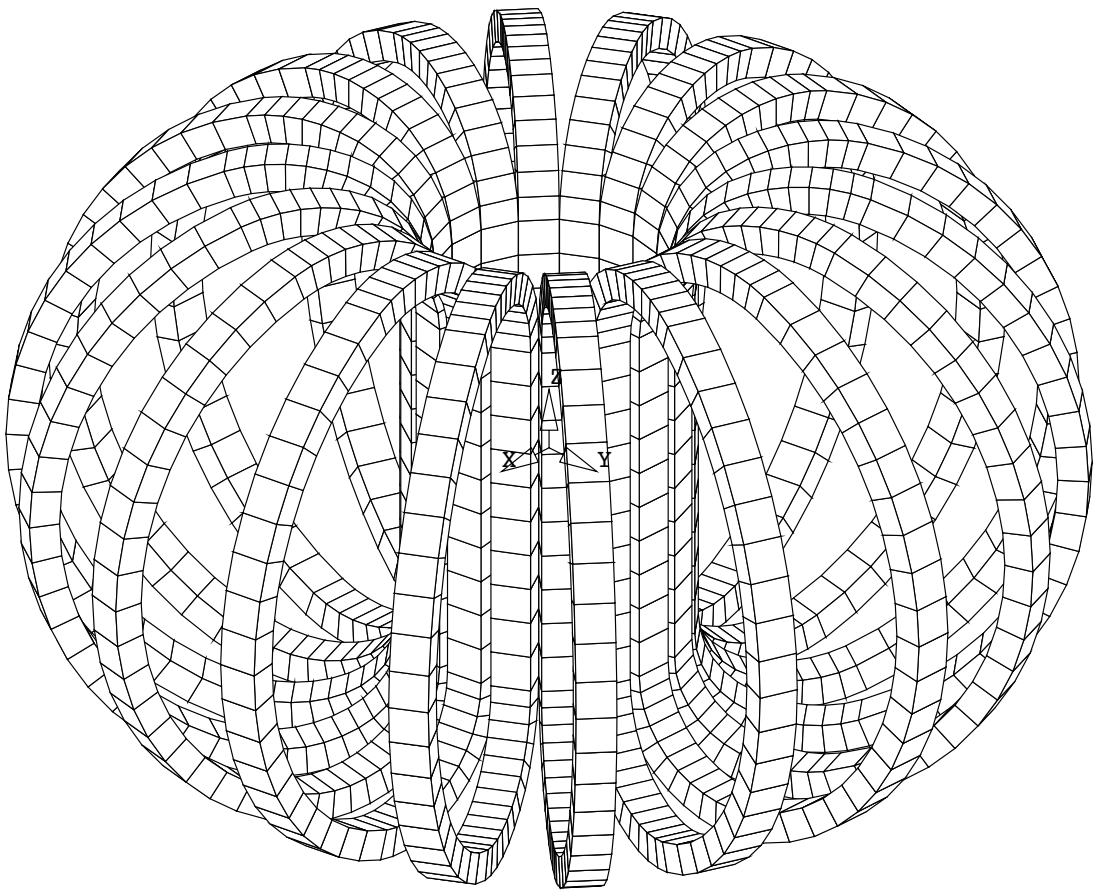

Figure 4: Details of the 18 ITER Toroidal Field coils.

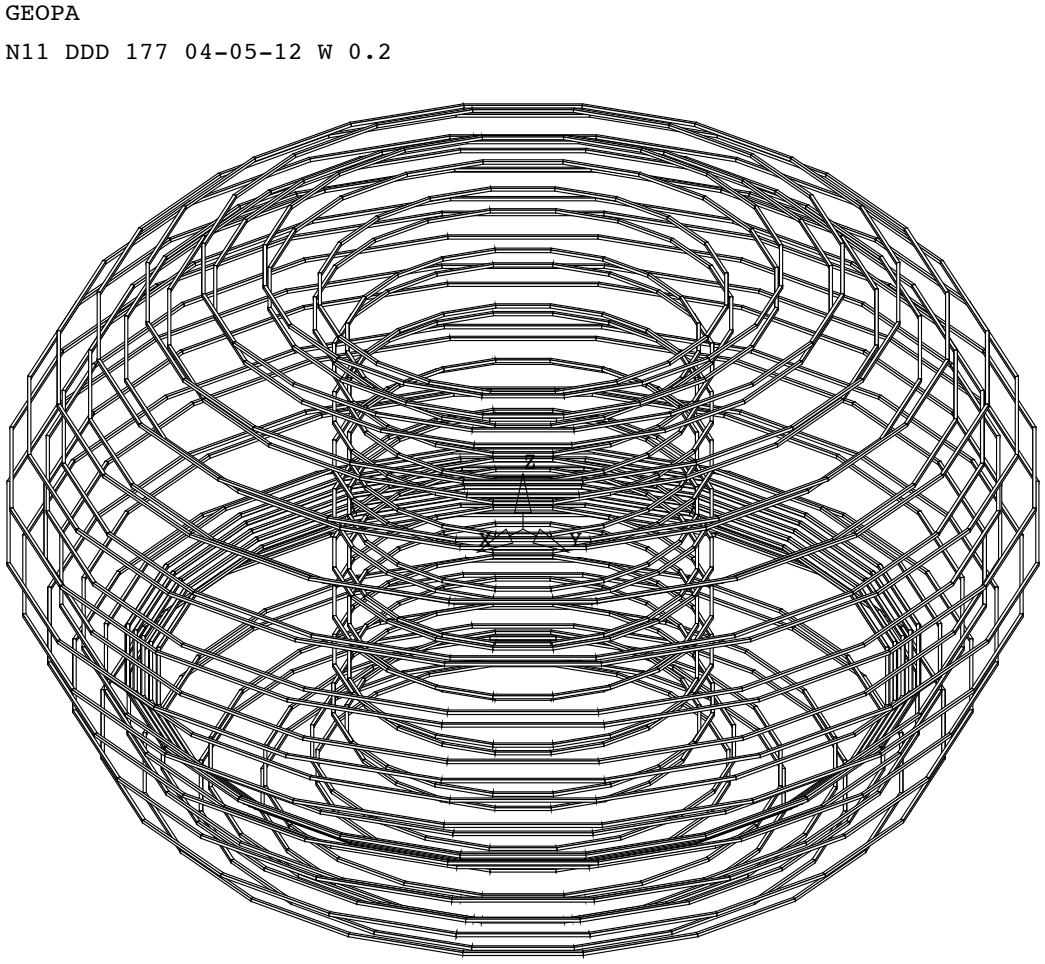

Figure 5: Details of the 60 passive coils to simulated the eddy current in the ITER vessel.

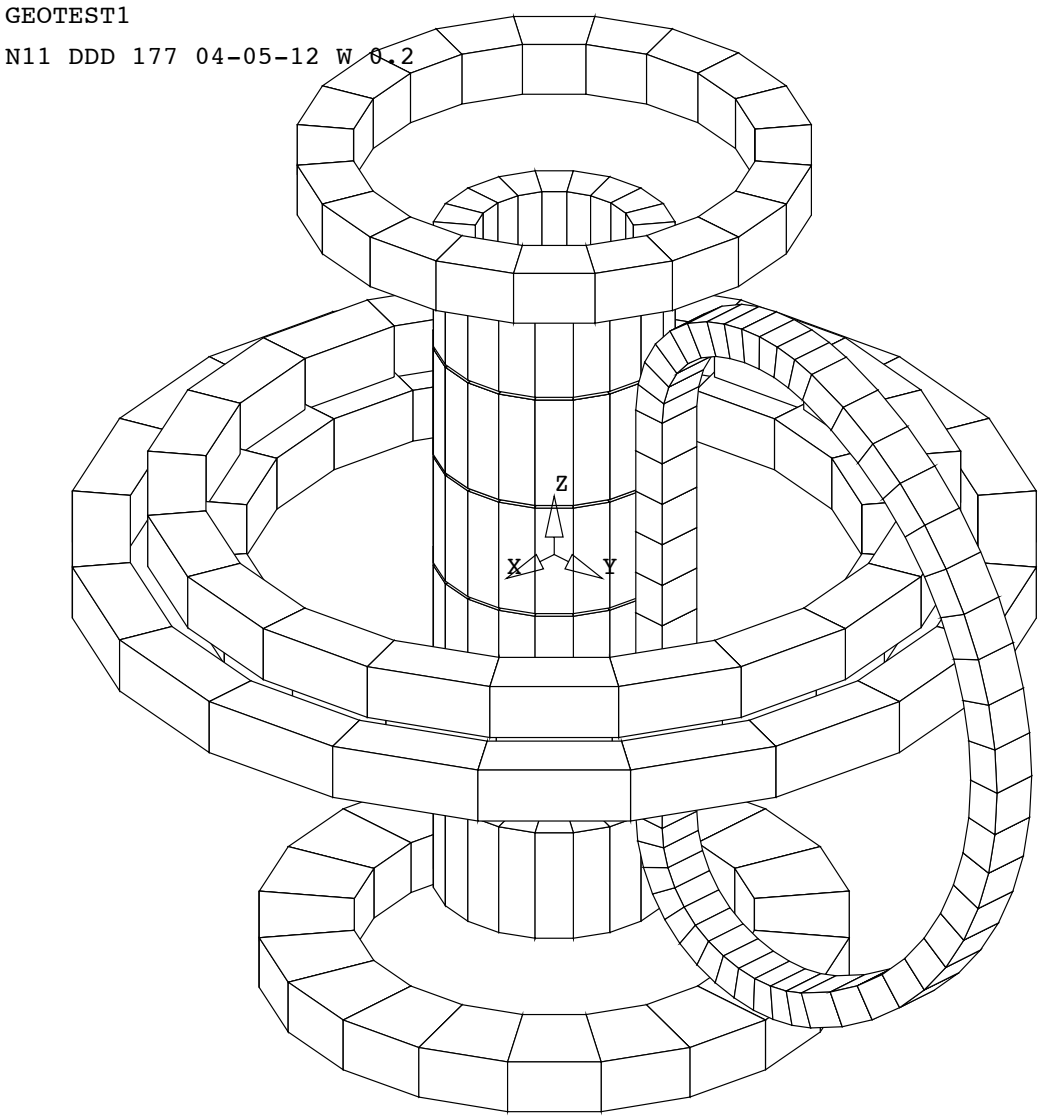

Figure 6: Details of some of the ITER coils and plasma used to test the geometric compatibility of the model.

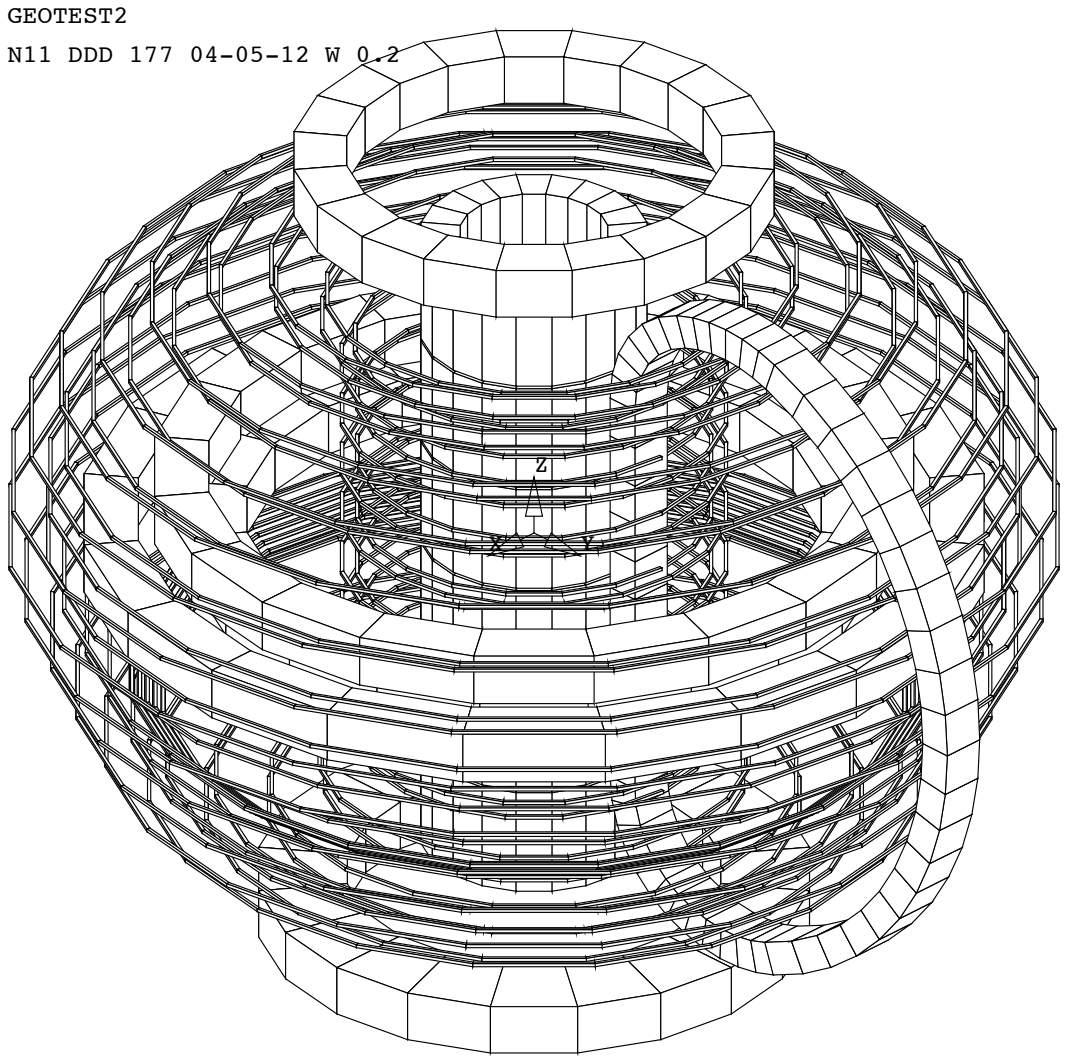

Figure 7: Details of some of the ITER coils, plasma and passive coils used to test the geometric compatibility of the model.

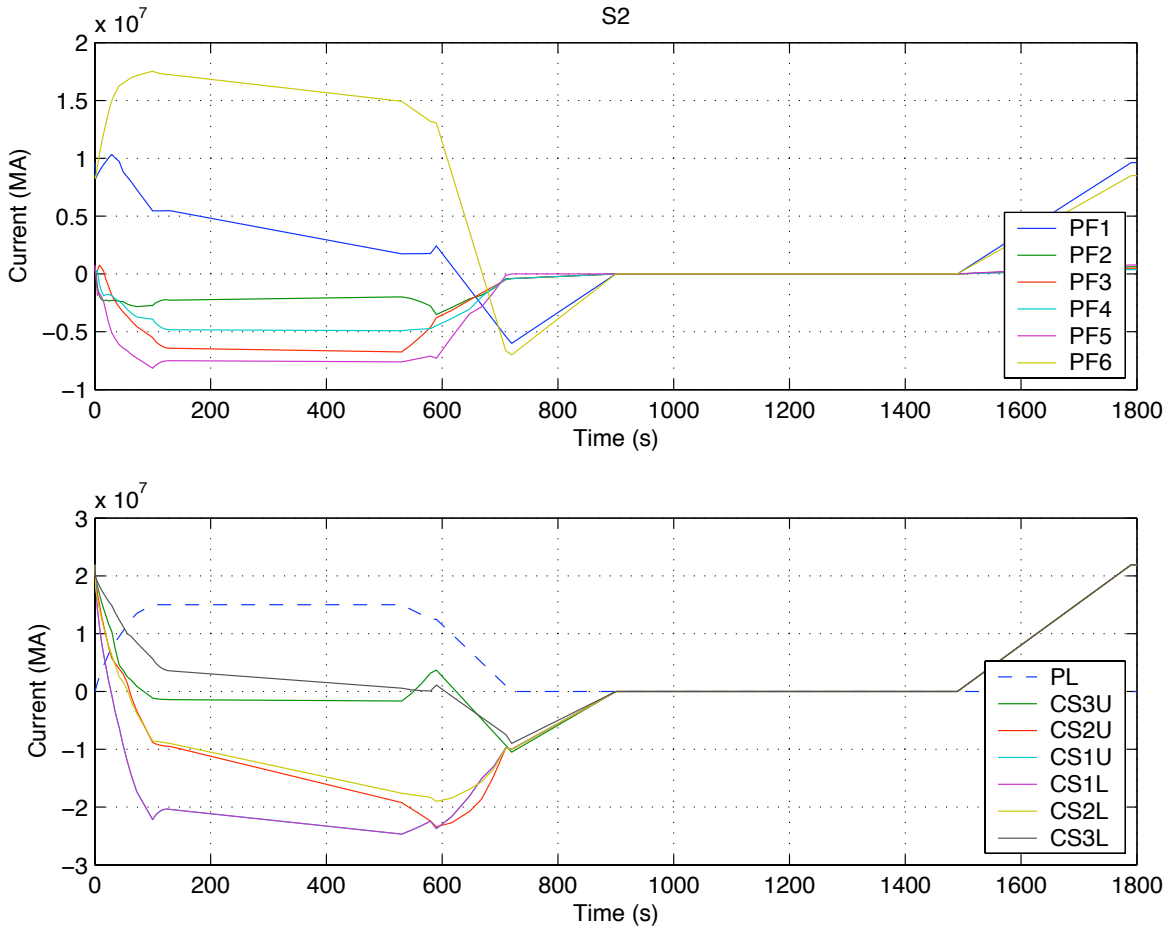

Figure 8: Operation scenario S2. Time history of the current in the ITER coils and in the plasma.

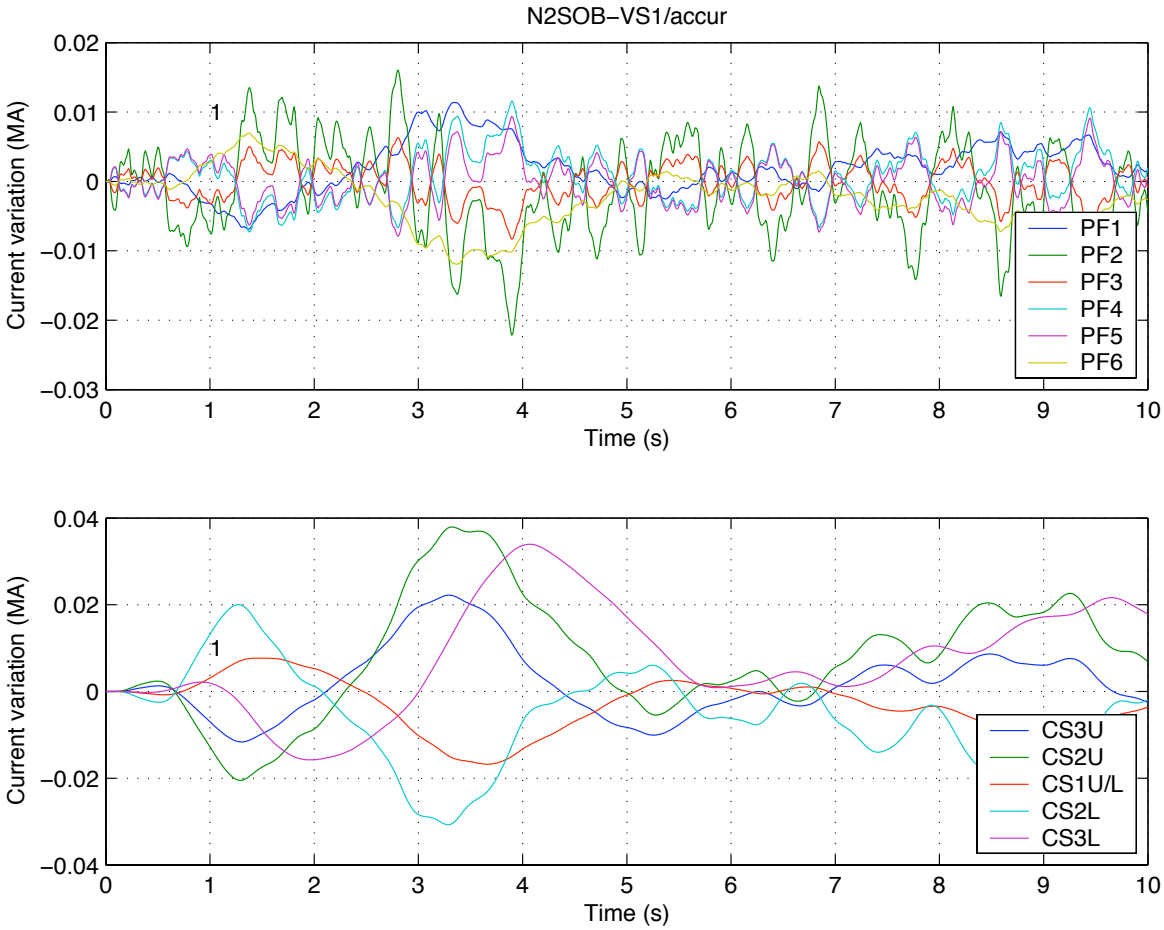

Figure 9: Control scenario SOBVS1. Time history of the current variation, i.e. to be added to the current of the operation scenario S2, in the ITER coils. The data set it complete.

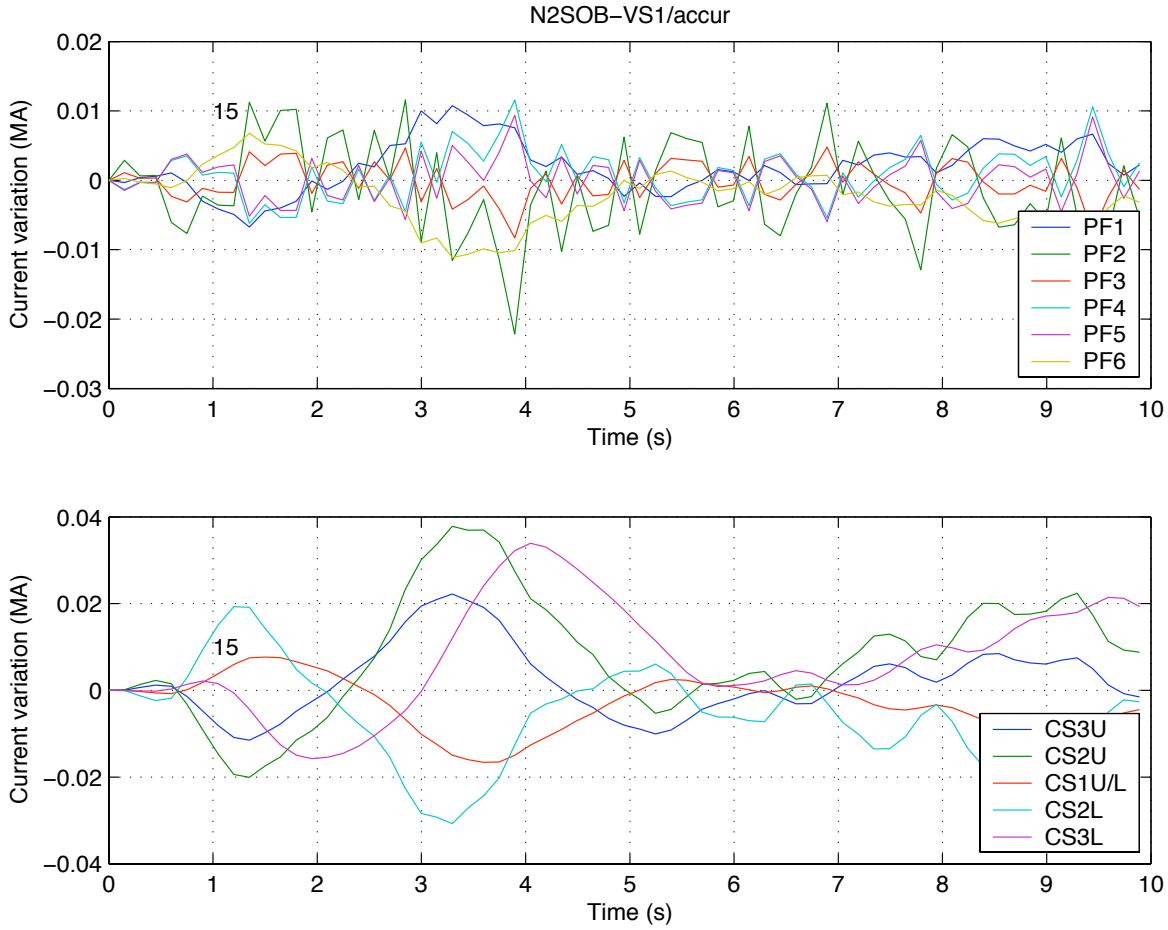

Figure 10: Control scenario SOBVS1. Same as Fig. 9 but the data set is decimated by a factor 15.

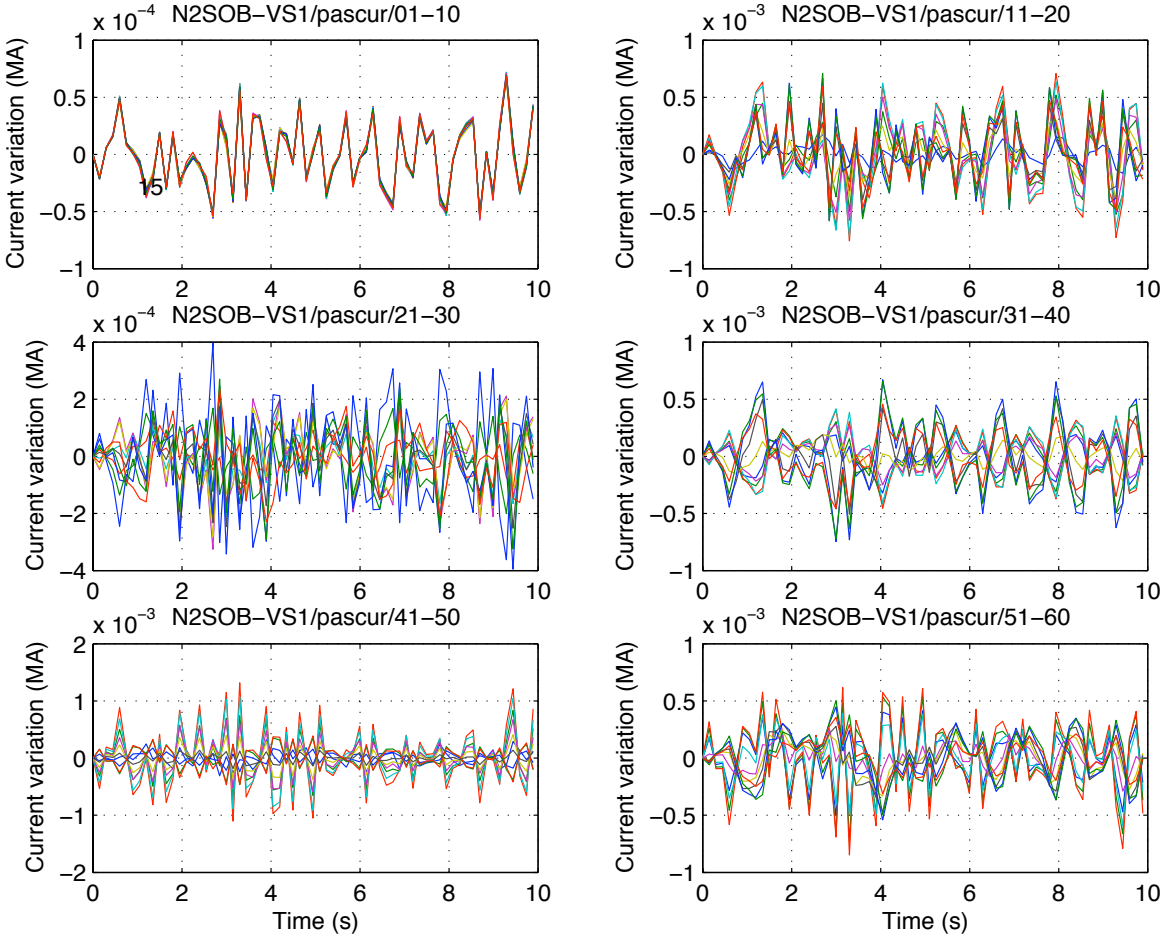

Figure 11: Control scenario SOBVS1. Time history of the current in the 60 passive coils (1–10 top–left plot, 11–20 top–right plot, etc.). The data set is decimated by a factor 15.

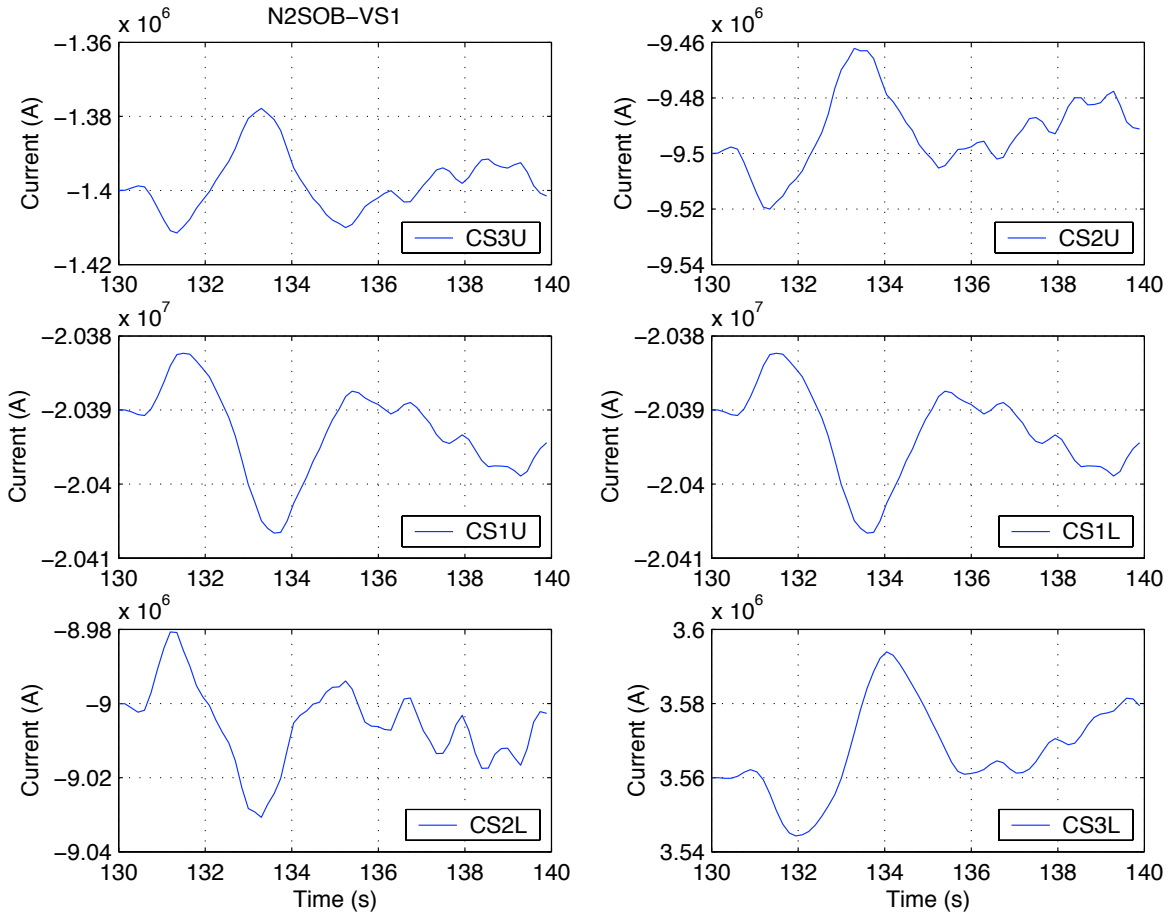

Figure 12: Control scenario SOBVS1. Details of the time history of the current in the CS coils after integration with the operation scenario S2.

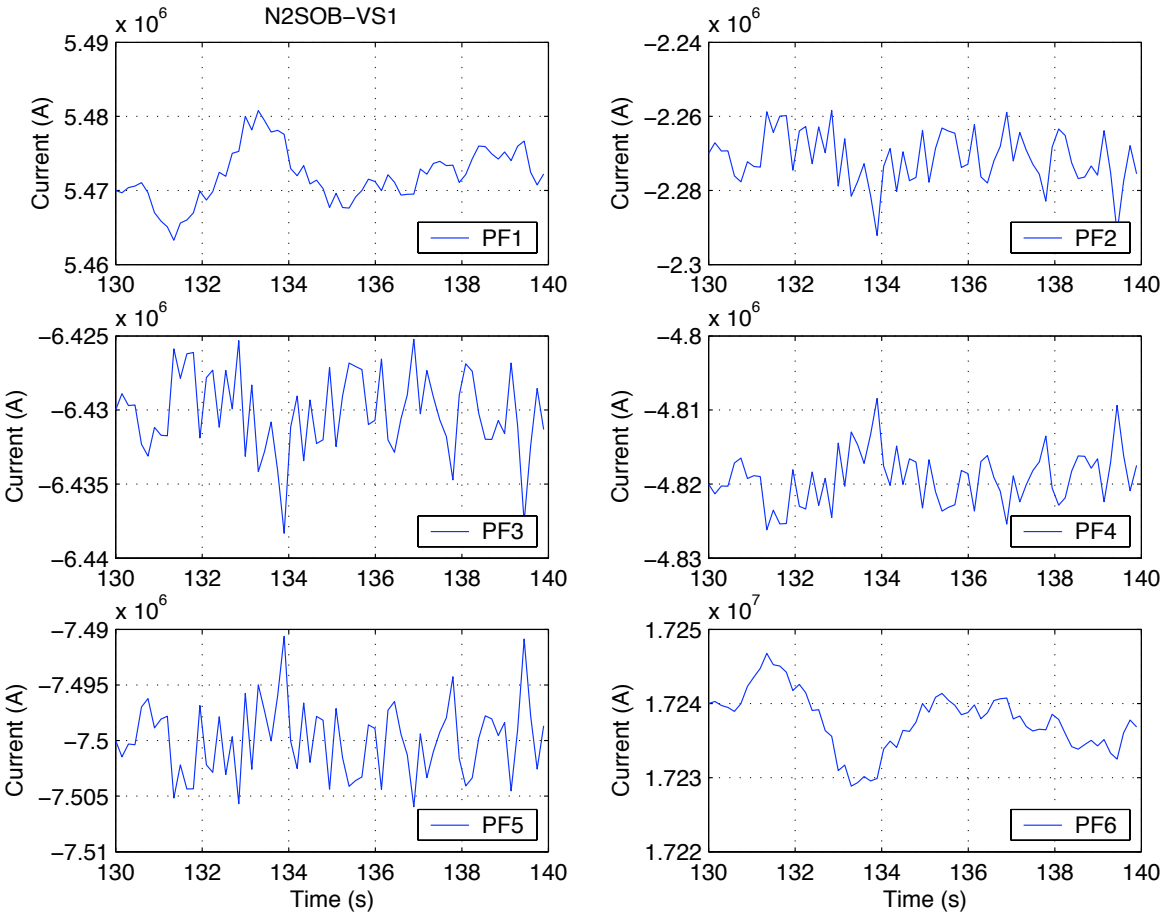

Figure 13: Control scenario SOBVS1. Details of the time history of the current in the PF coils after integration with the operation scenario S2.

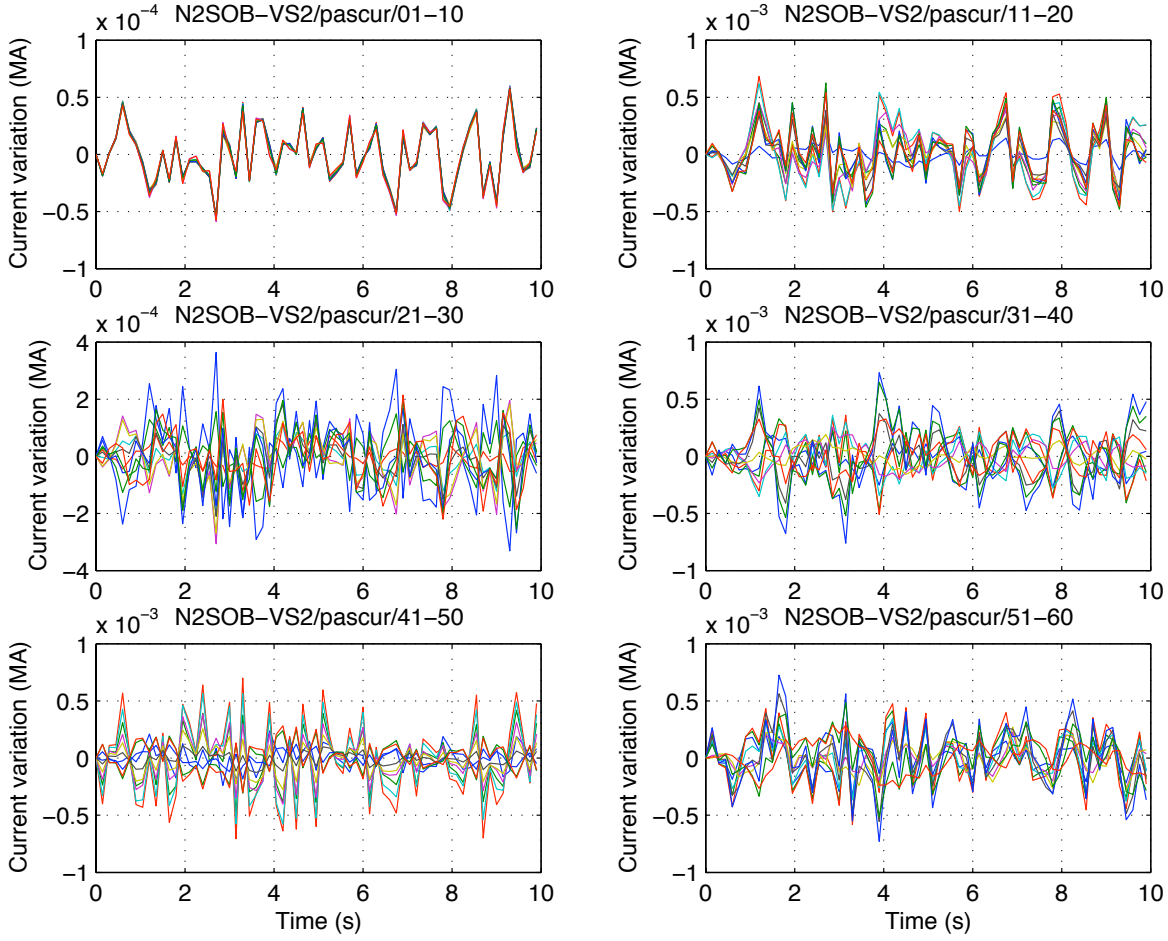

Figure 14: Control scenario SOBVS2. Time history of the current in the 60 passive coils (1–10 top–left plot, 11–20 top–right plot, etc.). The data set is decimated by a factor 15.

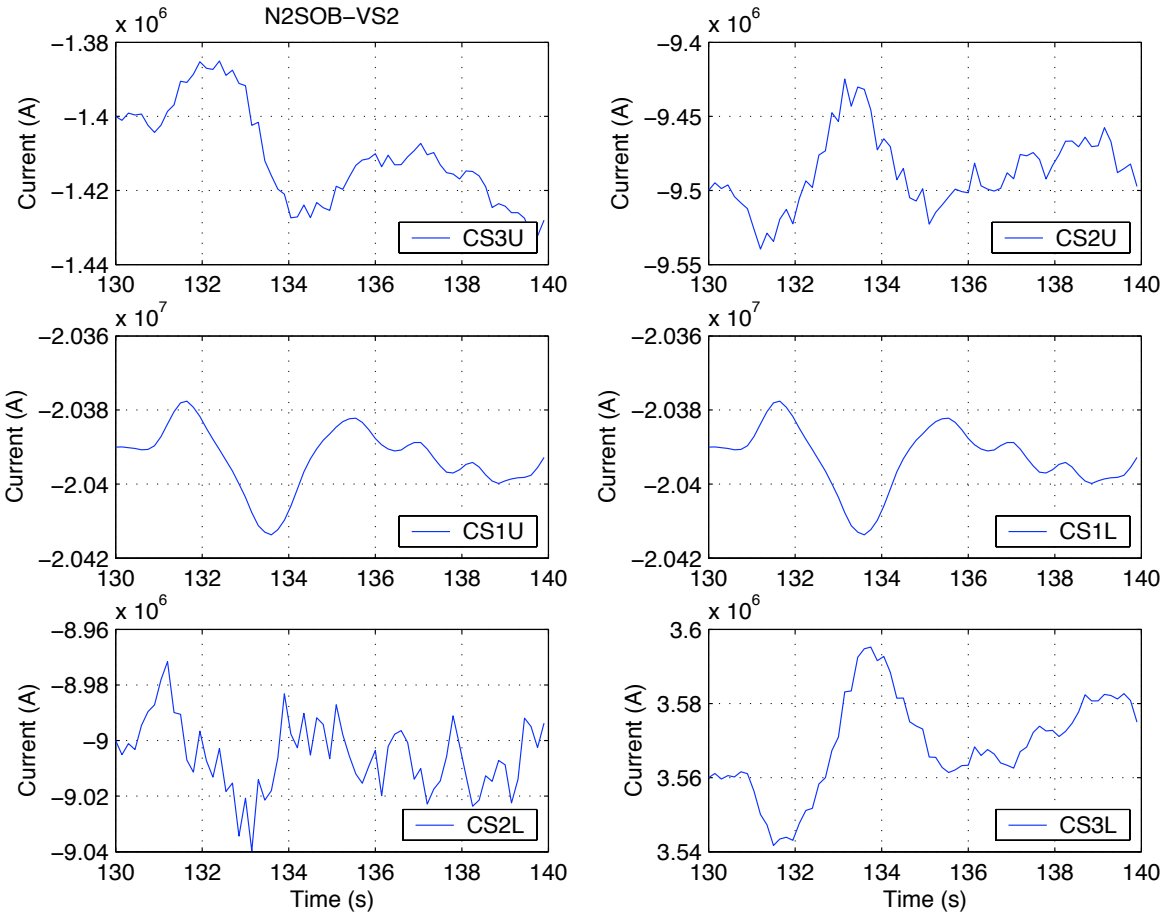

Figure 15: Control scenario SOBVS2. Details of the time history of the current in the CS coils after integration with the operation scenario S2.

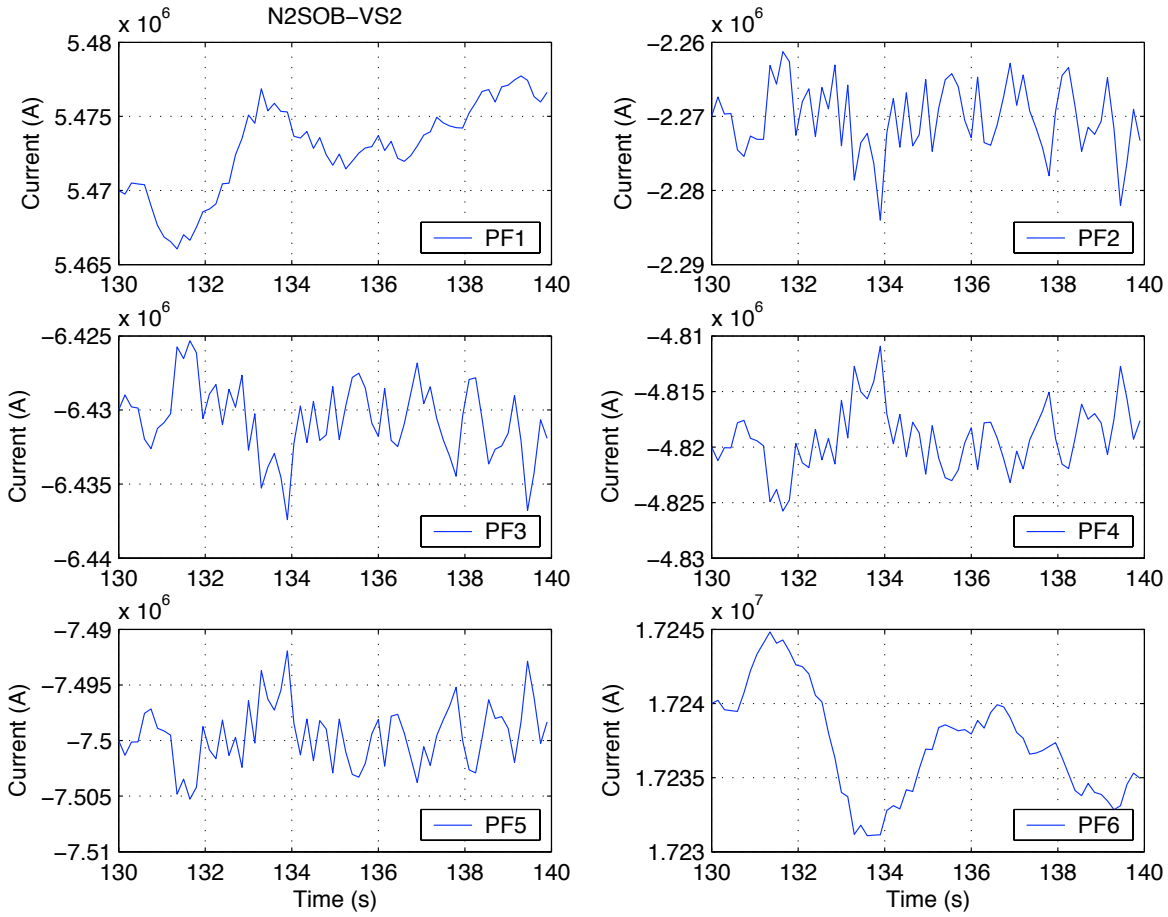

Figure 16: Control scenario SOBVS2. Details of the time history of the current in the PF coils after integration with the operation scenario S2.

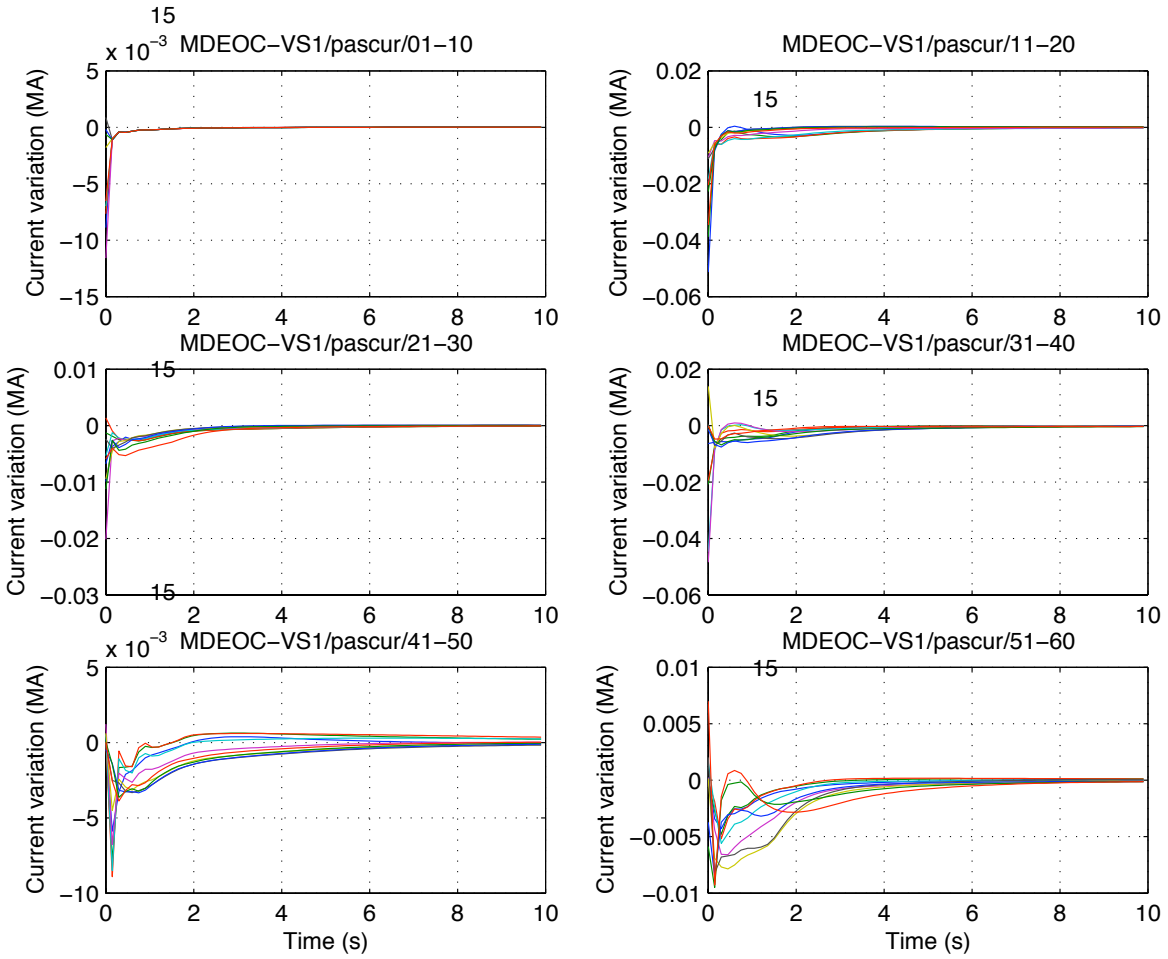

Figure 17: Control scenario EOCVS1. Time history of the current in the 60 passive coils (1–10 top–left plot, 11–20 top–right plot, etc.). The data set is decimated by a factor 15.

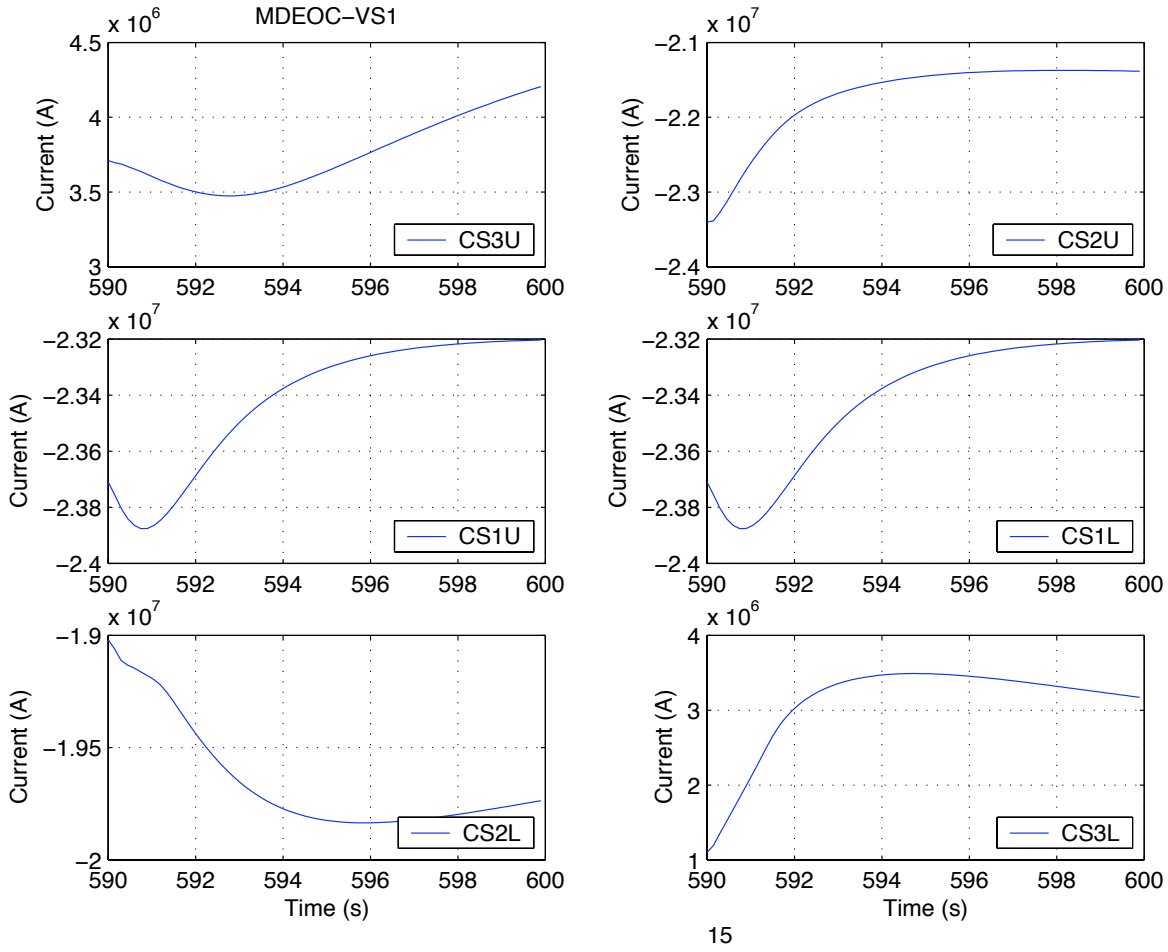

Figure 18: Control scenario EOCVS1. Details of the time history of the current in the CS coils after integration with the operation scenario S2.

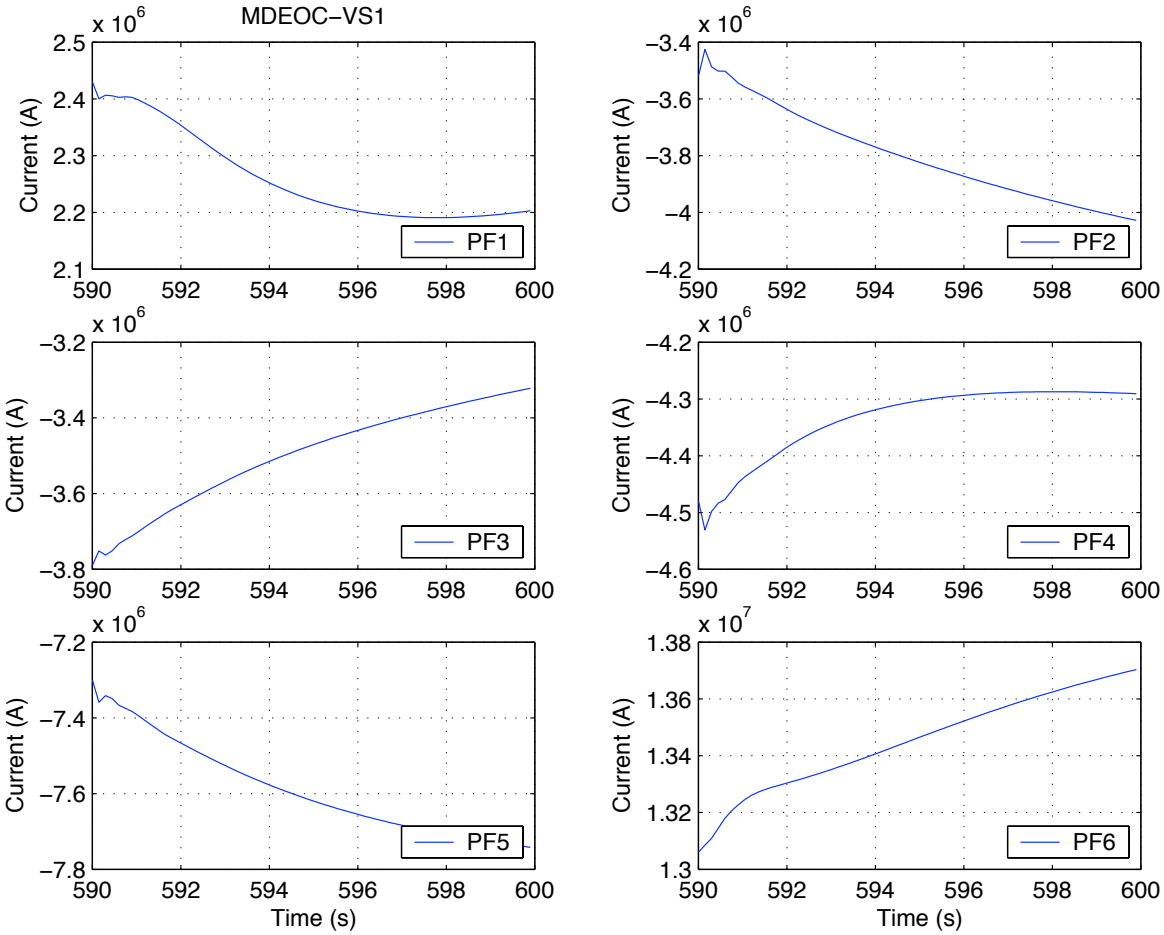

Figure 19: Control scenario EOCVS1. Details of the time history of the current in the PF coils after integration with the operation scenario S2.

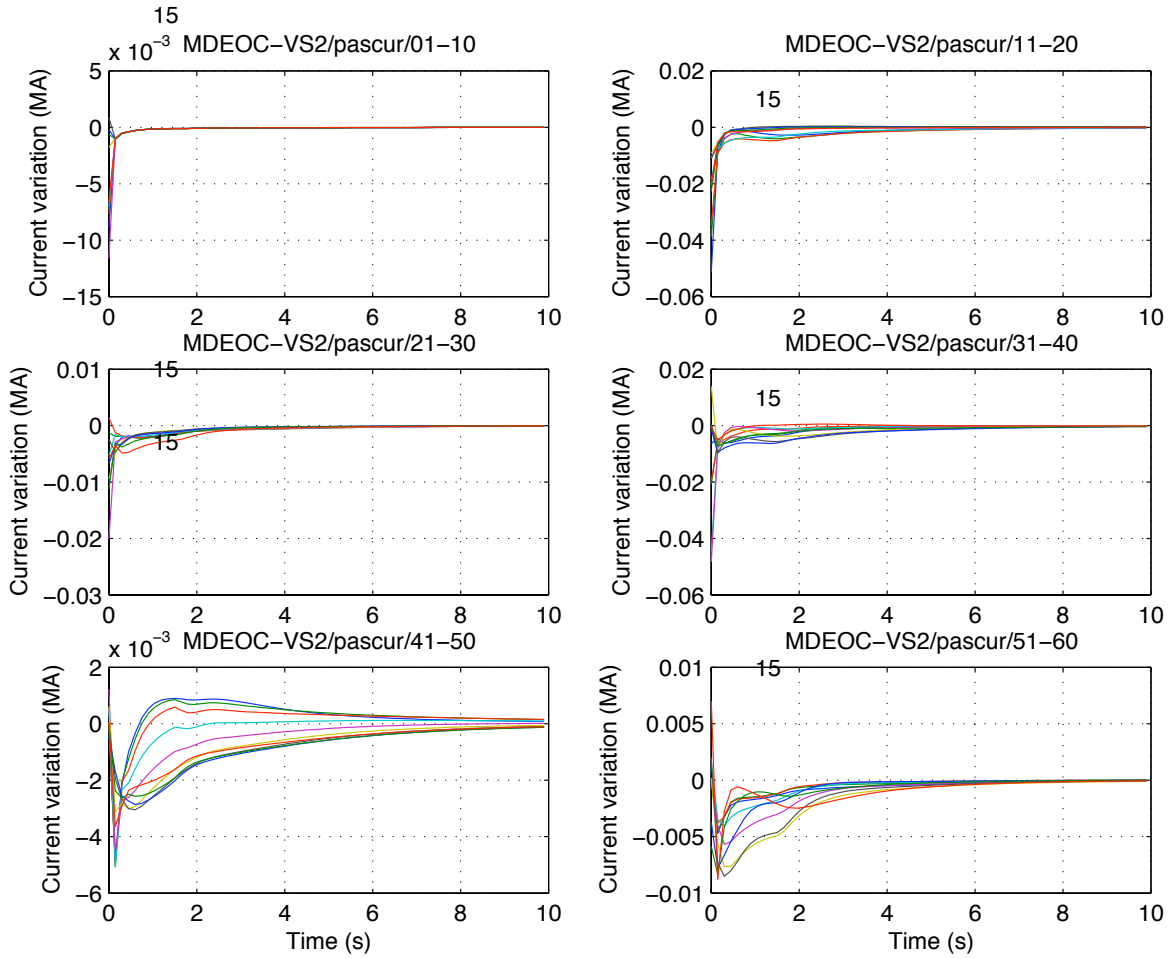

Figure 20: Control scenario EOCVS2. Time history of the current in the 60 passive coils (1–10 top–left plot, 11–20 top–right plot, etc.). The data set is decimated by a factor 15.

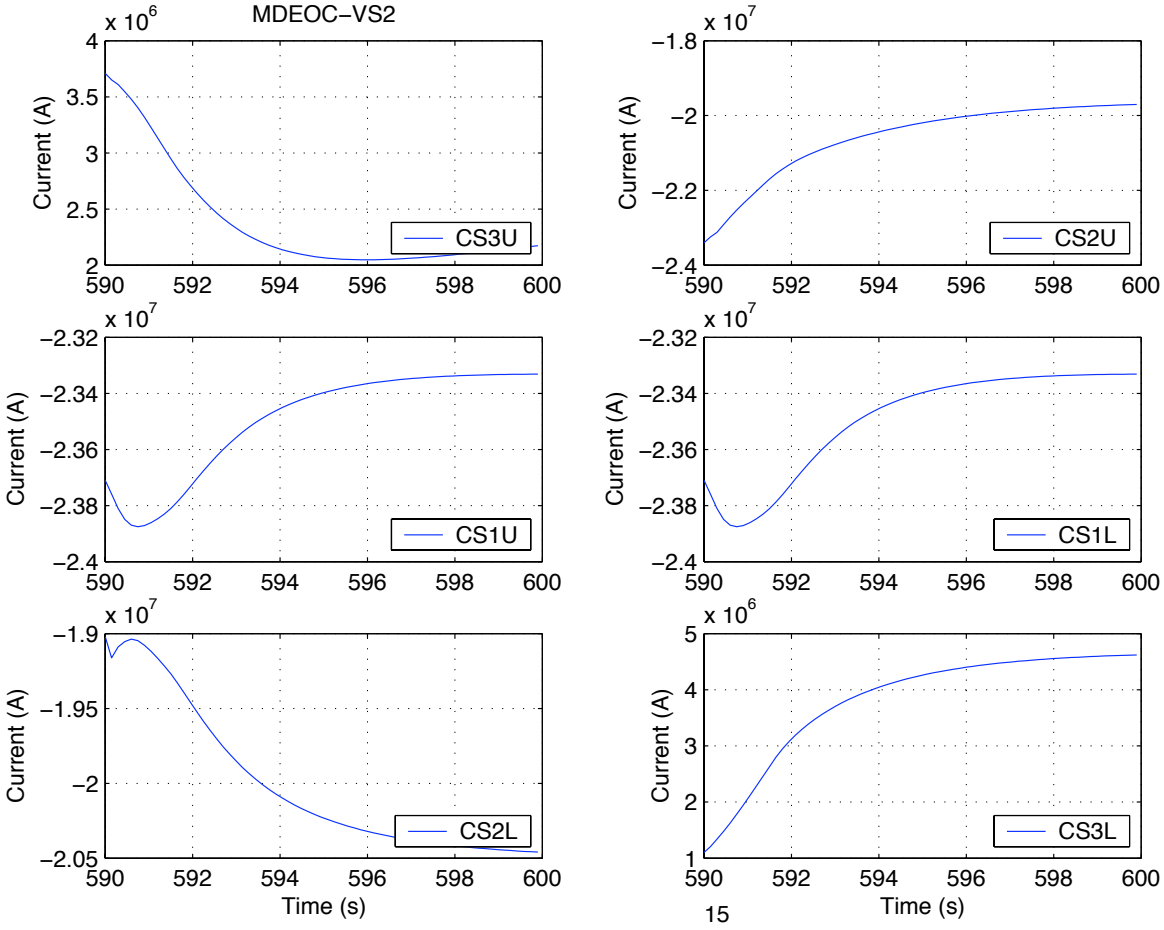

Figure 21: Control scenario EOCVS2. Details of the time history of the current in the CS coils after integration with the operation scenario S2.

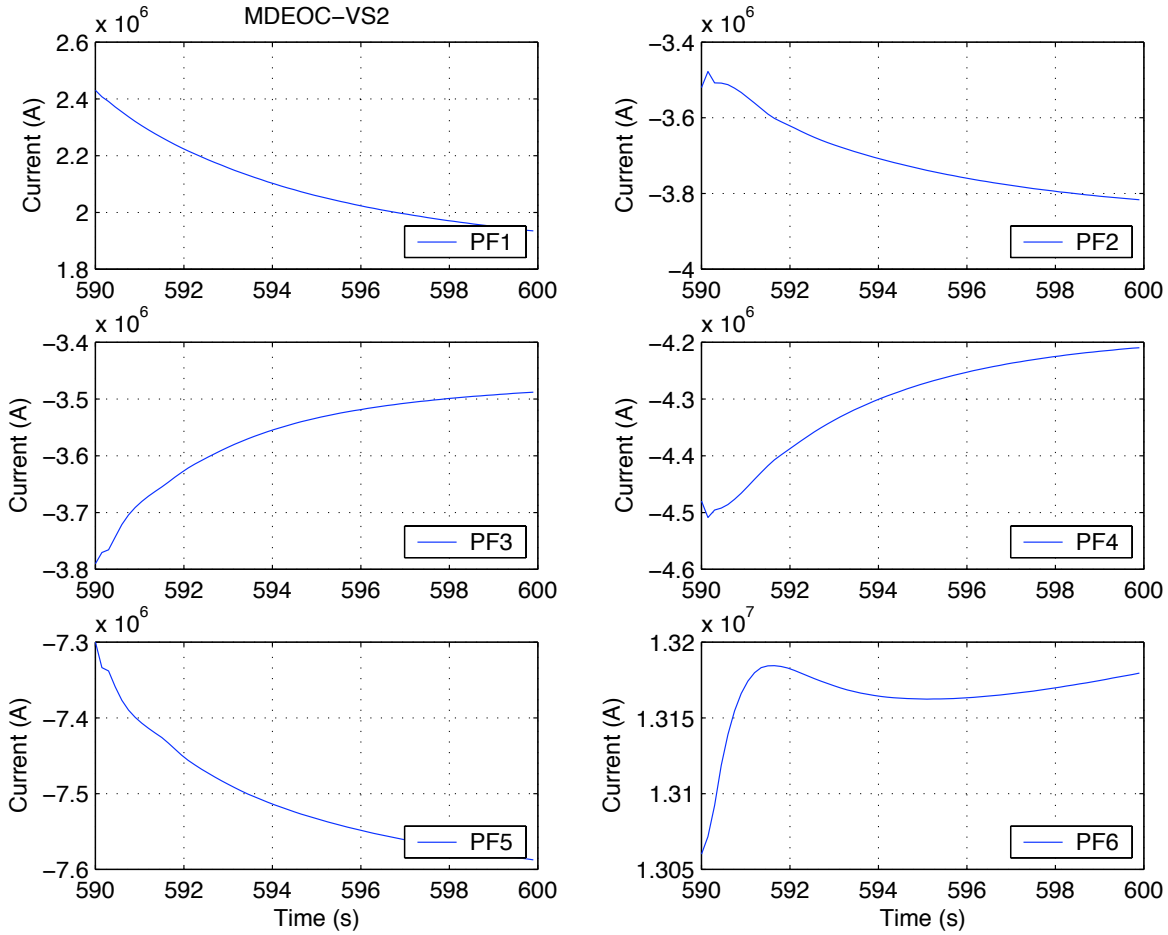

Figure 22: Control scenario EOCVS2. Details of the time history of the current in the PF coils after integration with the operation scenario S2.

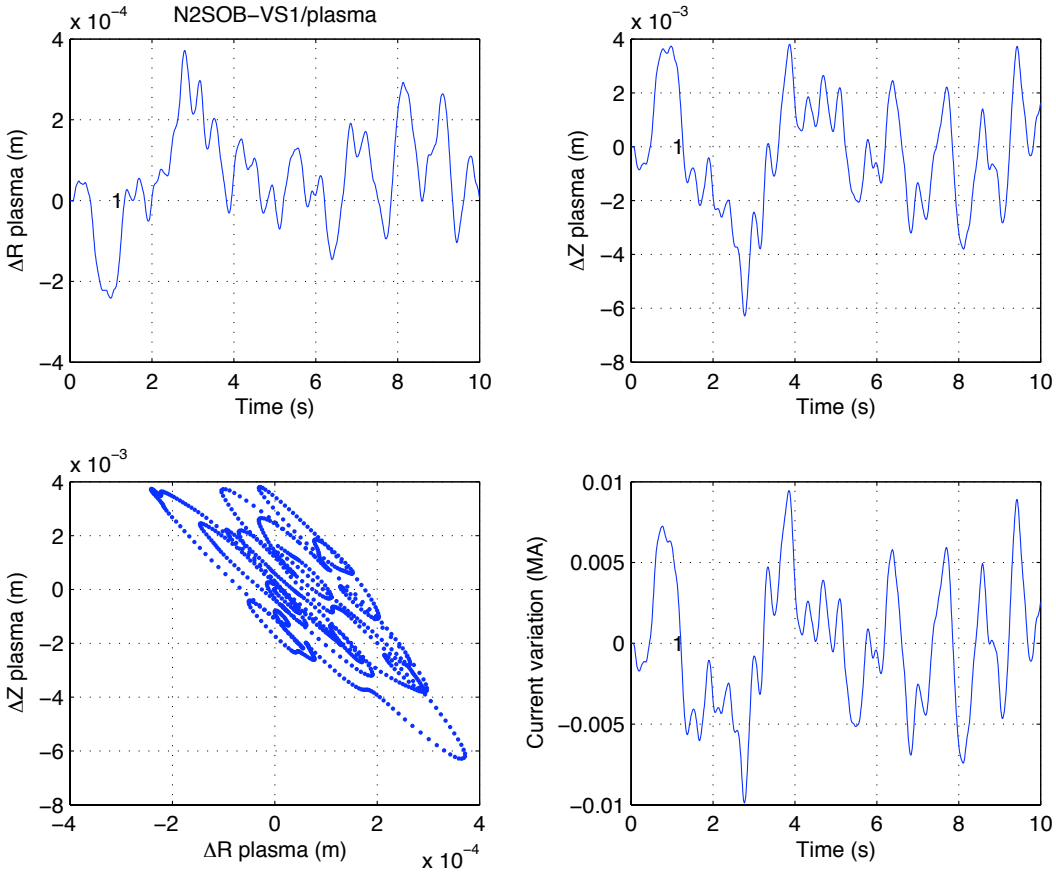

Figure 23: Control scenario SOBVS1. Offset of the plasma centroid coordinates (ΔR and ΔZ) with respect to the S2 scenario and plasma current variation (to be added to the plasma current of operation scenario S2). The data set is complete.

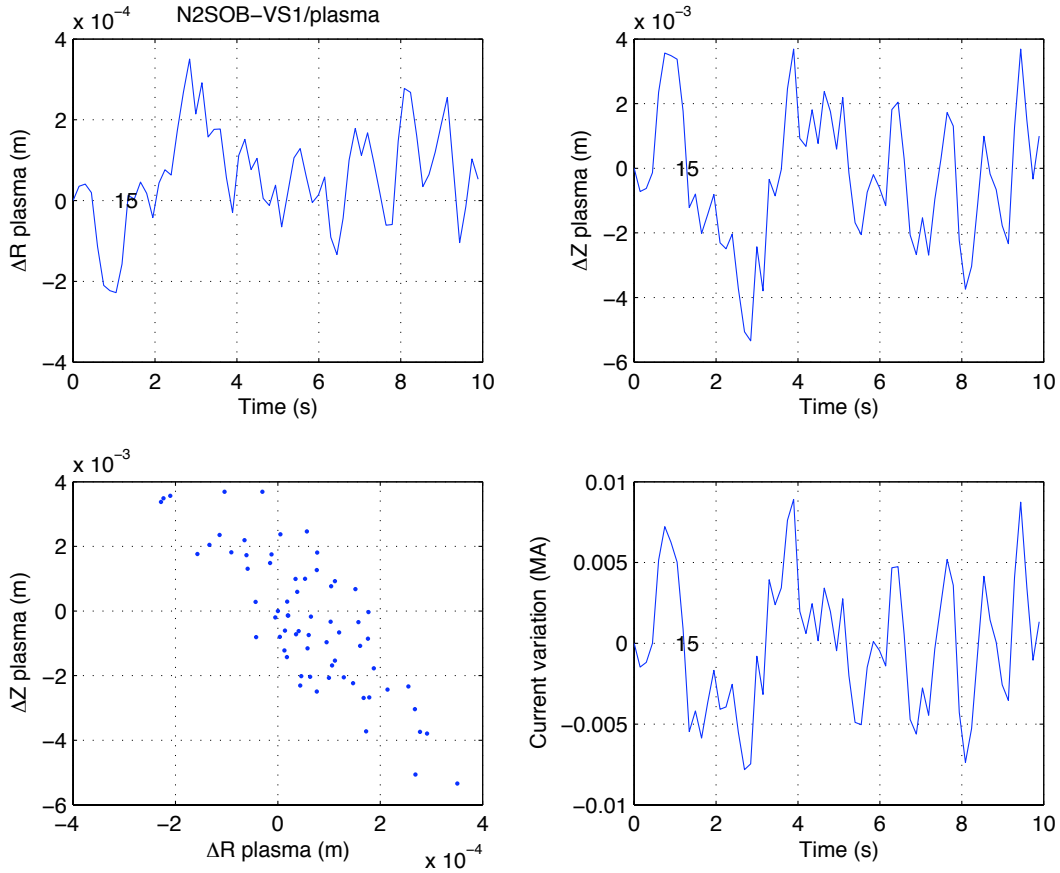

Figure 24: Control scenario SOBVS1. Offset of the plasma centroid coordinates (ΔR and ΔZ) with respect to the S2 scenario and plasma current variation (to be added to the plasma current of operation scenario S2). The data set is decimated by a factor 15.

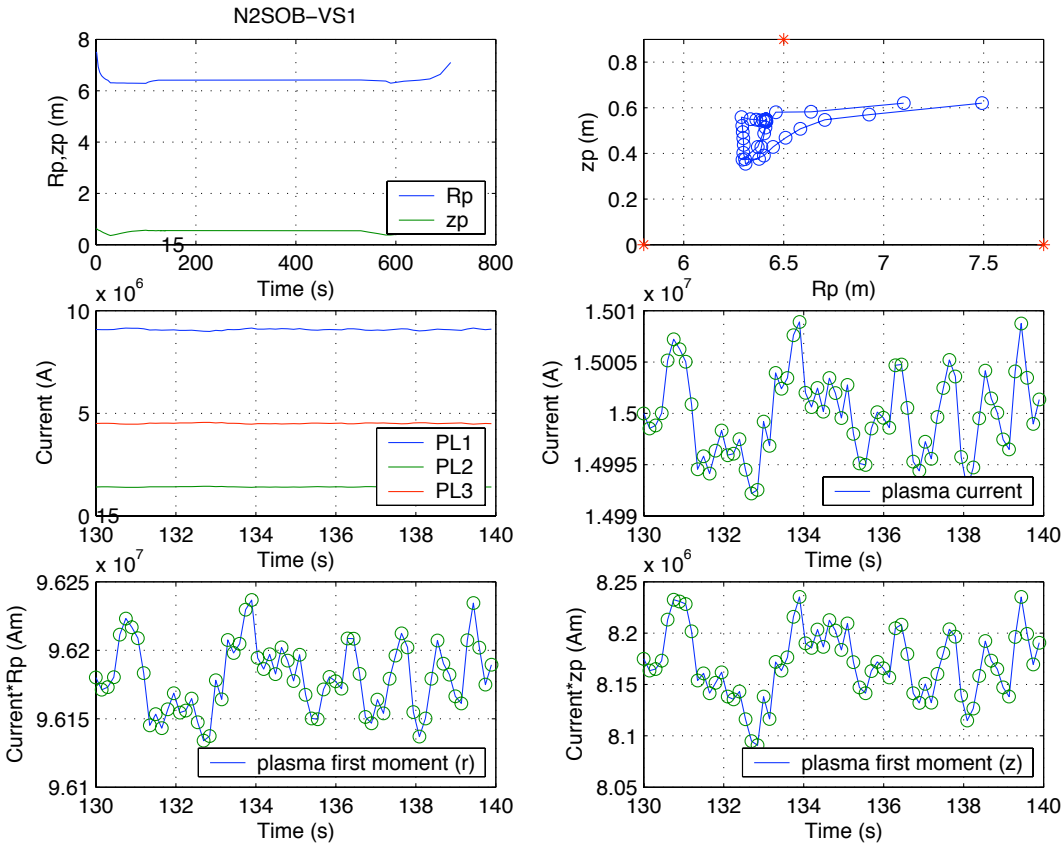

Figure 25: Control scenario SOBVS1. Moving plasma interpolation.

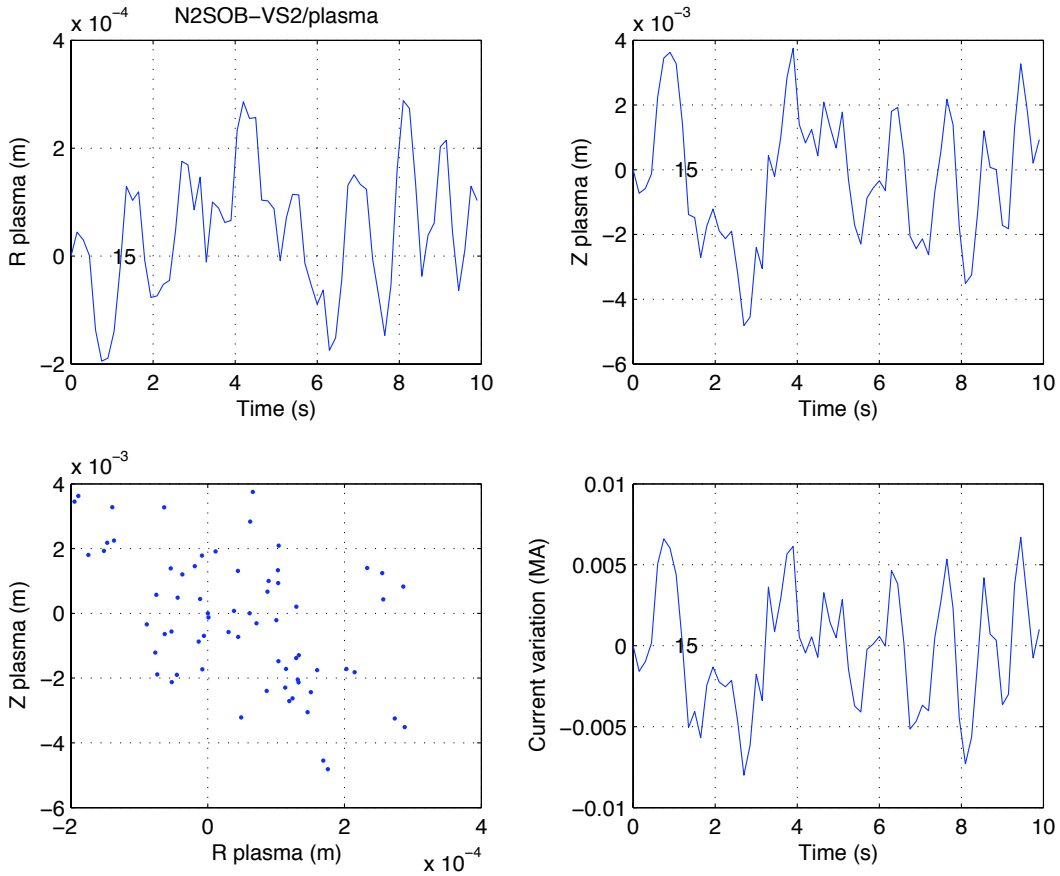

Figure 26: Control scenario SOBVS2. Offset of the plasma centroid coordinates (ΔR and ΔZ) with respect to the S2 scenario and plasma current variation (to be added to the plasma current of operation scenario S2). The data set is decimated by a factor 15.

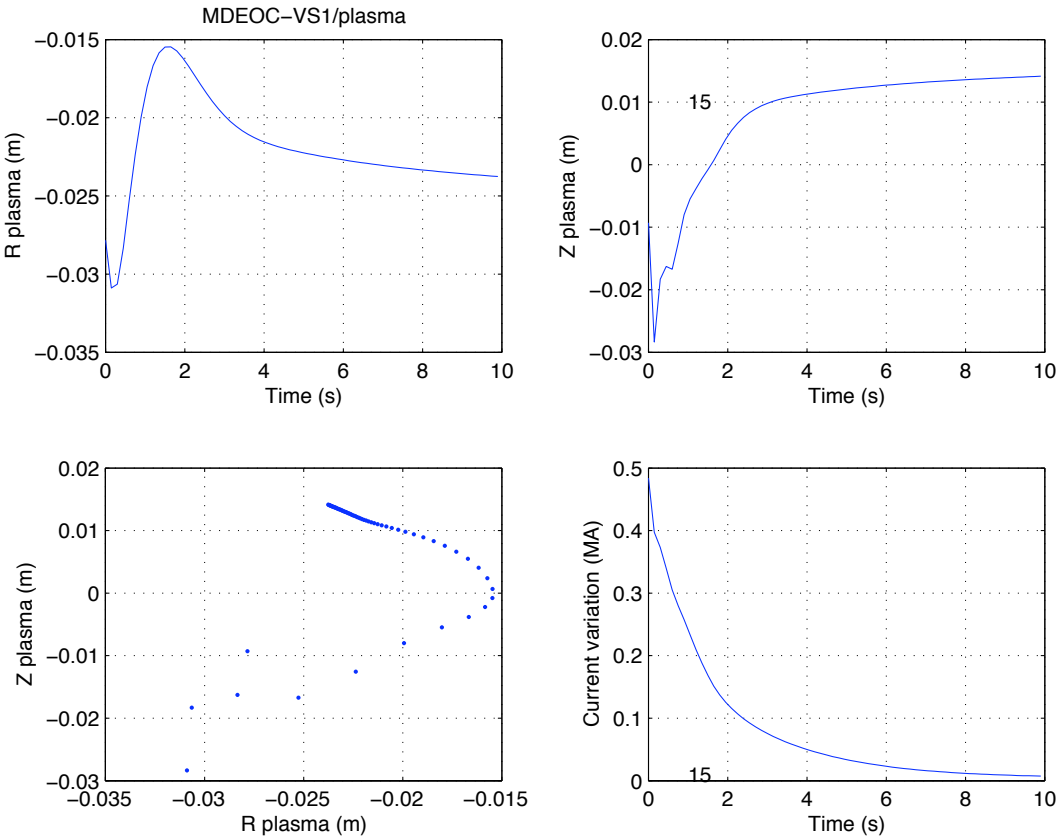

Figure 27: Control scenario EOCVS1. Offset of the plasma centroid coordinates (ΔR and ΔZ) with respect to the S2 scenario and plasma current variation (to be added to the plasma current of operation scenario S2). The data set is decimated by a factor 15.

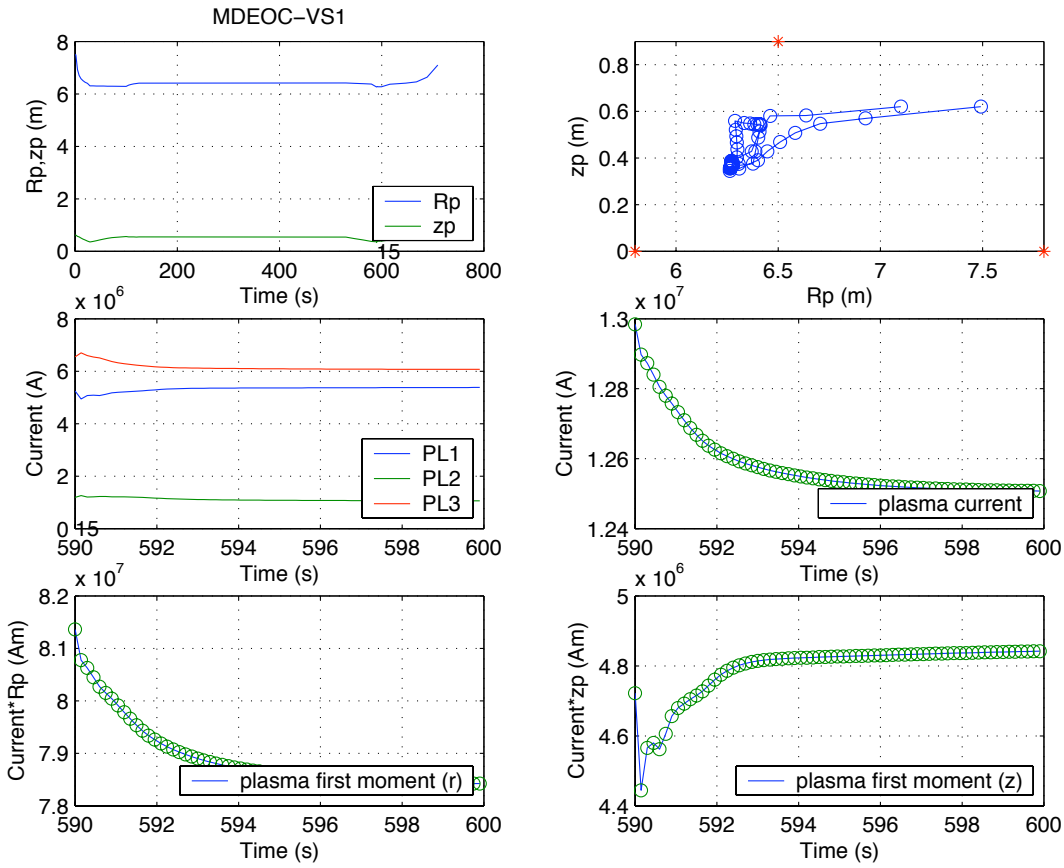

Figure 28: Control scenario SOBVS1. Moving plasma interpolation.

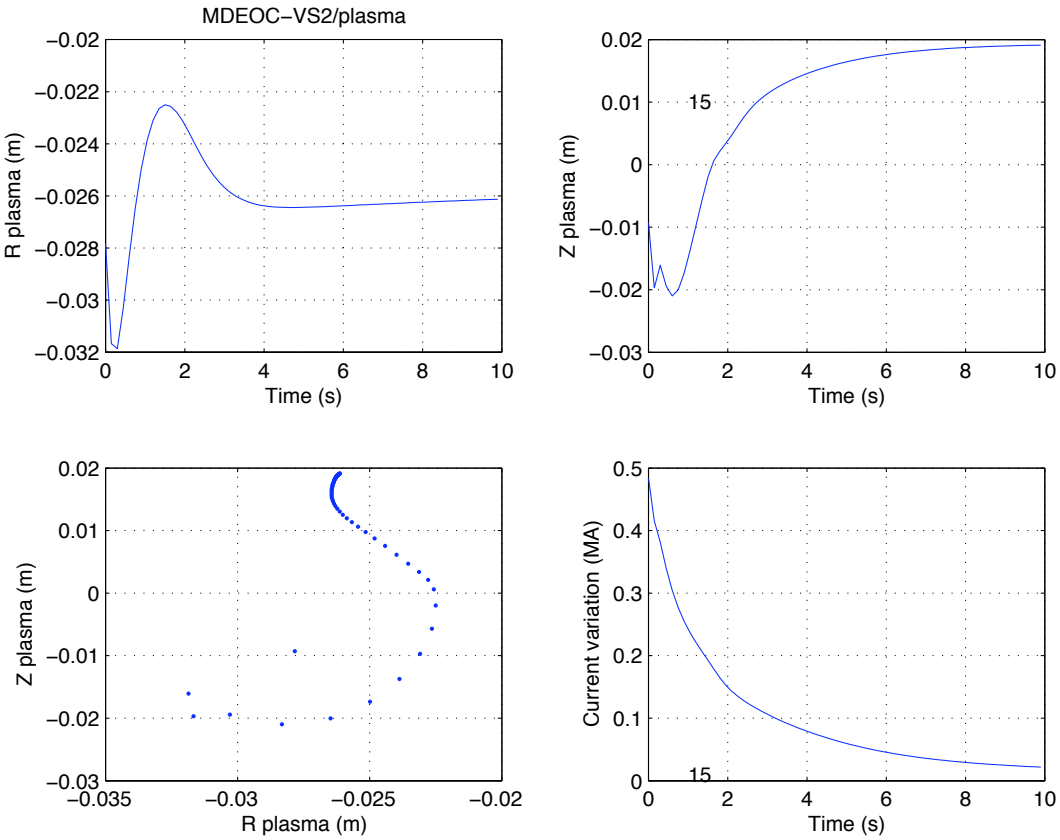

Figure 29: Control scenario EOCVS2. Offset of the plasma centroid coordinates (ΔR and ΔZ) with respect to the S2 scenario and plasma current variation (to be added to the plasma current of operation scenario S2). The data set is decimated by a factor 15.

3 Magnetic field

The magnetic field during the operation scenario S2 has been calculated in two ways, with and without non axis symmetric (TF) coils. To avoid unnecessary long computational times the analysis is limited to the part of S2 with plasma, i.e. from t=0s to the end-of-plasma (EOP, t=720s). The computations are performed using the static plasma data.

3.1 Without TF coils

The first computation is done including only the axis symmetric coils.[2] The calculated maximum magnetic field (B_{max}) in the ITER coils is in good agreement with the nominal values [4]-[5], as shown in the Fig. 30 for the CS coils, and in Fig. 31 for the PF coils. The CPU time for this run is $\approx$ 120 (M'C option AXIS ON).

A detailed M'C output, which includes the time history of B_{max} as well as the distribution of the module of the magnetic field ($\mid B \mid$) along the pancake length at SOD (t=0s), SOB (t=130s), EOC (t=590s) and shortly before the EOP (t=710s), is provided for all coils in the electronic documentation (file FIELD/FIELD.ps).

3.2 With TF coils

A second computation is performed including also the non axial symmetric coils in order to assess the effect of the ripple due to the TF coils on the magnetic field in CS and PF coils. The results have shown that, as expected, this ripple effect is negligible on the CS coils (Fig. 32) but not negligible on the PF coils, in particular PF2 and PF4, as shown in the Fig. 33. A detailed analysis of the PF2 coils, using a much finer discretization (90 GCE's instead of 20), have confirmed that the above results are not due to an artifact, i.e. the distribution of the magnetic field along one turn of the pancake length shows the TF ripple effect (Fig. 34). The CPU time for this run is $\approx$ 5000 s (M'C option AXIS OFF).

The detailed electronic documentation of this case is available (file FIELDTF/FIELDTF.ps).

[2] The passive coils are not included as they are relevant for control scenarios only.

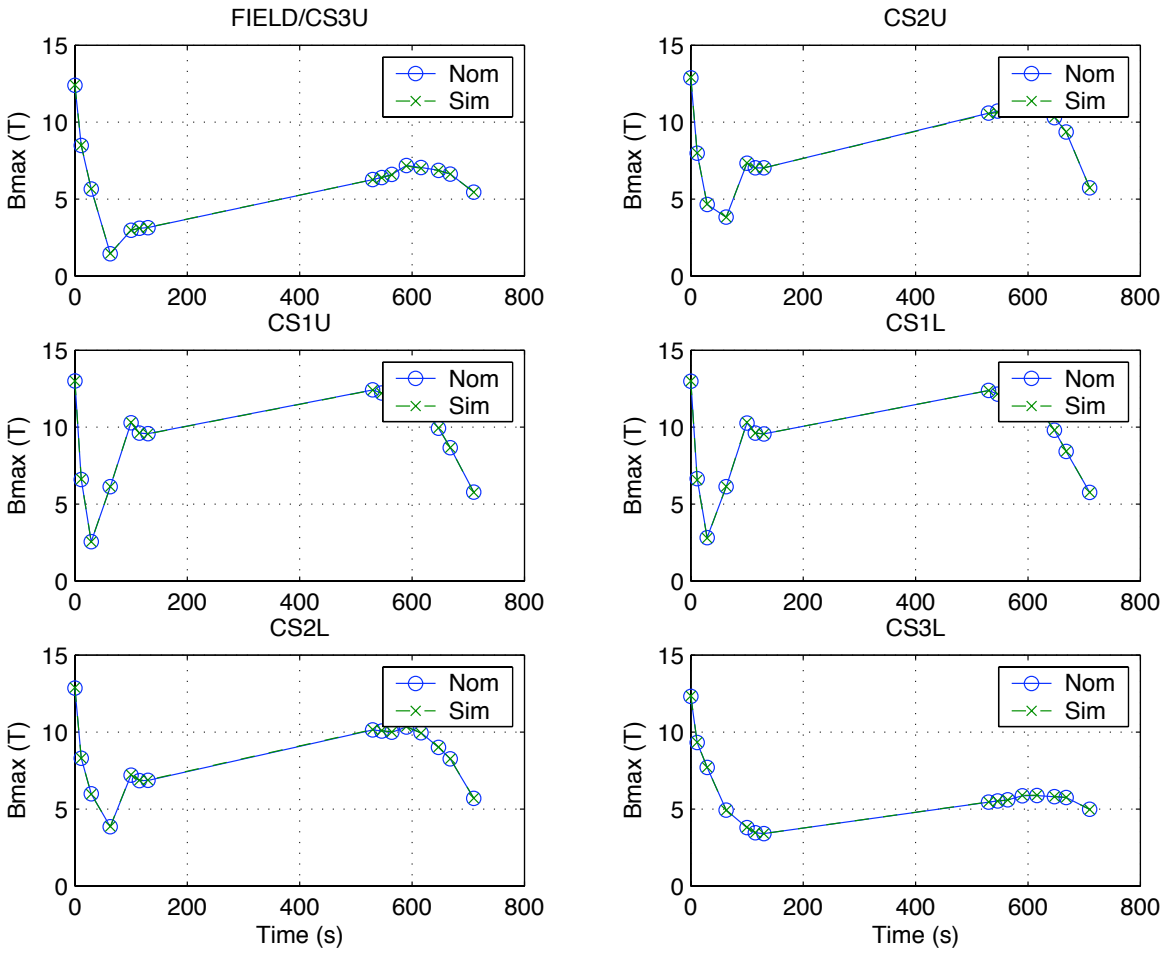

Figure 30: Time history of the maximum magnetic field in the CS coils (analysis without TF coils). The nominal [4] and the simulated results are shown.

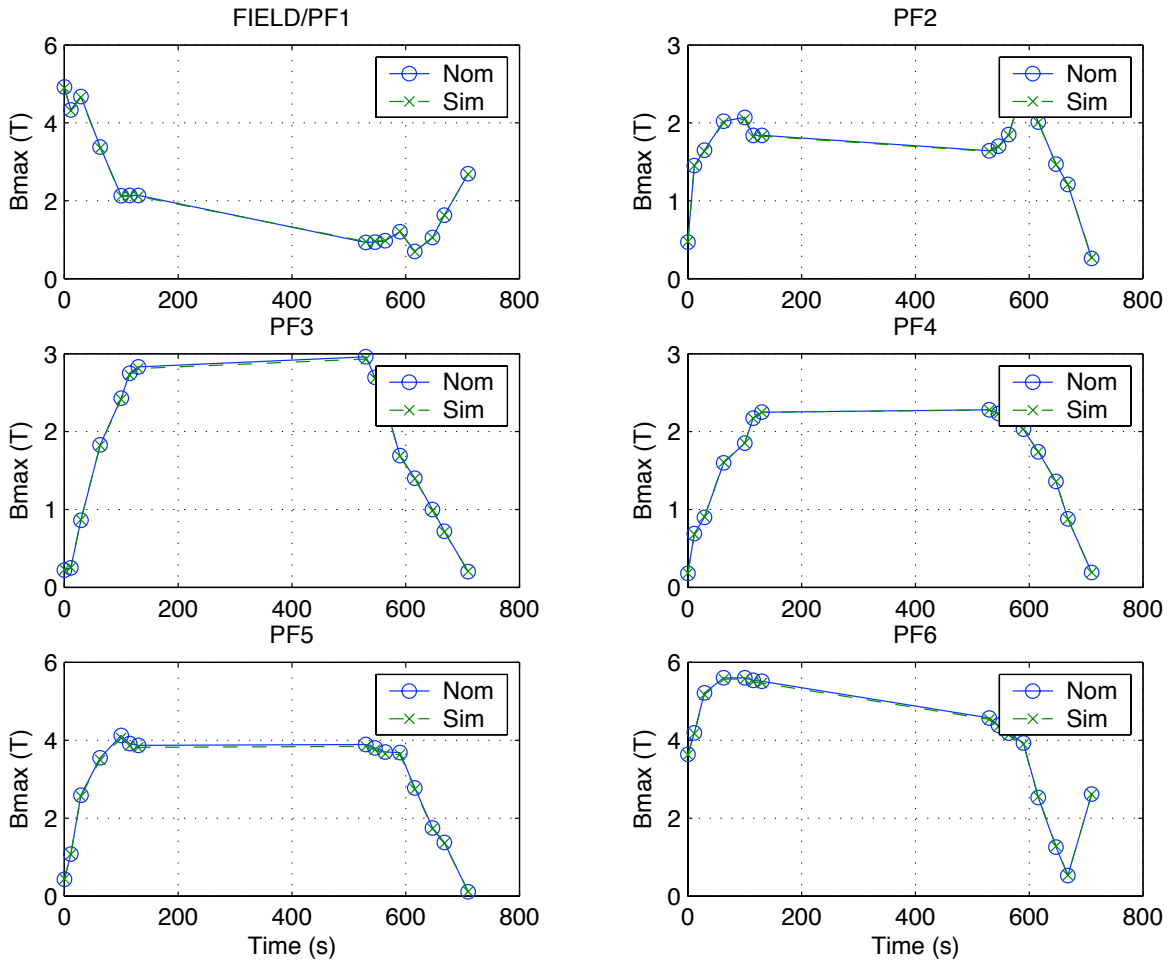

Figure 31: Time history of the maximum magnetic field in the PF coils (analysis without TF coils). The nominal [4] and the simulated results are shown.

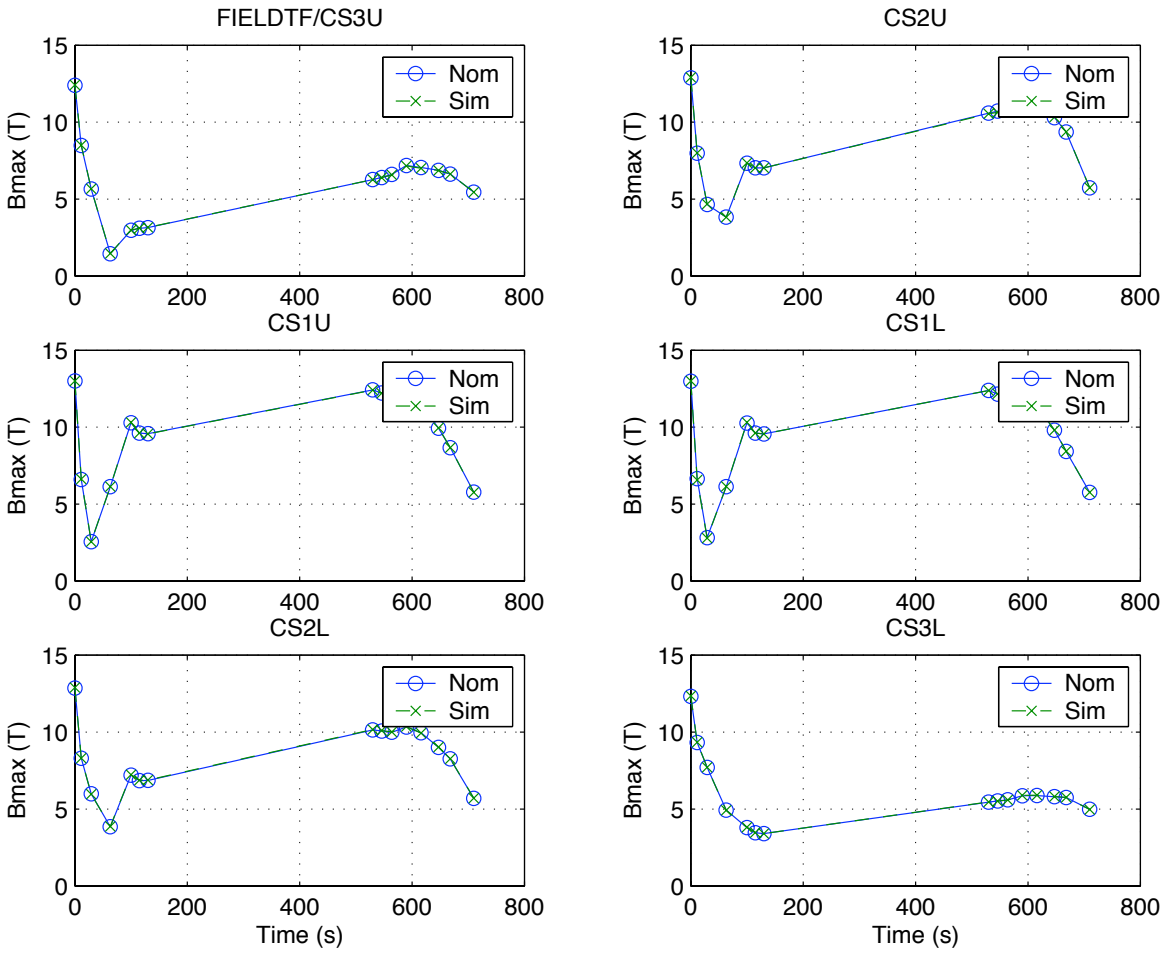

Figure 32: Time history of the maximum magnetic field in the CS coils (analysis with TF coils). The nominal [4] and the simulated results are shown.

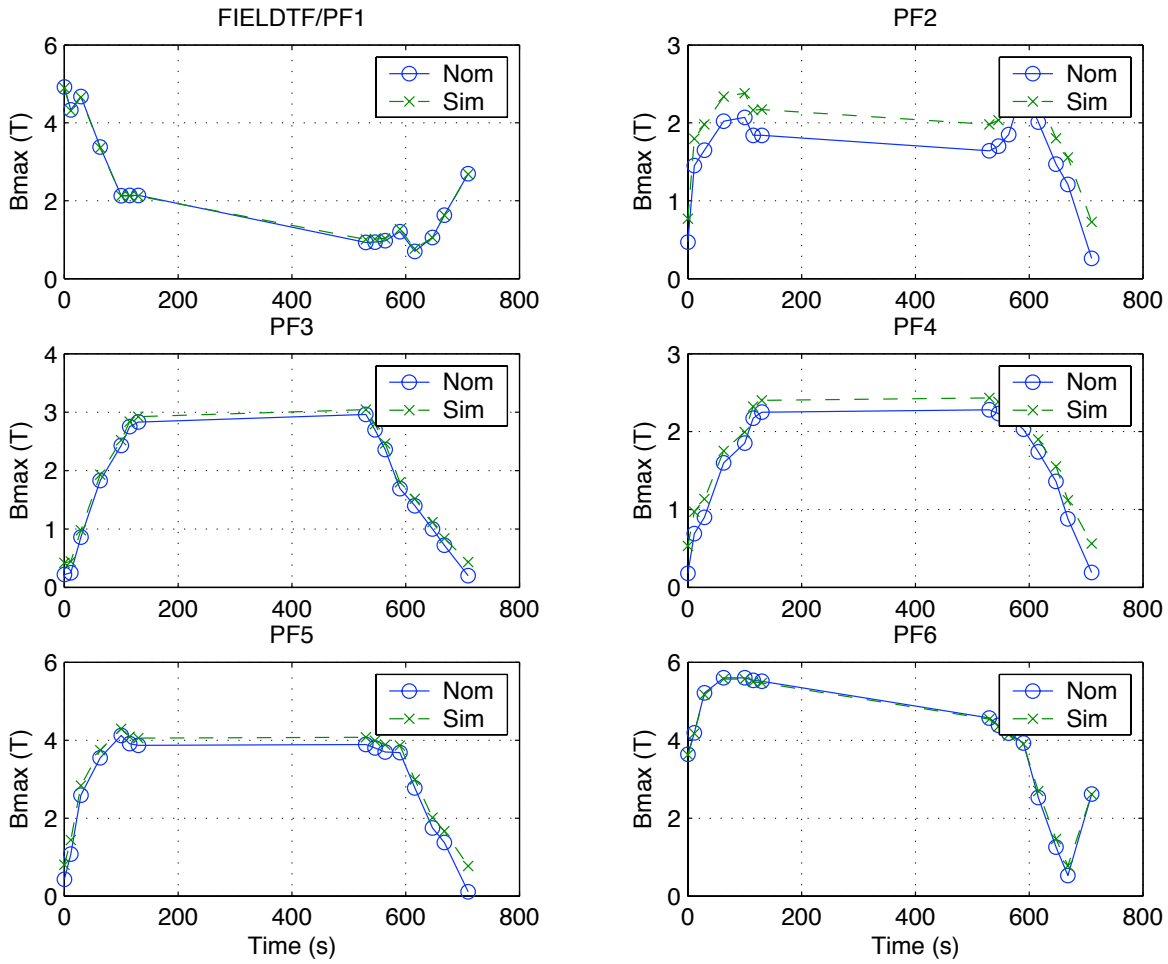

Figure 33: Time history of the maximum magnetic field in the PF coils (analysis with TF coils). The nominal [4] and the simulated results are shown.

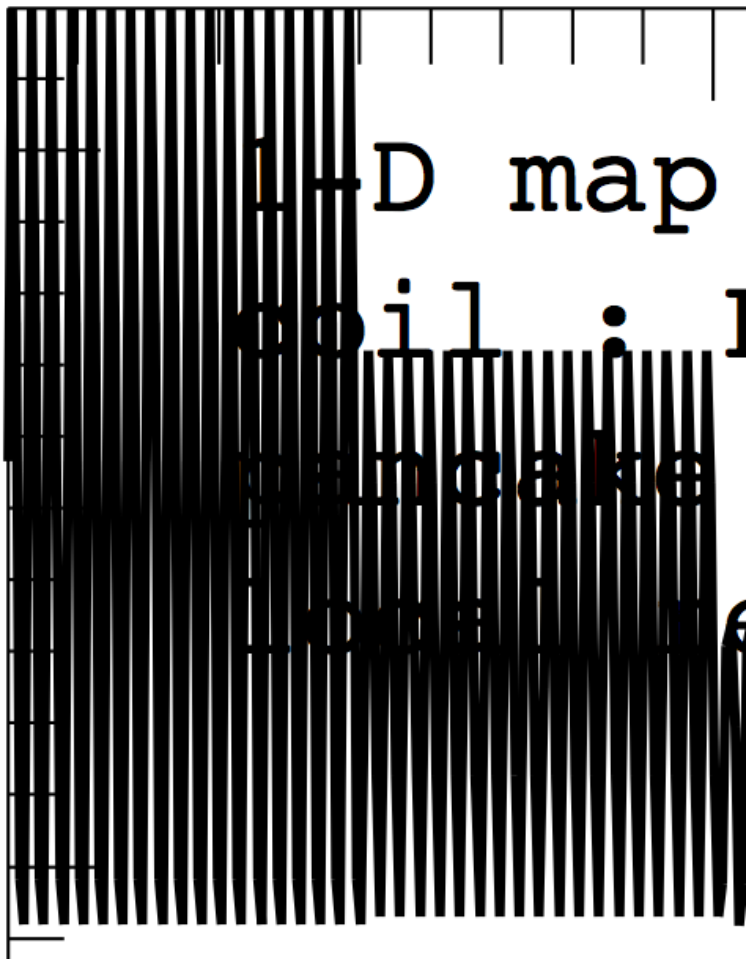

Figure 34: Zoom of the distribution of the maximum magnetic field along two turns of the PF2 coil (anaysis with TF coils), showing qualitatively the ripple effect due to the 18 TF coils.

4 AC losses during the operation scenario S2

The AC losses during the full operation scenario S2 (0–1800s) have been computed in two steps:

- in the axis symmetric (CS and PF) coils with the AXIS ON option. The goal is to save computation time without loss of accuracy, as discussed in detail in Section 7.1;
- in the non axis symmetric (TF) coils with the AXIS OFF option.

M'C calculates average AC losses as a function of time per unit length, $P_{av}(t)$ [W/m]. The total AC losses as a function of time are $P_{to}(t) = P_{av}(t) * L$ [W], where L is the total coil length. By time integration of $P_{to}(t)$ we obtain the energy E [J]. Finally we get the total power dissipation during a given scenario as $P = E/\Delta t$ where Δt is the duration of the given scenario. This procedure is applied to all components of the AC losses provided by M'C, i.e. hystereris losses due to normal magnetic field (HN), hystereris losses due to parallel magnetic field (PN), coupling losses due to normal magnetic field (CN), coupling losses due to parallel magnetic field, and total losses (TO). In the CS and PF coils (axis symmetric coils) the HP and CP losses are zero.

4.1 Losses in the CS and PF coils

The total AC losses are 2.6 kW in the CS coils and 1.2 kW in the PF coils, as summarized in Table 7. The losses are approximately the same in all CS coils (Fig. 35) and the dominant contributions are the HN losses (Fig. 36). In the PF coils the higher AC losses are in PF1 and PF6, (Fig. 37) and the dominant contributions are also the HN losses in all coils except PF2 where HN and CN losses are approximately the same (Fig. 38).

The electronic documentation contains:

1. Coil model, time history of the maximum magnetic field, time history of the average AC losses, time history of the maximum AC losses, contour plots of the module of the magnetic field at time 0s. 29.4s, 100s, 130s, 530s, 590s, 720s, 1800s and contour plots of the module of the AC losses at time 0s. 29.4s, 100s, 130s, 530s, 590s, 720s, 1800s. We have used the observed distribution of the AC losses in the coil cross sections to select the pancakes to analyze in detail. These data are in the file `S2/S2.ps` (total of 202 pages).
2. Distribution of the total AC losses along the length of the coil at time 0s. 29.4s, 100s, 130s, 530s, 590s, 720s, 1800s in three pancakes, i.e. two on both sides of the coil and one at the center of the coil. There are a total of 36 files in the folder `S2/matlab` (file name: `ACmod_coilname_pancake.eps`).
3. Coil model and time history of all contribution of the losses in the file `S2x/S2x.ps`.

4.2 Losses in the TF coils

The total losses in the TF coils, i.e. 18 times the losses in TF1, are 428 W (Table 8), with HN (44 %) and HP (40 %) as the dominant components (Fig. 39). The electronic documentation of this case is similar to the one described above, but in the folder `S2TFx` (instead of `S2x`).

4.3 Discussion

A comparison of the above results with the AC losses in the ITER DDD [4] shows that these are different but comparable, e.g. in the CS coils the total losses are 2572 W (our model) vs. 3734 W, in the PF 1215 W vs. 747 W, and in the TF coils 428 W vs. 673 W. The differences are due to a combination of several reasons, e.g. parametric description of the critical current, computation algorithm, etc. The difference in the coupling losses, i.e. a factor 1/3 lower in our model, can be explained by the different input data used. In fact, the total time constant is $n\tau = 50$ ms in our model and 150 ms in the other model.

Table 7: Summary of AC losses in the full operation scenario S2 (0–1800s) in the CS and PF coils. P_{HN} are the hysterisis losses due to normal magnetic field, P_{CN} are the coupling losses due to normal magnetic field, and $P_{TO} = P_{HN} + P_{CN}$ are the total losses.

Coil	P_{HN} [W]	P_{CN} [W]	P_{TO} [W]
CS3U	353.5	85.0	438.6
CS2U	303.9	124.7	428.6
CS1U	292.8	170.7	463.5
CS1L	293.2	173.1	466.3
CS2L	281.4	128.4	409.8
CS3L	300.5	65.3	365.8
Total CS	1825.3	747.2	2572.5
PF1	247.3	45.9	293.2
PF2	26.0	27.6	53.6
PF3	62.0	27.1	89.1
PF4	45.2	24.7	69.9
PF5	103.2	76.3	179.5
PF6	439.1	90.7	529.8
Total PF	922.7	292.3	1215.0

Table 8: Summary of AC losses in the full operation scenario S2 (0–1800s) in the TF coils. P_{HN} are the hysterisis losses due to normal magnetic field, P_{HP} are the hysterisis losses due to parallel magnetic field, P_{CN} are the coupling losses due to normal magnetic field, P_{CP} are the coupling losses due to normal magnetic field, and $P_{TO} = P_{HP} + P_{CP} + P_{HN} + P_{CN}$ are the total losses.

Coil	P_{HN} [W]	P_{HP} [W]	P_{CN} [W]	P_{CP} [W]	P_{TO} [W]
TF1	10.4	9.4	1.7	2.3	23.8
Total TF	187.1	169.3	30.4	41.7	428.4

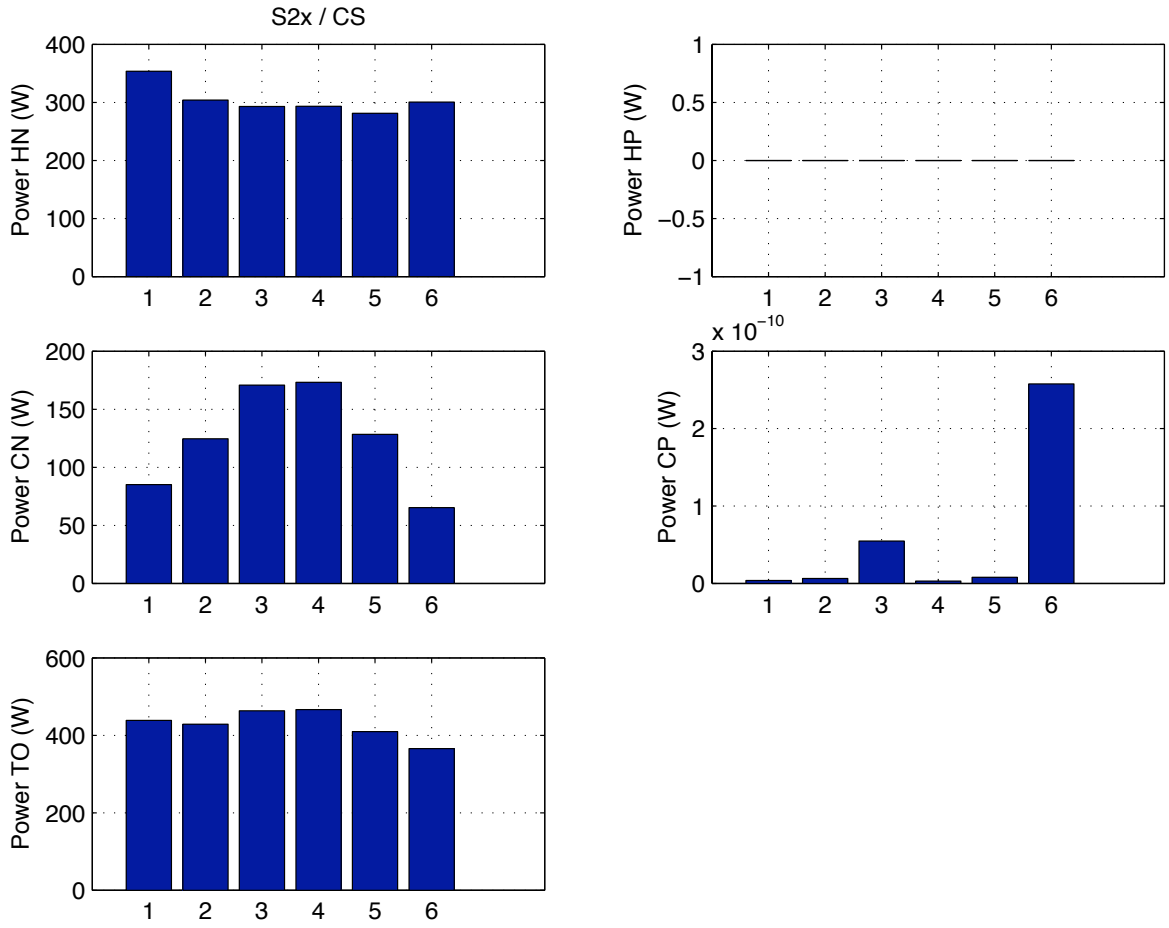

Figure 35: Operation scenario S2. Summary of AC losses at the end of the full scenario in the CS coils.

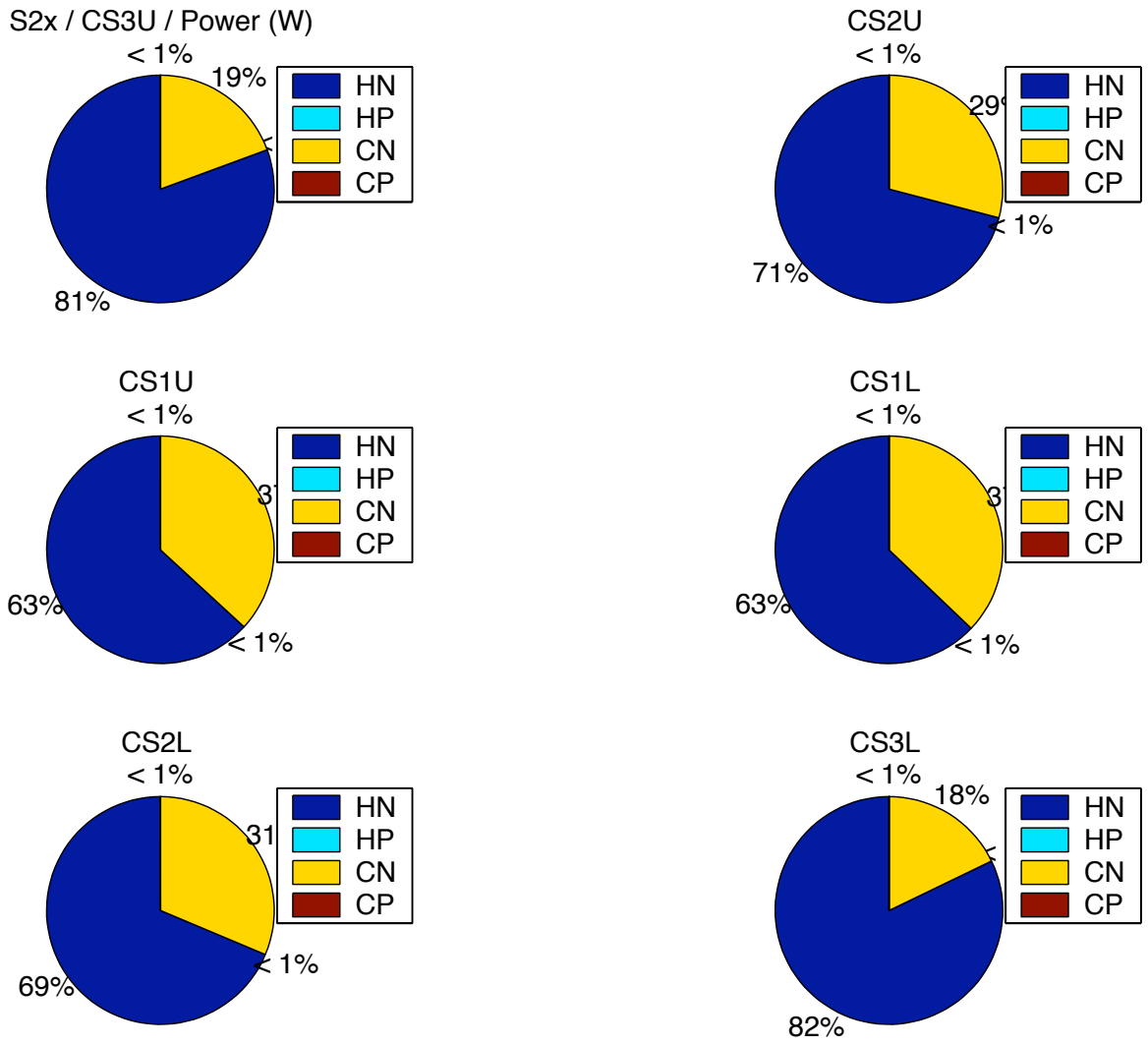

Figure 36: Operation scenario S2. Contributions to the total AC losses (power) at the end of the full scenario, in the CS coils.

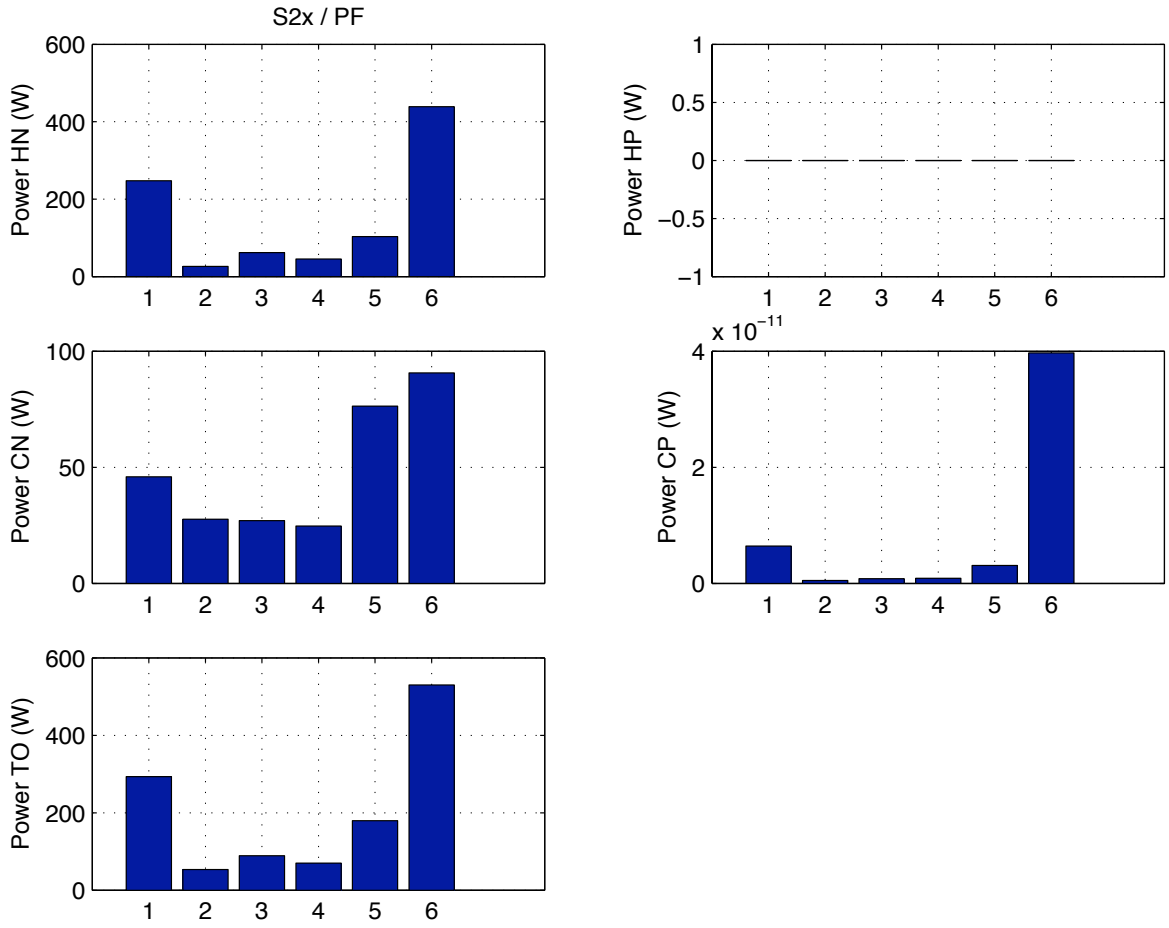

Figure 37: Operation scenario S2. Summary of AC losses at the end of the full scenario in the PF coils.

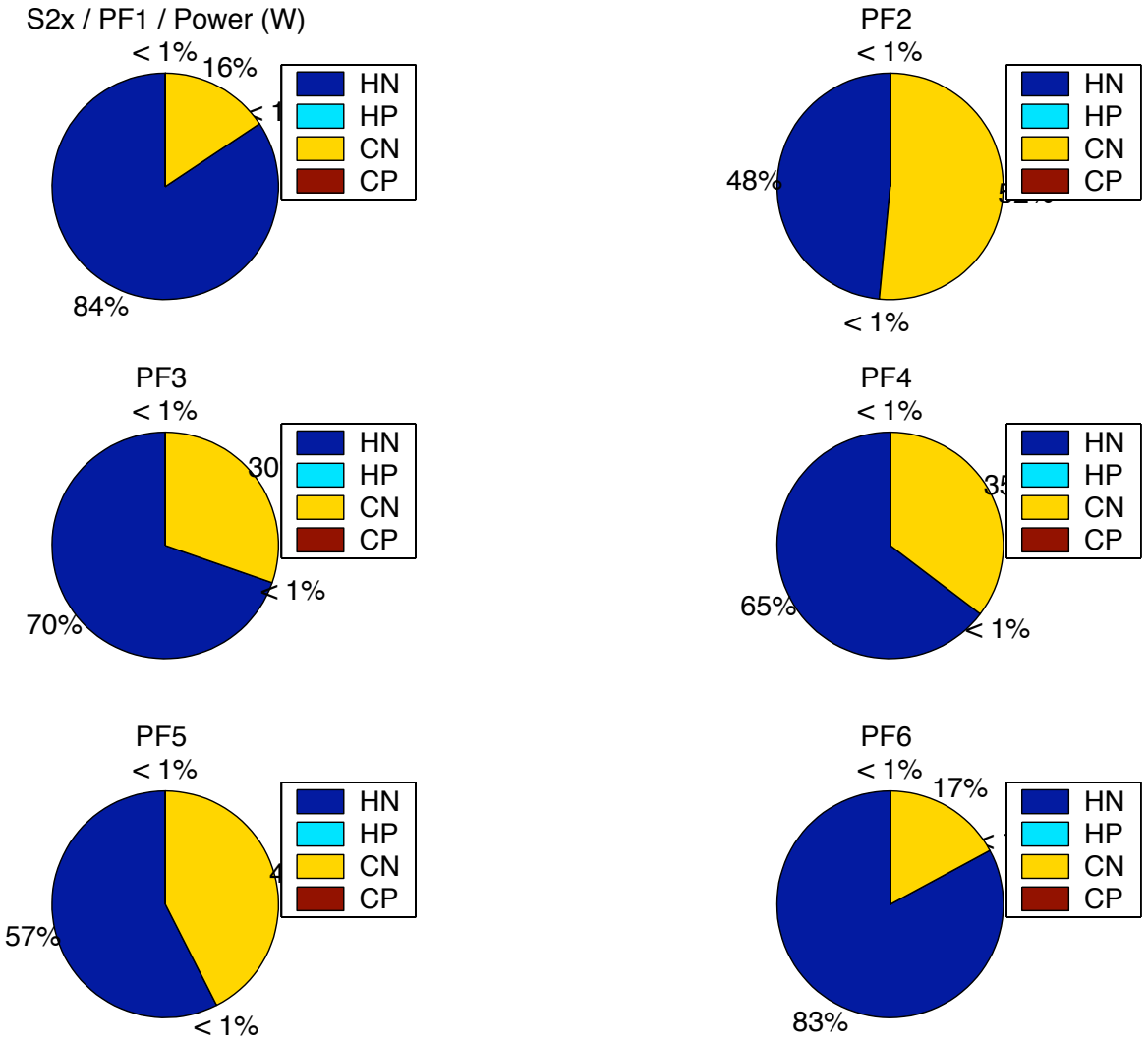

Figure 38: Operation scenario S2. Contributions to the total AC losses (power) at the end of the full scenario, in the PF coils.

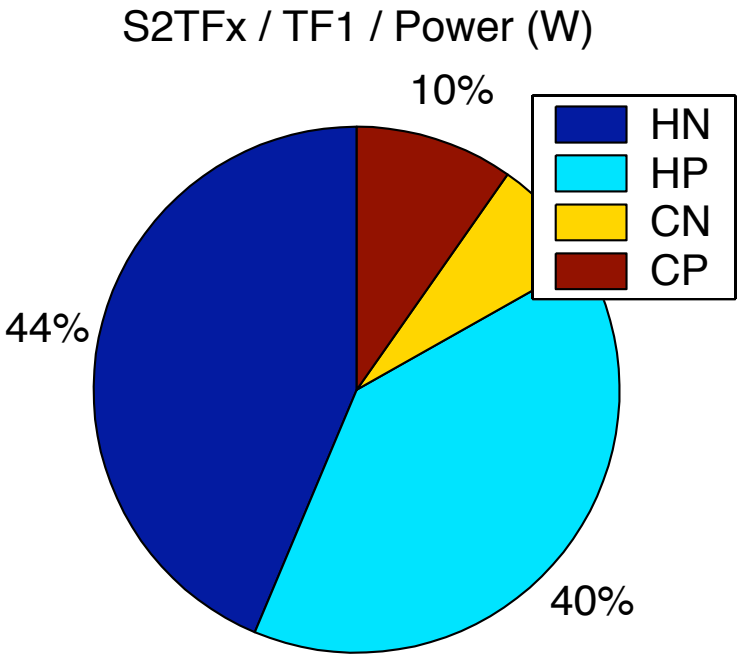

Figure 39: Operation scenario S2TF. Contributions to the total AC losses (power) at the end of the full scenario, in the TF1 coil.

5 AC losses in the control scenario 'Noise at SOB'

As done for the analysis of the operation scenario S2, the AC losses in the control scenarios 'Noise at SOB' have been calculated in two steps, i.e. using the AXIS ON option to assess the losses in the CS and PF coils, and using the AXIS OFF option to assess the losses in the TF coils. A discussion of this approach is given in Section 7.

The AC losses have been calculated using the vertical stabilization VS1 (SOBVS1) and VS2 (SOBVS2), from t=0s to the end of the scenario (t=140s). The moving plasma has been used in all cases. In the axis symmetric model the losses due to parallel field (HP and CP) are zero.

5.1 Vertical stabilization VS1

5.1.1 Losses in the CS and PF coils

The total AC losses are 56 W in the CS coils and 254 W in the PF coils, as summarized in Table 9. The losses are higher in CS3U, CS2L and CS3L (Fig. 40) and the dominant contributions are the HN losses (Fig. 41). In the PF coils the higher AC losses are in PF2 (Fig. 42) and the dominant contributions are the CN losses in all coils except PF1 and PF6 (Fig. 43).

The standard electronic documentation contains:

1. Coil model, time history in the time interval 130s–140s of the maximum magnetic field, of the average AC losses and of the maximum AC losses, as well as contour plots of at time 130s, 135s and 140s of the module of magnetic field and of AC losses. The observed distribution of the AC losses in the coil cross sections has been used to select the pancakes to analyze in detail. These data are in the file `SOBVS1MP1/SOBVS1MP1.ps` (total of 94 pages).
2. Distribution of the total AC losses along the length of the coil at 10 times equally spaced in the interval 130s –140s in three pancakes, i.e. two on both sides of the coil and one at the center of the coil. There are a total of 36 files in the folder `SOBVS1MP1/matlab` (file name: `ACmod_coilname_pancake.eps`).
3. Coil model and time history of all contribution of the losses in the time interval 0s–140s, in the file `SOBVS1MP1x/SOBVS1MP1x.ps`.

5.1.2 Losses in the TF coils

The total losses in the TF coils, i.e. 18 times the losses in TF1, are 70 W (Table 10), with CP (63 %) as the dominant component (Fig. 44).

The standard electronic documentation of this case, with details in the CS, PF and TF coils, can be found in the folders `SOBVS1MPTF` and `SOBVS1MPTFx`.

5.2 Vertical stabilization VS2

5.2.1 Losses in the CS and PF coils

Although the total AC losses in all CS and PF coils are approximately the same in the scenarios SOBVS2 and SOBVS1, i.e. 262 W and 310 W respectively, the contributions of the two coil groups is different, as listed in Table 11. In particular, in all CS coils the losses are 144.7 W with SOBVS2 and 55.9 W with SOBVS1, whereas in all PF coils the losses are 117.2 W (SOBVS2) and 254.4 W (SOBVS1).

The ratio of all losses VS2/VS1 in all coils is shown in Fig. 45. Compared with the currents in the two scenarios (Fig. 46 for CS, Fig. 47 for PF) these results show that (a) in all PF coils the losses are closely dependent on the magnetic field variation ΔB, i.e hinting at the fact that the dominating mechanism is driven by the hysteresis losses, and (b) the same is true in all CS coils except CS2U and CS1U where the losses show a dependence on ΔB^2, i.e. hinting at the fact that the dominating mechanism is driven by the coupling losses.

The standard electronic documentation of this case, with details in the CS and PF coils, can be found in the folders `SOBVS2MP1` and `SOBVS2MP1x`.

5.2.2 Losses in the TF coils

The total losses in the TF coils, i.e. 18 times the losses in TF1, are 58.1 W (Table 12), $\approx$ 15 % less than in scenario SOBVS1. The dominant component is given by the CP losses (58 %) as (Fig. 48).

The standard electronic documentation of this case, with details in the CS, PF and TF coils, can be found in the folders `SOBVS2MPTF` and `SOBVS2MPTFx`.

5.3 Comparison between vertical stabilization VS1 and VS2

We report in Fig. 49 a summary of the overall results of the two simulations SOBVS1 and SOBVS2. The bars represent the total loss, split among each of the three main coil systems, and further subdivided in the different mechanism (coupling and hysteresis). Loads are reported as average power during the time simulated, 10 s. The calculation provides a quick means to qualify the controller scenarios in terms of the cryogenic load, as we see a clear distinction in the loss at the level of the CS and PF system. We note further that the contribution of the two loss mechanisms in the CS and PF coil systems is massively different in the two scenarios. This is due to the combined effect of the different current amplitudes as well as the different dynamic characteristics of the current waveforms in the CS and PF coils, affecting both hysteresis and coupling loss. Interestingly enough, the situation on the TF coil (close to the plasma) is essentially unaffected by the control scenario, as we should have expected.

Table 9: Summary of AC losses in the control scenario SOBVS1 in the CS and PF coils. P_{HN} are the hysterisis losses due to normal magnetic field, P_{CN} are the coupling losses due to normal magnetic field, and $P_{TO} = P_{HN} + P_{CN}$ are the total losses.

Coil	P_{HN} [W]	P_{CN} [W]	P_{TO} [W]
CS3U	12.6	1.8	14.4
CS2U	4.8	3.3	8.1
CS1U	1.7	1.4	3.2
CS1L	4.0	1.2	5.2
CS2L	9.9	3.3	13.2
CS3L	9.7	2.2	11.9
Total CS	42.8	13.1	55.9
PF1	7.1	4.1	11.2
PF2	8.7	122.5	131.2
PF3	3.6	22.2	25.7
PF4	3.3	32.2	35.4
PF5	5.8	34.2	40.1
PF6	7.2	3.5	10.7
Total PF	35.7	218.6	254.4

Table 10: Summary of AC losses in the control scenario SOBVS1 in the TF coils. P_{HN} are the hysterisis losses due to normal magnetic field, P_{HP} are the hysterisis losses due to parallel magnetic field, P_{CN} are the coupling losses due to normal magnetic field, P_{CP} are the coupling losses due to normal magnetic field, and $P_{TO} = P_{HP} + P_{CP} + P_{HN} + P_{CN}$ are the total losses.

Coil	P_{HN} [W]	P_{HP} [W]	P_{CN} [W]	P_{CP} [W]	P_{TO} [W]
TF1	0.4	0.5	0.5	2.4	3.9
Total TF	6.8	9.6	9.5	44.1	70.0

Table 11: Summary of AC losses in the control scenario SOBVS2 in the CS and PF coils. P_{HN} are the hysterisis losses due to normal magnetic field, P_{CN} are the coupling losses due to normal magnetic field, and $P_{TO} = P_{HN} + P_{CN}$ are the total losses.

Coil	P_{HN} [W]	P_{CN} [W]	P_{TO} [W]
CS3U	26.0	6.9	32.9
CS2U	13.6	23.1	36.7
CS1U	4.7	6.4	11.1
CS1L	5.5	5.6	11.1
CS2L	13.6	20.6	34.3
CS3L	11.7	7.0	18.7
Total CS	75.1	69.6	144.7
PF1	4.8	1.3	6.0
PF2	3.5	50.4	53.9
PF3	3.0	11.1	14.1
PF4	2.6	13.6	16.2
PF5	4.3	15.5	19.8
PF6	5.7	1.5	7.2
Total PF	23.9	93.3	117.2

Table 12: Summary of AC losses in the control scenario SOBVS2 in the TF coils. P_{HN} are the hysterisis losses due to normal magnetic field, P_{HP} are the hysterisis losses due to parallel magnetic field, P_{CN} are the coupling losses due to normal magnetic field, P_{CP} are the coupling losses due to normal magnetic field, and $P_{TO} = P_{HP} + P_{CP} + P_{HN} + P_{CN}$ are the total losses.

Coil	P_{HN} [W]	P_{HP} [W]	P_{CN} [W]	P_{CP} [W]	P_{TO} [W]
TF1	0.4	0.5	0.4	1.9	3.2
Total TF	7.4	9.3	7.8	33.7	58.1

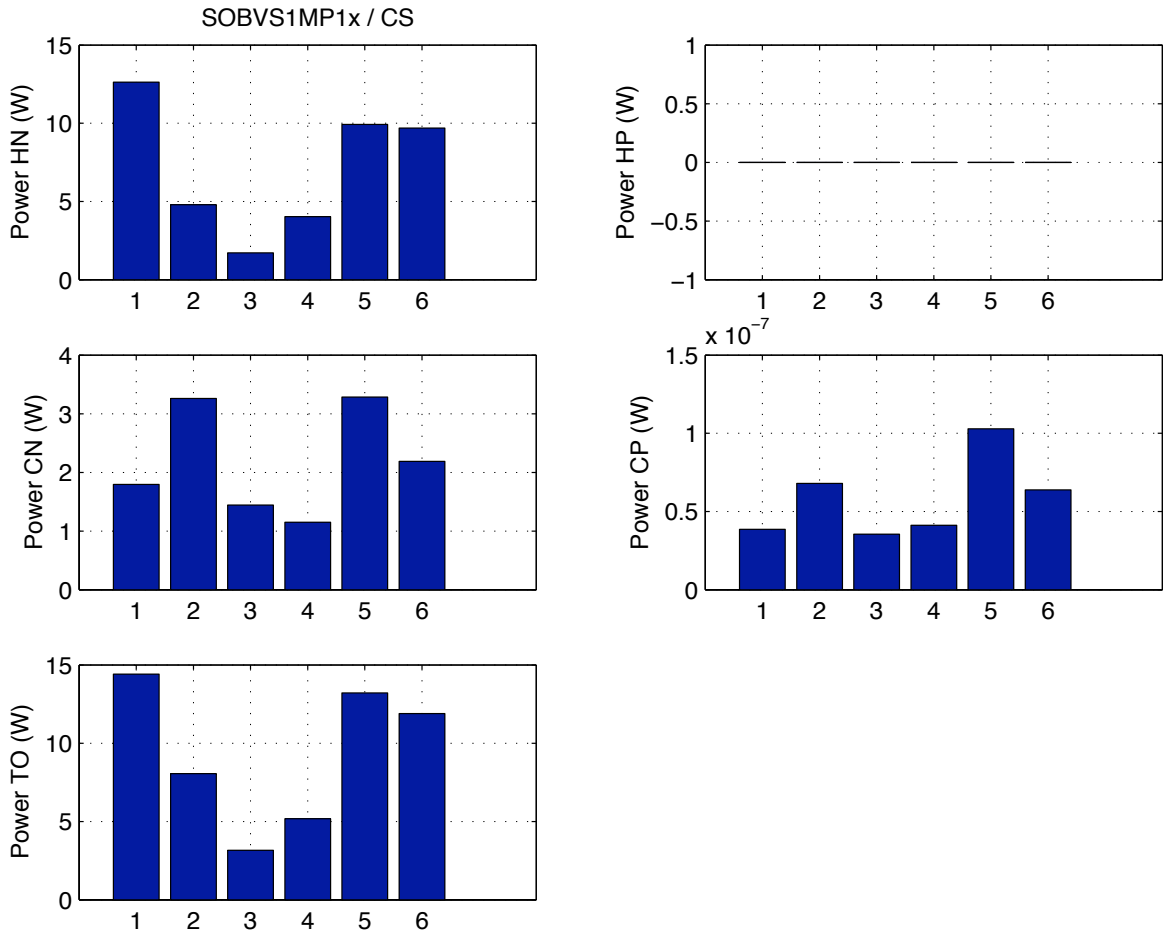

Figure 40: Control scenario SOBVS1. Summary of AC losses at the end of the scenario in the CS coils.

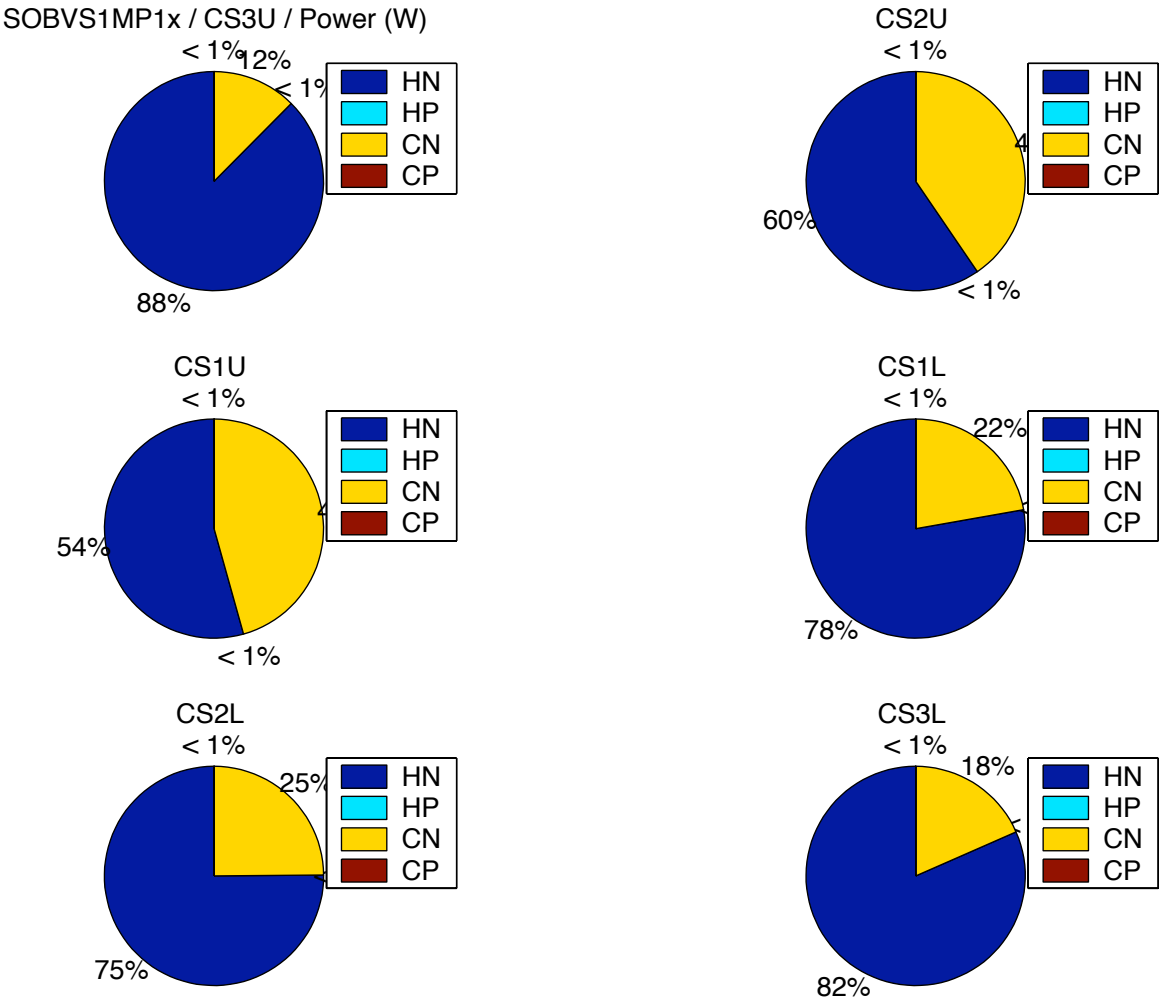

Figure 41: Control scenario SOBVS1. Contributions to the total AC losses (power) at the end of the scenario, in the CS coils.

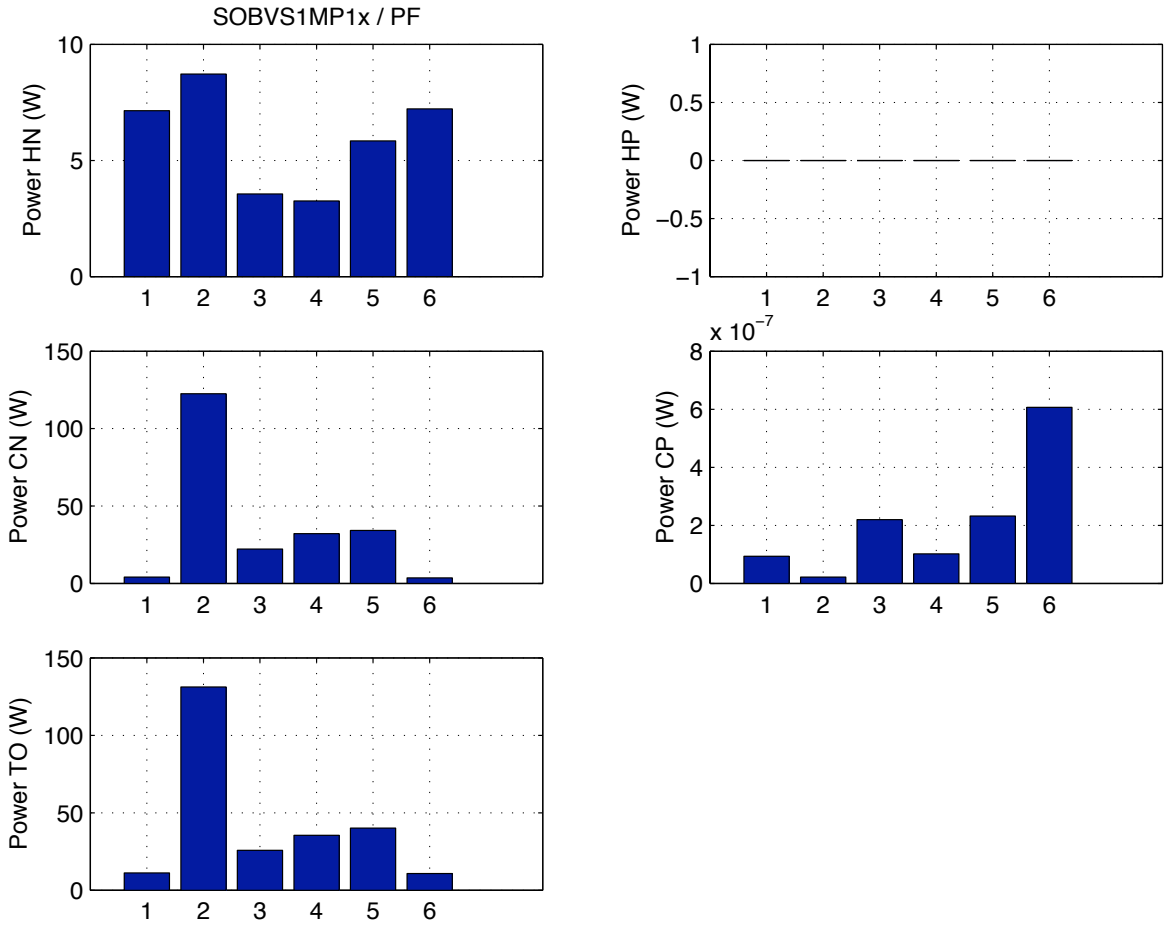

Figure 42: Control scenario SOBVS1. Summary of AC losses at the end of the scenario in the PF coils.

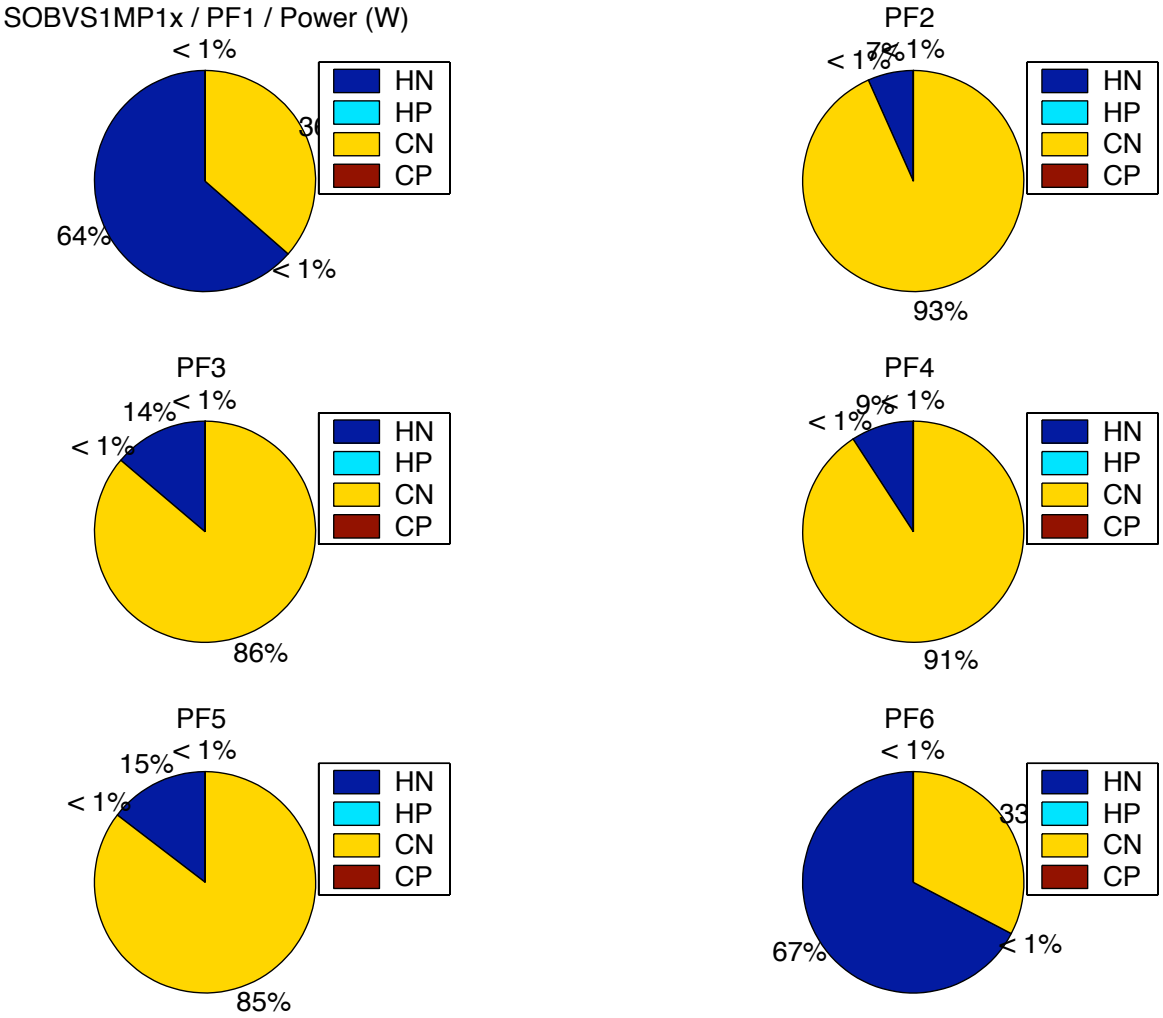

Figure 43: Control scenario SOBVS1. Contributions to the total AC losses (power) at the end of the scenario, in the PF coils.

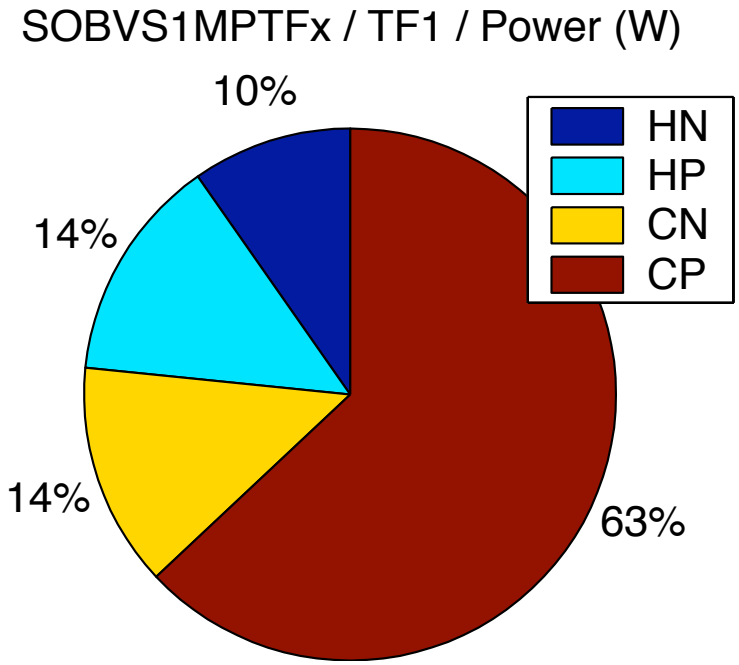

Figure 44: Control scenario SOBVS1. Contributions to the total AC losses (power) at the end of the scenario, in the TF1 coil.

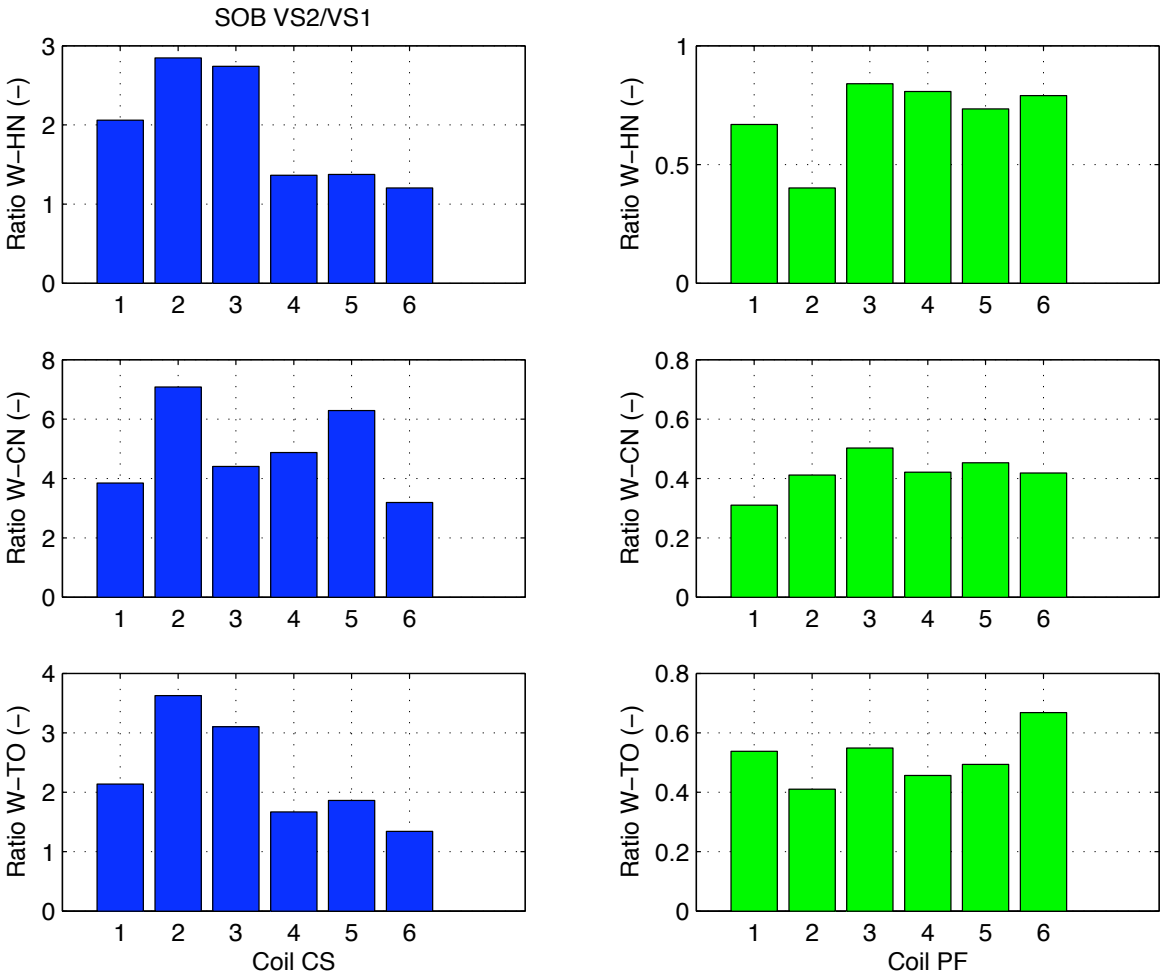

Figure 45: Ratio of the AC losses (power) SOBVS2/SOBVS1 at the end of the scenarios, in the CS coils (blue) and the PF coils (green).

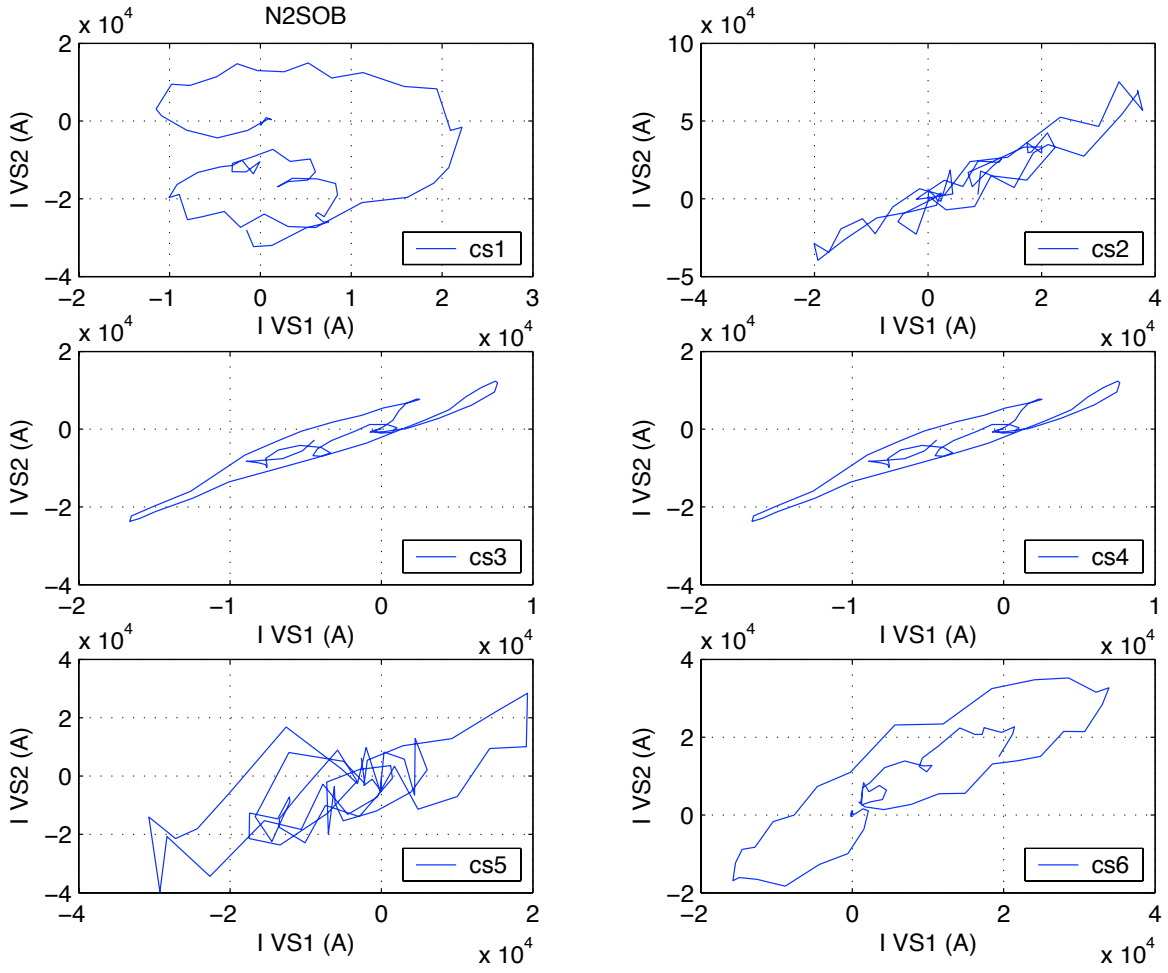

Figure 46: Currents in the CS coils, in the control scenarios SOBVS1 and SOBVS2.

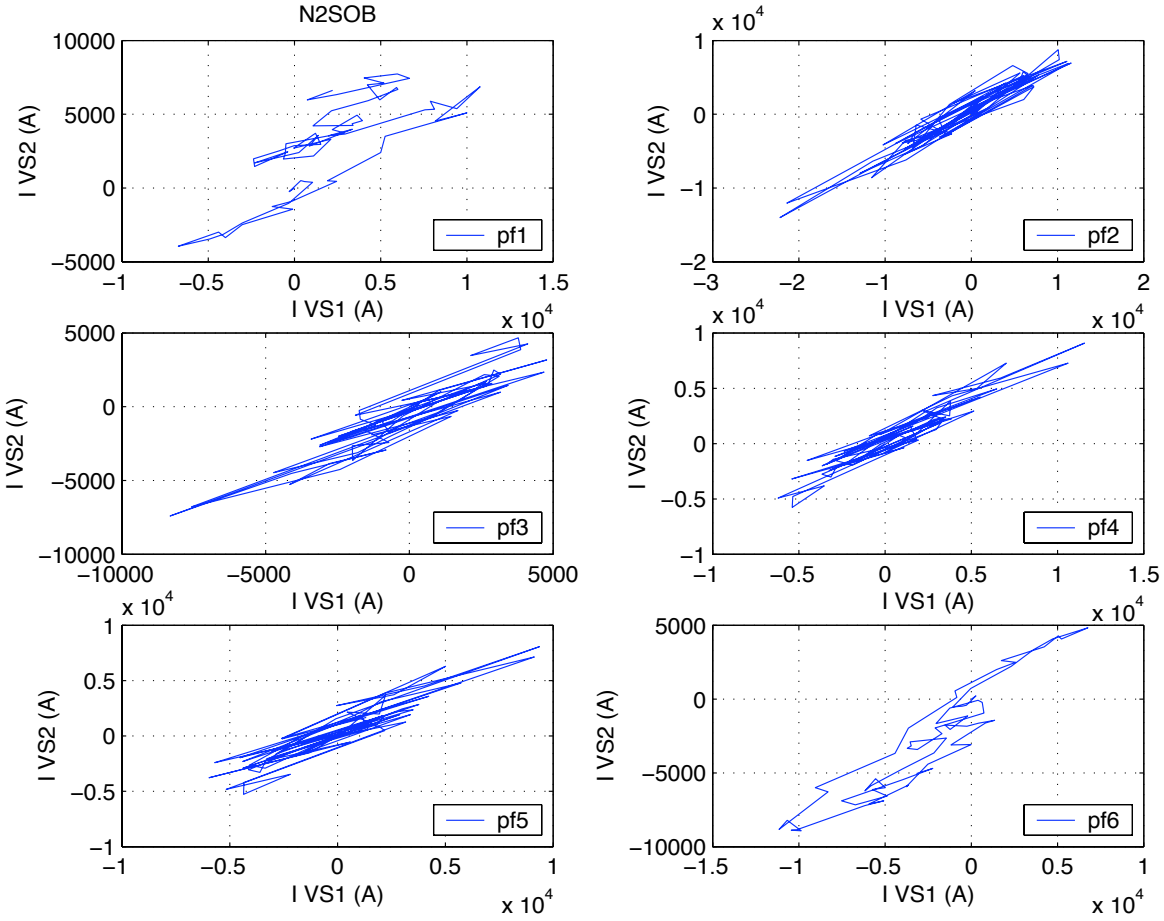

Figure 47: Currents in the PF coils, in the control scenarios SOBVS1 and SOBVS2.

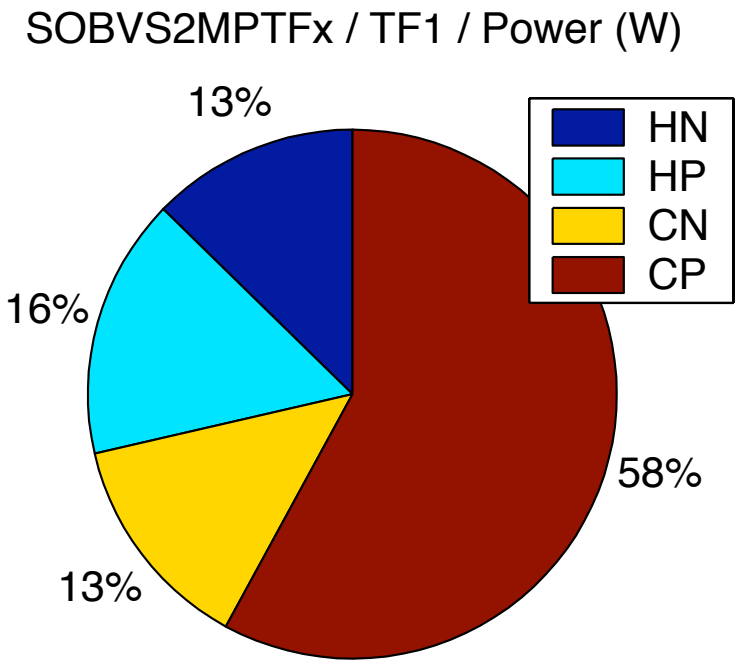

Figure 48: Control scenario SOBVS2. Contributions to the total AC losses (power) at the end of the scenario, in the TF1 coil.

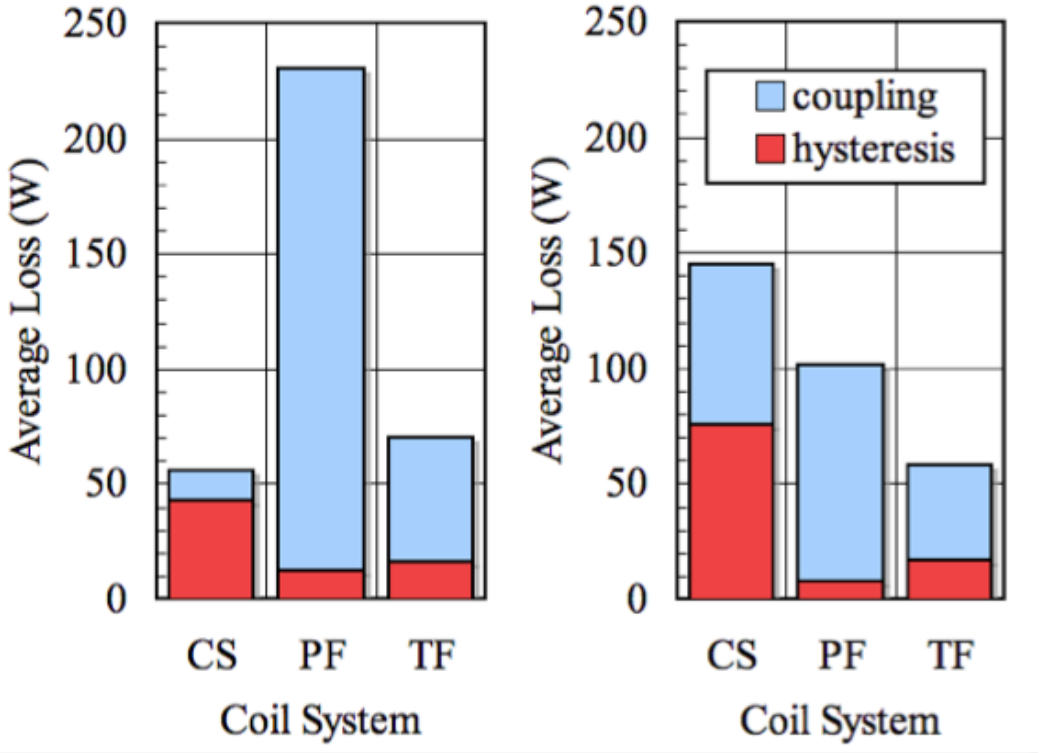

Figure 49: Average AC loss power computed for the vertical stabilization scenario SOBVS1 (left) and SOBVS2 (right) at SOB.

6 AC losses in the control scenario 'Minor disruption at EOC'

The AC losses in the control scenarios 'Minor disruption at EOC' have been computed in two steps, i.e. using the AXIS ON option to assess the losses in the CS and PF coils, and using the AXIS OFF option to assess the losses in the TF coils. A discussion of this approach is given in Section 7.

The AC losses have been calculated using the vertical stabilization VS1 (EOCVS1) and VS2 (EOCVS2), from t=590s to the end of the scenario (t=600s). The moving plasma has been used in all cases. In the axis symmetric model the losses due to parallel field (HP and CP) are zero.

6.1 Vertical stabilization VS1

6.1.1 Losses in the CS and PF coils

The total AC losses are ≈6.2 KW in the CS coils and ≈ 2.6 KW in the PF coils, as summarized in Table 13. The losses are by far higher in CS3L (Fig. 51) and the individual contributions to the losses are shown in Fig. 50. In the PF coils the higher AC losses are in PF2 and PF6 (Fig. 52) and the dominant contributions are: the CN losses in PF1, PF3 and PF6, the HN losses in PF2 and PF4 (Fig. 53).

The standard electronic documentation contains:

1. Coil model, time history in the time interval 590s–600s of the maximum magnetic field, of the average AC losses and of the maximum AC losses, as well as contour plots of at time 590s, 595s and 600s of the module of magnetic field and of AC losses. The observed distribution of the AC losses in the coil cross sections has been used to select the pancakes to analyze in detail. The data are in the file `EOCVS1MP1/EOCVS1MP1.ps` (total of 94 pages).

2. Distribution of the total AC losses along the length of the coil at 10 times equally spaced in the interval 590s –600s in three pancakes, i.e. two on both sides of the coil and one at the center of the coil. There are a total of 36 files in the folder `EOCVS1MP1/matlab` (file name: `ACmod_coilname_pancake.eps`).

3. Coil model and time history of all contribution of the losses in the time interval 590s–600s, in the file `EOCVS1MP1x/EOCVS1MP1x.ps`.

6.1.2 Losses in the TF coils

The total losses in the TF coils, i.e. 18 times the losses in TF1, are ≈ 1.6 KW(Table 14), with HN (36 %) as the dominant component (Fig. 54).

The standard electronic documentation of this case, with details in the CS, PF and TF coils, can be found in the folders `EOCVS1MPTF` and `EOCVS1MPTFx`.

6.2 Vertical stabilization VS2

6.2.1 Losses in the CS and PF coils

The total AC losses in all the CS and PF coils are considerably different in the scenarios EOCVS2 and EOCVS, i.e. $\approx$ 11.4 KW and $\approx$ 8.9 KW respectively. The contributions of the two coil groups are also very different, as listed in Table 15. In particular, in all CS coils the losses are $\approx$ 11.5 KW with EOCVS2 and $\approx$6.2 KW with EOCVS1. In all PF coils the losses are $\approx$ 1.8 KW (EOCVS2) and $\approx$ 2.6 KW (EOCVS1).

The ratio of all losses VS2/VS1 in all coils is shown in Fig. 55. Compared with the currents in the two scenarios (Fig. 46 for CS, Fig. 47 for PF) these results show that (a) in all PF coils the losses are closely dependent on the magnetic field variation ΔB, i.e hinting at the fact that the dominating mechanism is driven by the hysteresis losses, and (b) the same is true in all coils CS coils except CS2U and CS1U where the losses show a dependence on ΔB^2, i.e. hinting hinting at the fact that the dominating mechanism is driven by the coupling losses.

The standard electronic documentation of this case, with details in the CS and PF coils, can be found in the folders `EOCVS2MP1` and `EOCVS2MP1x`.

6.2.2 Losses in the TF coils

The total losses in the TF coils, i.e. 18 times the losses in TF1, are $\approx$ 2.0 KW (Table 16), $\approx$ 25 % more than in scenario EOCVS1. The dominant component is given by the HN losses (35 %) as (Fig. 58).

The standard electronic documentation of this case, with details in the CS, PF and TF coils, can be found in the folders `EOCVS2MPTF` and `EOCVS2MPTFx`.

Table 13: Summary of AC losses in the control scenario EOCVS1 in the CS and PC coils. P_{HN} are the hysterisis losses due to normal magnetic field, P_{CN} are the coupling losses due to normal magnetic field, and $P_{TO} = P_{HN} + P_{CN}$ are the total losses.

Coil	P_{HN} [W]	P_{CN} [W]	P_{TO} [W]
CS3U	781.0	220.6	1001.6
CS2U	390.4	706.0	1096.4
CS1U	216.3	253.7	470.1
CS1L	148.7	113.4	262.1
CS2L	373.9	371.5	745.4
CS3L	1471.4	1170.6	2642.0
Total CS	3381.6	2835.9	6217.5
PF1	266.5	45.9	312.4
PF2	150.4	443.5	593.8
PF3	248.5	175.3	423.8
PF4	94.7	152.5	247.2
PF5	215.6	198.7	414.3
PF6	494.6	175.1	669.7
Total PF	1470.4	1190.9	2661.3

Table 14: Summary of AC losses in the control scenario EOCVS1 in the TF coils. P_{HN} are the hysterisis losses due to normal magnetic field, P_{HP} are the hysterisis losses due to parallel magnetic field, P_{CN} are the coupling losses due to normal magnetic field, P_{CP} are the coupling losses due to normal magnetic field, and $P_{TO} = P_{HP} + P_{CP} + P_{HN} + P_{CN}$ are the total losses.

Coil	P_{HN} [W]	P_{HP} [W]	P_{CN} [W]	P_{CP} [W]	P_{TO} [W]
TF1	32.7	23.0	13.3	22.1	91.1
Total TF	589.5	414.3	239.0	397.1	1639.9

Table 15: Summary of AC losses in the control scenario EOCVS2 in the CS and PF coils. P_{HN} are the hysterisis losses due to normal magnetic field, P_{CN} are the coupling losses due to normal magnetic field, and $P_{TO} = P_{HN} + P_{CN}$ are the total losses.

Coil	P_{HN} [W]	P_{CN} [W]	P_{TO} [W]
CS3U	747.5	712.8	1460.2
CS2U	792.4	1559.5	2352.0
CS1U	393.1	396.2	789.3
CS1L	211.1	133.7	344.8
CS2L	554.3	594.4	1148.7
CS3L	2097.7	1460.7	3558.5
Total CS	4796.2	4857.3	9653.5
PF1	574.6	90.8	665.3
PF2	80.4	127.0	207.4
PF3	159.4	104.3	263.7
PF4	117.9	92.3	210.2
PF5	142.7	91.9	234.6
PF6	193.4	61.6	255.0
Total PF	1268.4	567.9	1836.2

Table 16: Summary of AC losses in the control scenario EOCVS2 in the TF coils. P_{HN} are the hysterisis losses due to normal magnetic field, P_{HP} are the hysterisis losses due to parallel magnetic field, P_{CN} are the coupling losses due to normal magnetic field, P_{CP} are the coupling losses due to normal magnetic field, and $P_{TO} = P_{HP} + P_{CP} + P_{HN} + P_{CN}$ are the total losses.

Coil	P_{HN} [W]	P_{HP} [W]	P_{CN} [W]	P_{CP} [W]	P_{TO} [W]
TF1	39.3	27.0	20.3	24.4	111.0
Total TF	708.2	485.1	366.1	438.4	1997.8

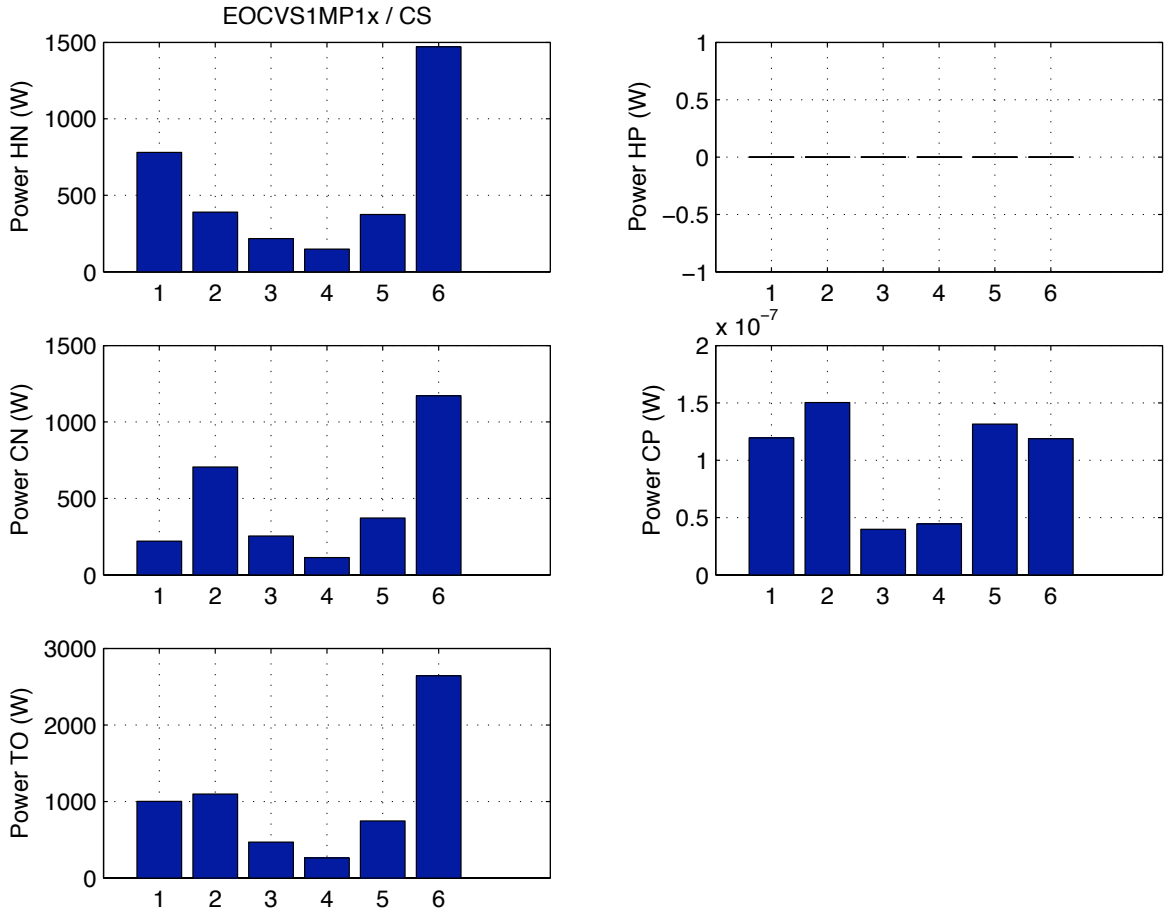

Figure 50: Control scenario EOCVS1. Summary of AC losses at the end of the scenario in the CS coils.

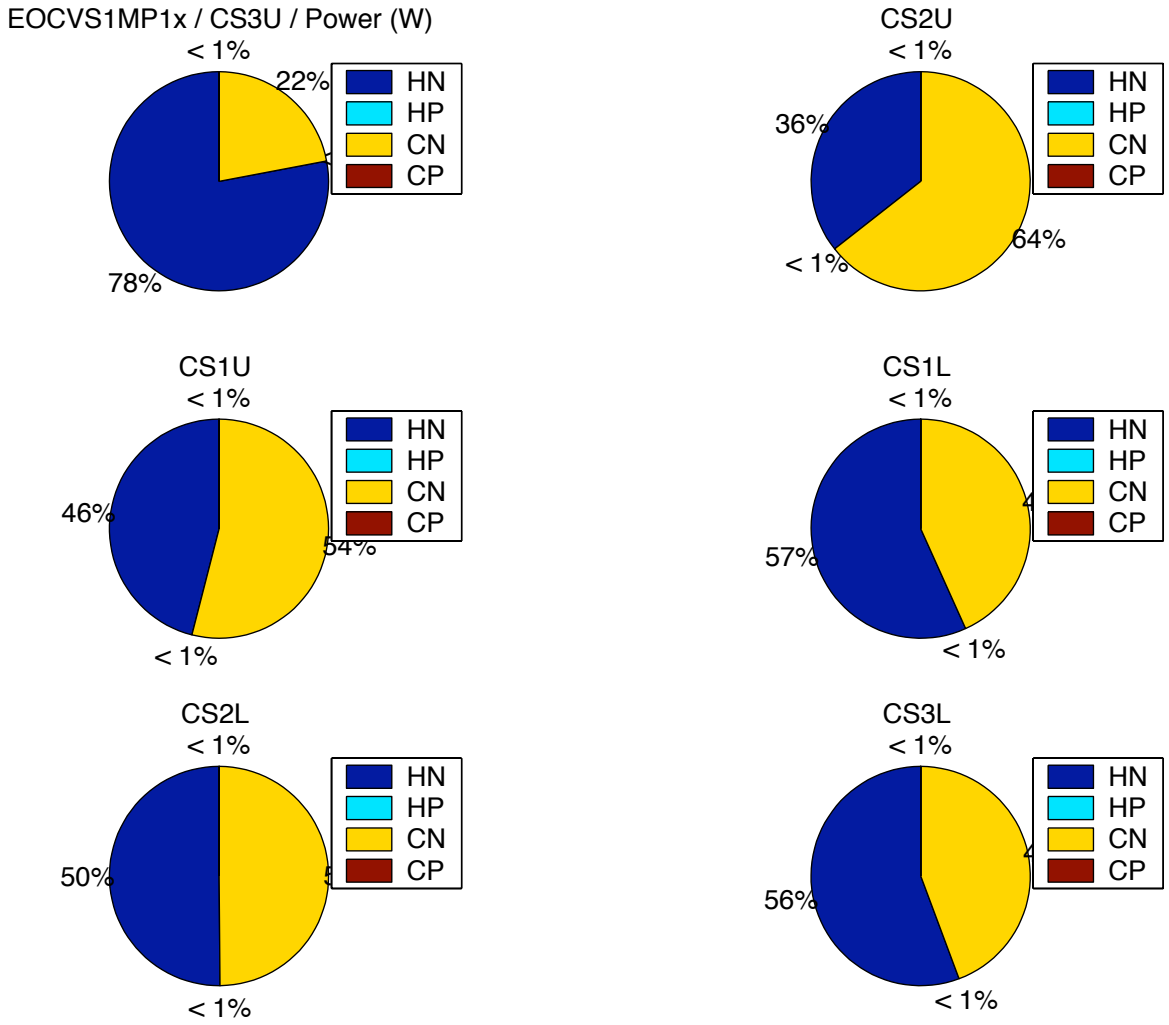

Figure 51: Control scenario EOCVS1. Contributions to the total AC losses (power) at the end of the scenario, in the CS coils.

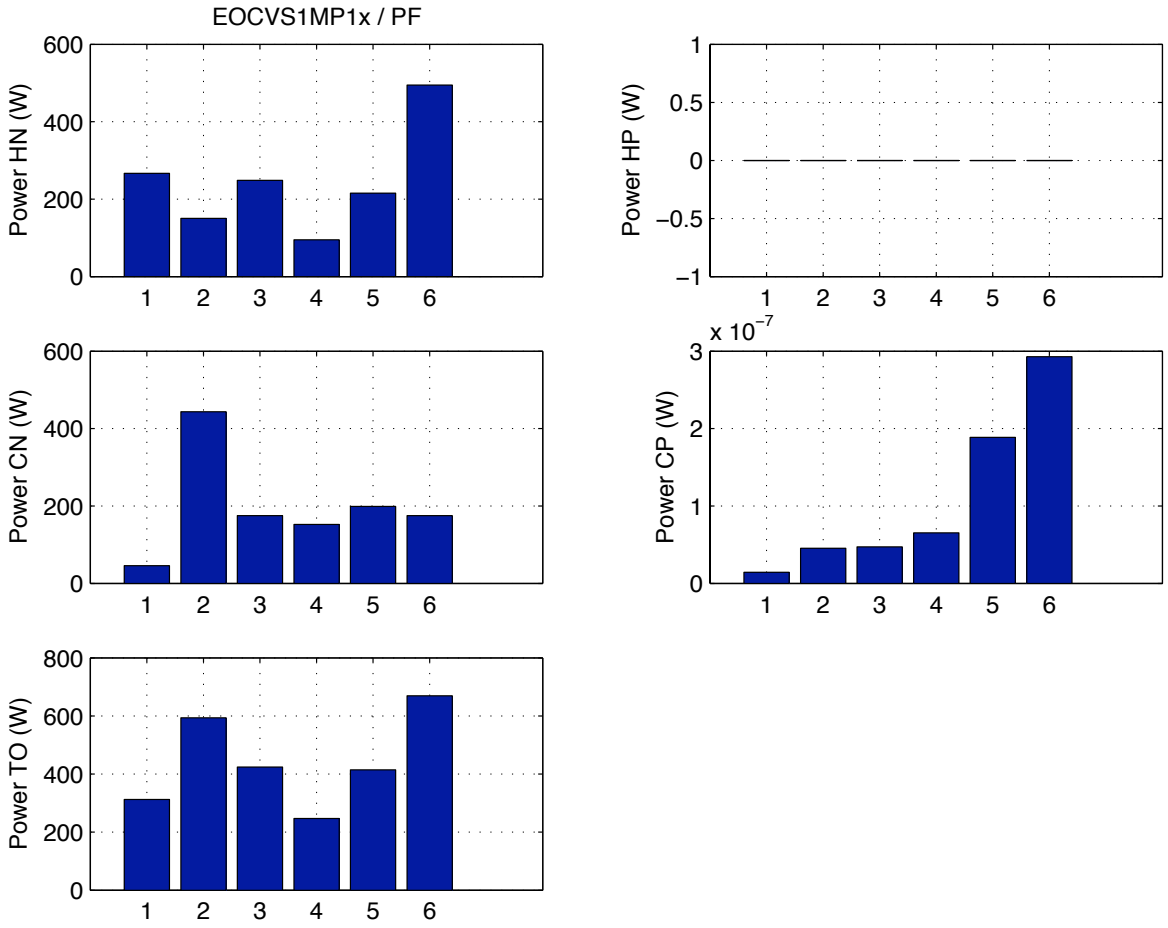

Figure 52: Control scenario EOCVS1. Summary of AC losses at the end of the scenario in the PF coils.

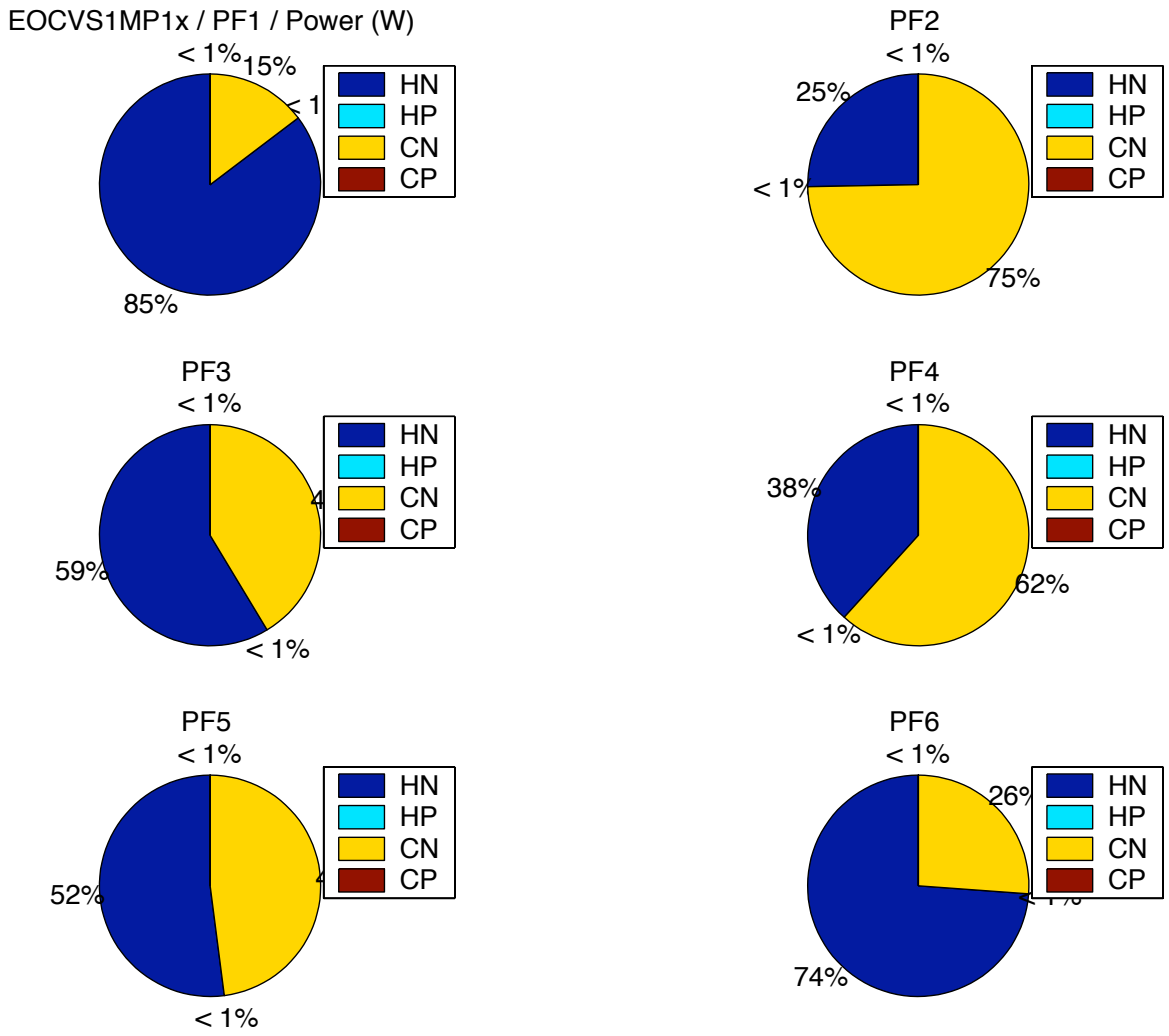

Figure 53: Control scenario EOCVS1. Contributions to the total AC losses (power) at the end of the scenario, in the PF coils.

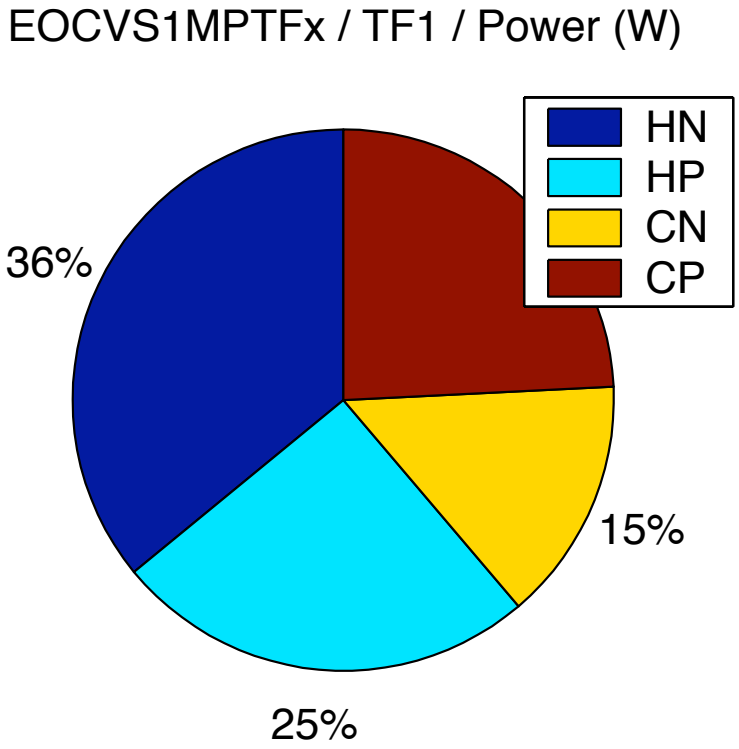

Figure 54: Control scenario EOCVS1. Contributions to the total AC losses (power) at the end of the scenario, in the TF1 coil.

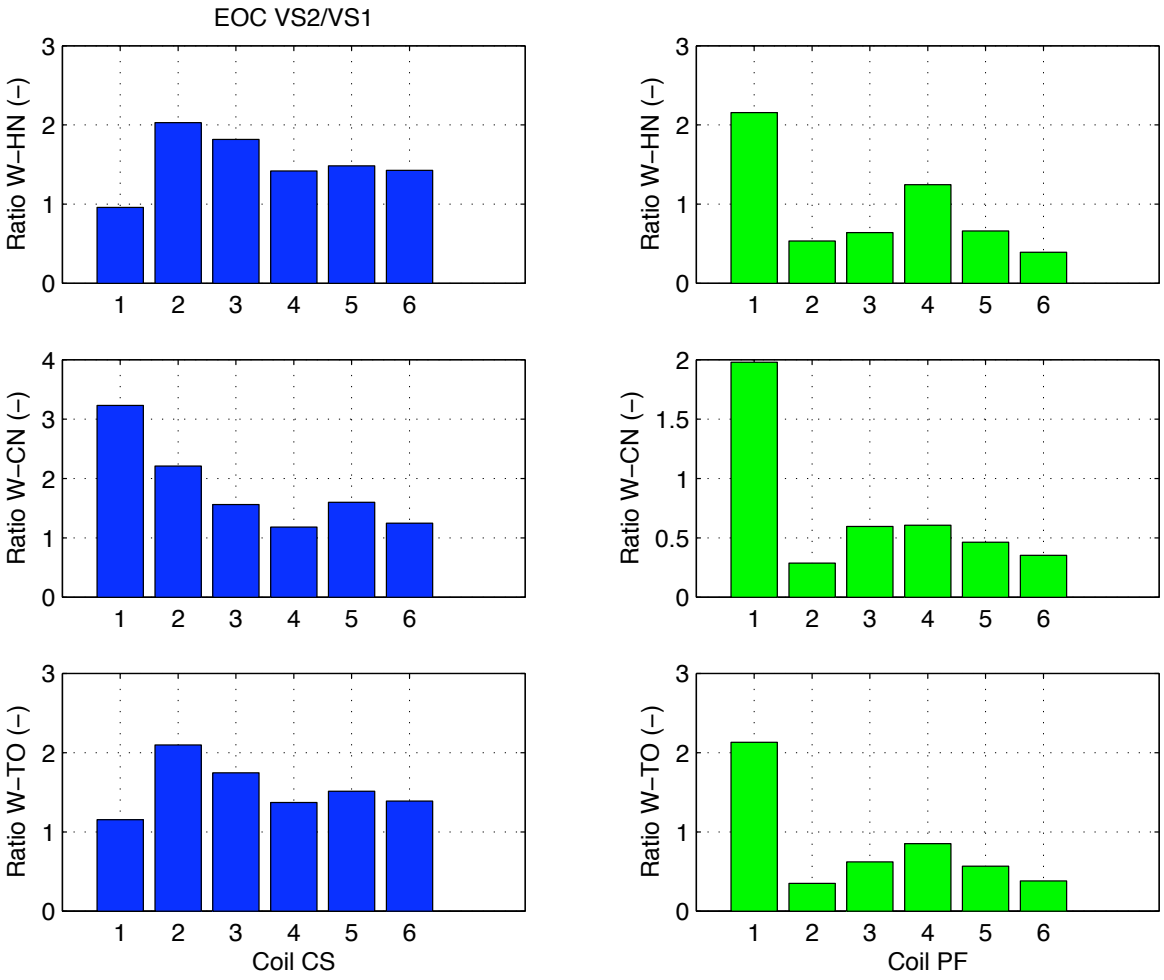

Figure 55: Ratio of the AC losses (power) EOCVS2/EOCVS1 at the end of the scenarios, in the CS coils (blue) and the PF coils (green).

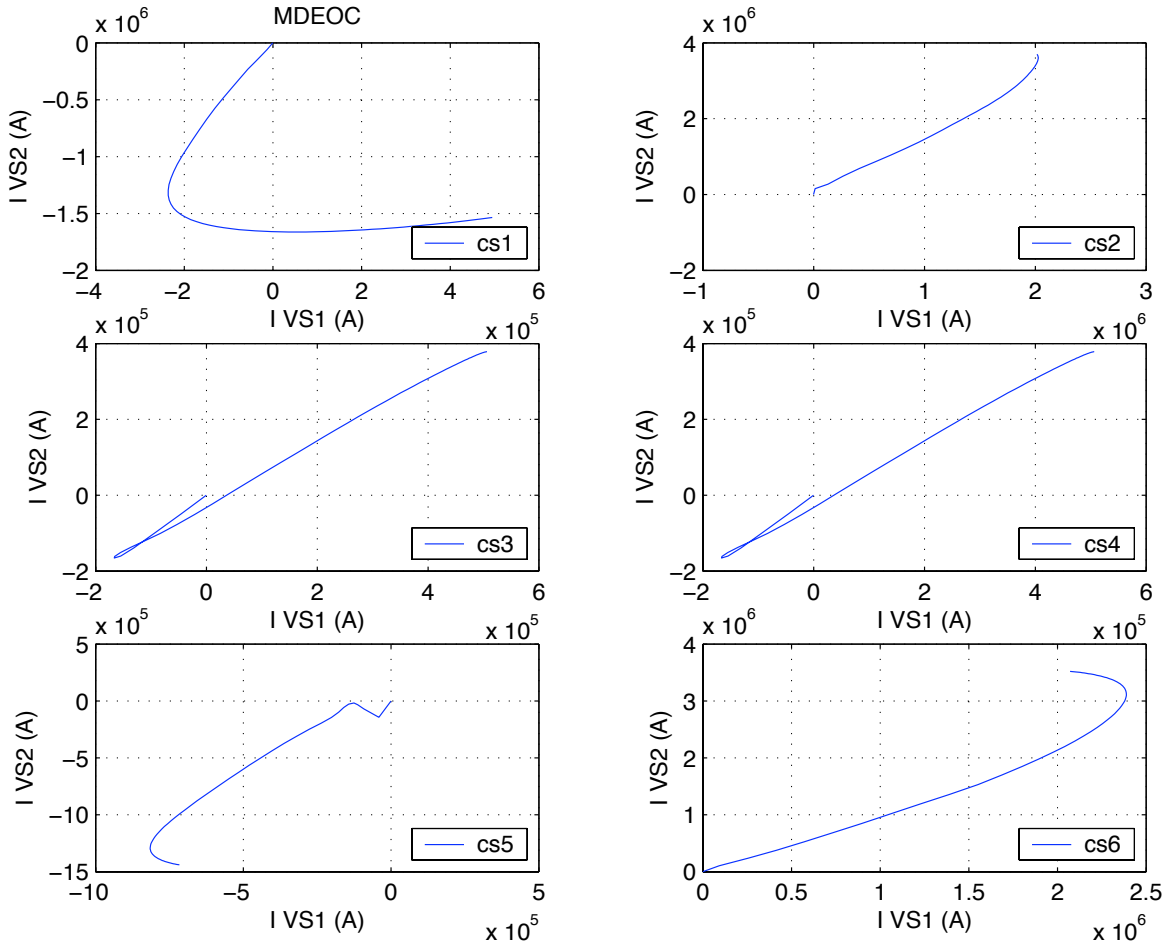

Figure 56: Currents in the CS coils, in the control scenarios EOCVS1 and EOCVS2.

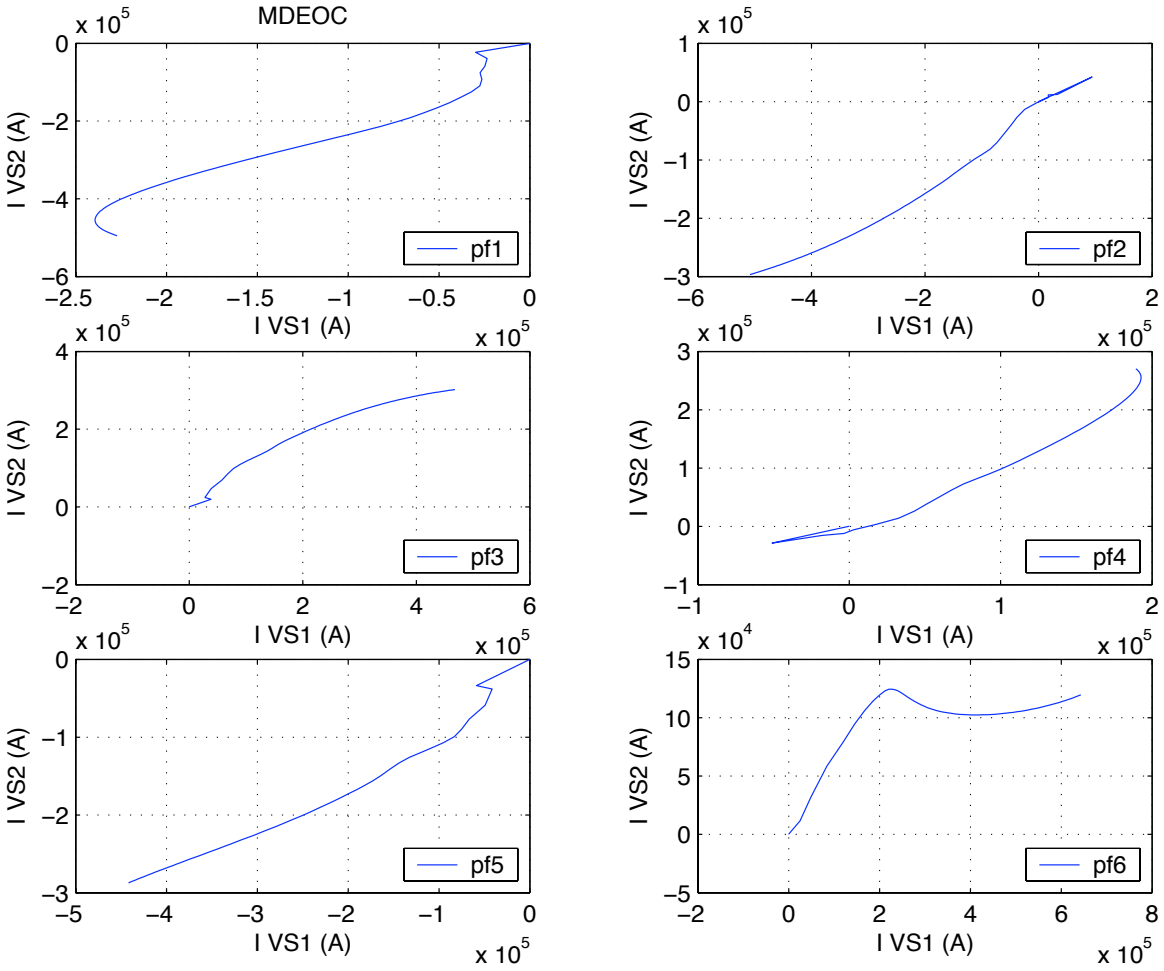

Figure 57: Currents in the PF coils, in the control scenarios EOCVS1 and EOCVS2.

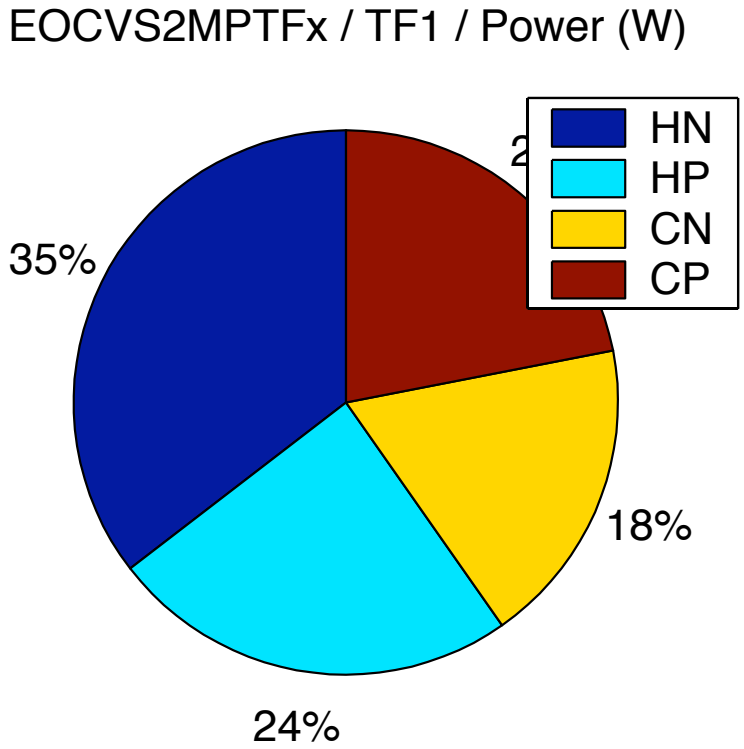

Figure 58: Control scenario EOCVS2. Contributions to the total AC losses (power) at the end of the scenario, in the TF1 coil.

7 AC losses in special cases

7.1 Effect of TF coil

The AC losses in the CS and PF coils are practically the same if the TF coils are included (non axis symmetric case) or not included (axis symmetric case) in the M'C model, as shown for example by the comparison in the SOBVS1 control scenario (Fig. 59). These comparison were confirmed in other control scenarios investigated (e.g. EOCVS1). Therefore the axis symmetric option was selected to obtain all the results in CS and PF coils reported in the previous Sections[3]. In this way a considerable reduction of the CPU time could be achieved without a loss of accuracy.

7.2 Moving and static plasma

The difference of AC losses in the CS and PF coils when using the moving plasma model instead of the static plasma model is not negligible as shown for example by the comparison in the SOBVS1 control scenario (Fig. 60). Therefore the moving plasma model was used to obtain all the results in CS and PF coils reported in the previous Sections, with practically no penalty for the CPU time.

7.3 Effect of passive coils

The difference of AC losses in the CS and PF coils when including or neglecting the passive coils is also not negligible, as shown for example by the comparison in the SOBVS1 control scenario (Fig. 61). Therefore the passive coils were included in the model to obtain all the results in CS and PF coils reported in the previous Sections. Again, this option has practically no influence on the total CPU time.

7.4 Sensitivity study

We have performed sensitivity studies on the effect of a change in the loss parameters, of the conductors, e.g. time constant and effective filament diameter.

7.4.1 Time constants

Figure 62 shows in particular the effect of a parametric change of the time constant τ by a factor 1/5 to 5 (i.e. from 5 ms to 125 ms) on the coupling loss in scenario SOBVS1. Three values of time constants were investigated: 25 ms (nominal case), 5 ms (case t1) and 125 ms (case t2). As a side remark, this range of variation is representative for the spread measured

[3]The TF coils were obviously included to calculate the AC losses in these coils.

on the large-scale ITER cables. The scaling of the coupling loss in the CS coil system is approximately linear, which indicates negligible shielding in the range of time constants explored for the specific scenario analyzed (low frequency regime). In the PF coil system, on the other hand, we clearly see the effect of shielding at high values of τ, which results in a coupling loss significantly smaller than would be expected by the low-frequency regime, linear extrapolation. These results are discussed in detail in Appendix A.

7.4.2 Effective filament diameter

Three values of effective filament diameter of the Nb3Sn conductors: 30 μm (nominal case), 15 μm (case d1) and 60 μm (case d2). The results are discussed in detail in Appendix A.

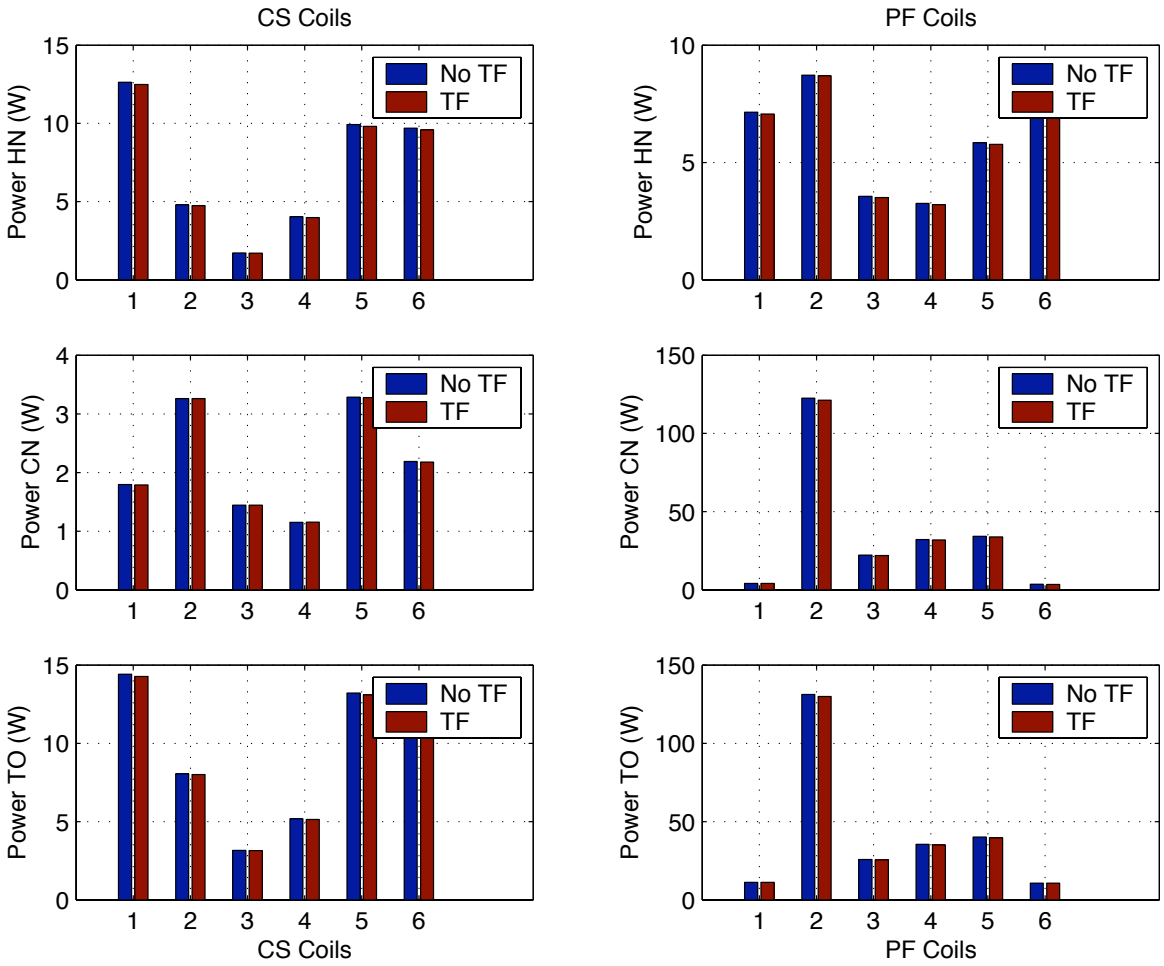

Figure 59: Comparison between AC losses power in the CS (left) and PF (right) coils: without TF (No TF) coils and with TF coils.

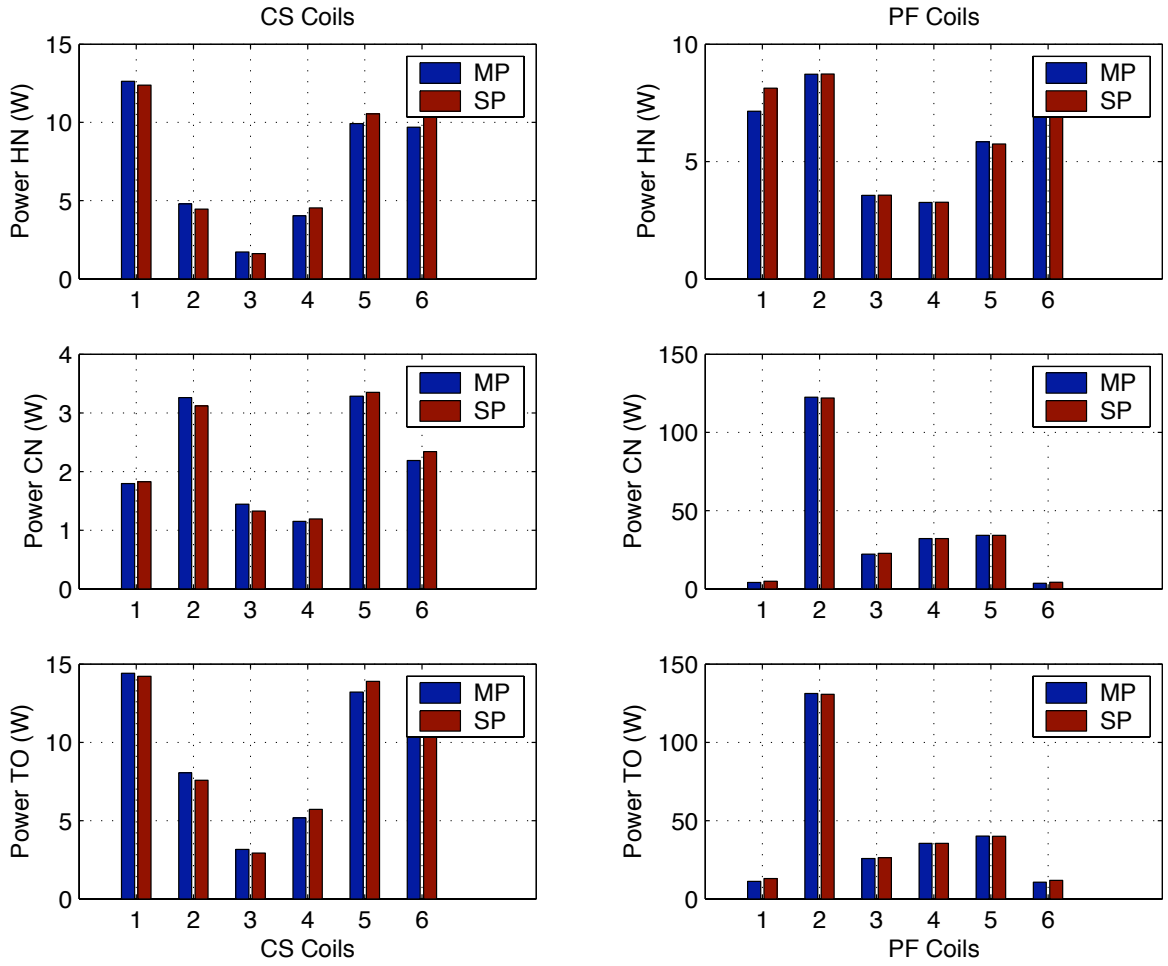

Figure 60: Comparison between AC losses power in the CS (left) and PF (right) coils: using moving (MP) and static (SP) plasma.

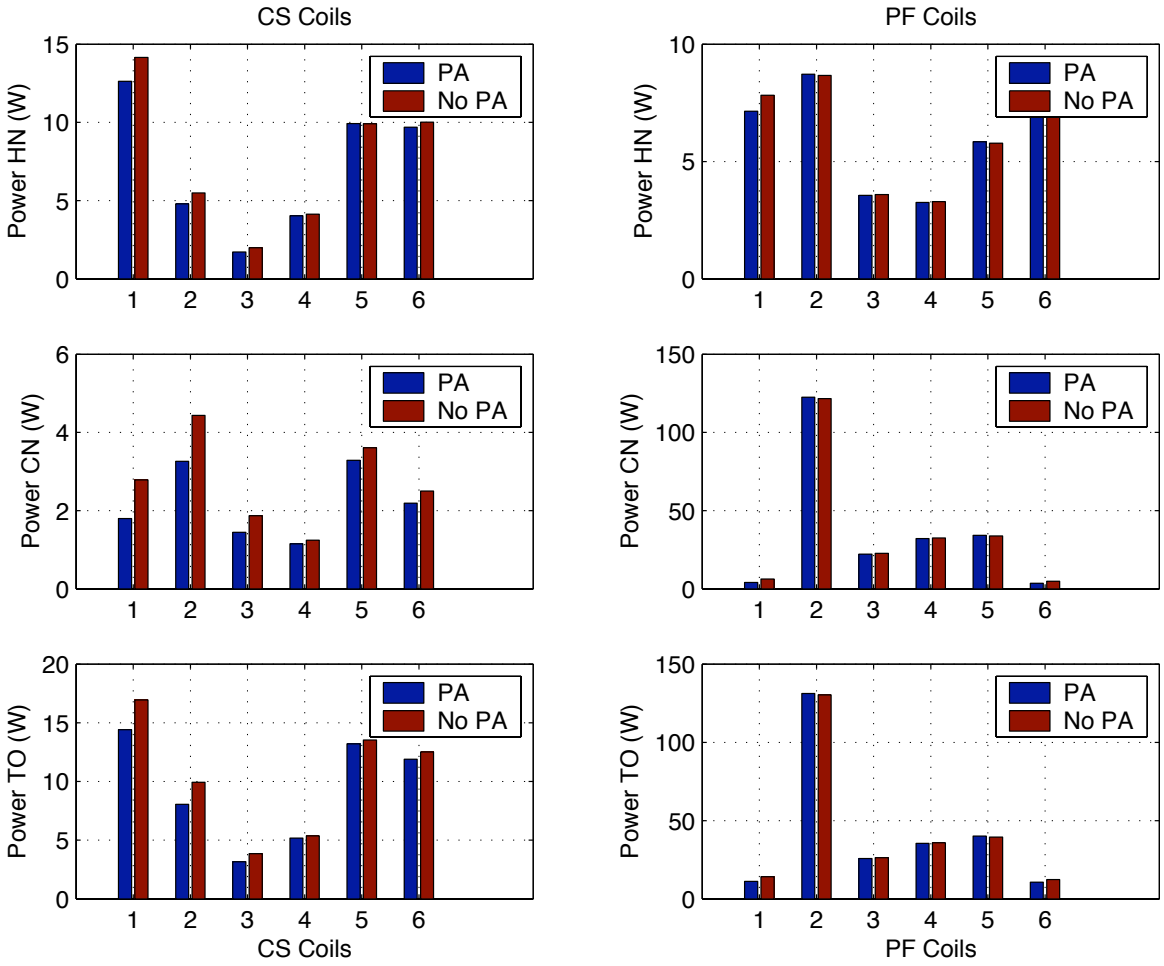

Figure 61: Comparison between AC losses power in the CS (left) and PF (right) coils: without passive coils (No PA) and with passive coils (PA).

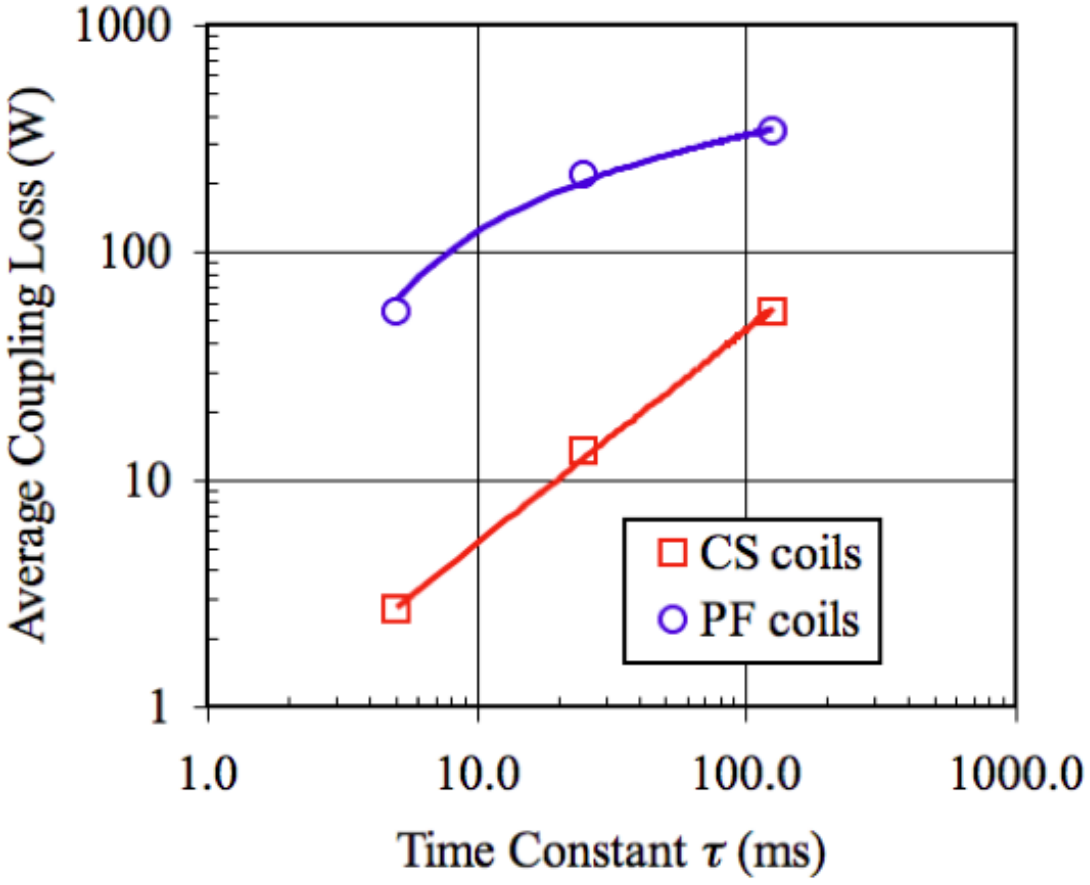

Figure 62: Sensitivity study: effect of time constant on coupling current loss in the CS and PF coil system during the SOBVS1 scenario.

8 Summary

Magnetic field and AC losses in the ITER CS, PF and TF coils have been calculated with the CryoSoft code M'C using an axis symmetric and a non axis symmetric model. In particular:

- The M'C code is suitable to accurately calculate the 3D magnetic field.
- The M'C code is suitable to calculate the AC losses in the complex ITER 3D configuration, i.e. 75 coils for the axis symmetric case and 93 coils for the non axis symmetric case. The losses in the CS and PF coils in the operation scenario S2 and in the control scenarios SOBVS1, SOBVS2, EOCVS1 and EOCVS2 are summarized in Table 17 and Fig. 63.
- The losses are in agreement with the losses calculated with a different code [4].
- The calculation method for AC losses in pulsed superconducting magnets is suitable over a wide regime of field changes (from partial to full penetration) and frequencies (from the low frequency limit to shielding). The examples reported, i.e. vertical control scenarios in ITER, provides a measure of the flexibility in dealing with complex geometric and powering conditions.

The ultimate goal of the above work was to introduce the model in the control optimization algorithm, which is presently based on plasma and electrical circuit parameters, thus allowing an integrated system design. Although the calculation has been proven to be stable and feasible in reasonable times (several scenarios were analysed with parametric variations of cable characteristics), the size and complexity of the model developed in the task TW5-TPO-ACLOSS is such that it does not allow an easy integration into the design procedure for the plasma control algorithm. We hence propose to proceed with the work, defining a simplified, fast, parametric AC loss calculation algorithm whose size allows integration in the control design procedure. The parameters will be adjusted based on numerical simulations to be performed using the detailed model now available.

$\mathcal{CM}$

First compiled: 17th July 2006
Last modified: 30th September 2006

Typeset by LaTeX

Table 17: Summary of total AC losses [W] in the CS, PF and TF coils in the operation scenario S2 and in 4 control scenarios investigated.

Scenario Coil	S2	SOBVS1	SOBVS2	EOBVS1	EOBVS2
CS3U	438.6	14.4	32.9	1001.6	1460.1
CS2U	428.6	18.1	36.7	1096.4	2352.0
CS1U	463.5	3.2	11.1	470.1	789.3
CS1L	466.3	5.2	11.1	262.1	344.8
CS2L	409.8	13.2	34.3	745.4	1148.7
CS3L	365.8	11.9	18.7	2642.0	3558.5
Total CS	2572,5	55.9	144.7	6217.5	9653.5
PF1	293.2	11.2	6.0	312.4	665.3
PF2	53.6	131.2	53.9	593.8	207.4
PF3	89.1	25.7	14.1	423.8	263.7
PF4	69.9	35.4	16.2	247.2	210.2
PF5	179.5	40.1	19.8	414.3	234.6
PF6	529.8	10.7	7.2	669.7	255.0
Total PF	1215.0	254.4	117.2	2661.3	1836.2
TF1	23.8	3.9	3.2	91.1	111.0
Total TF	428.4	70.0	58.1	1639.9	1997.8

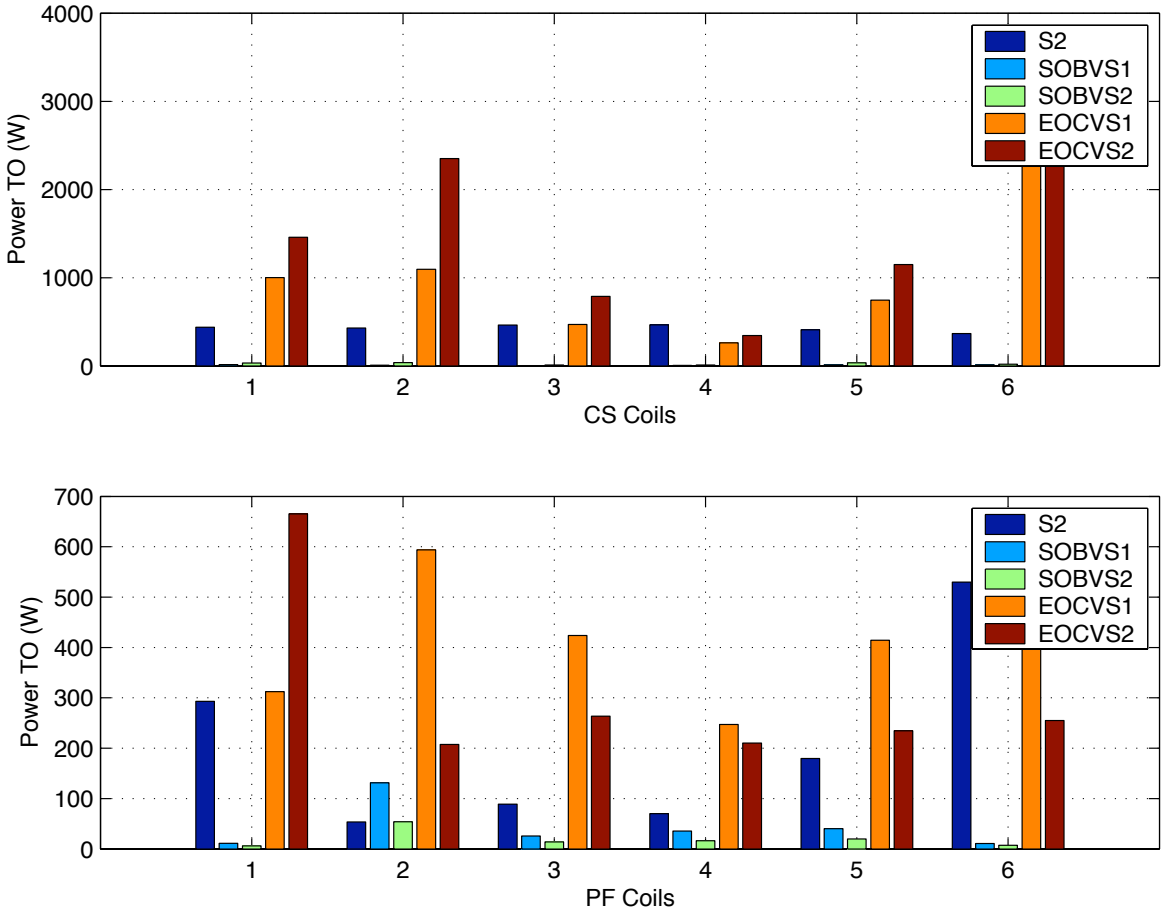

Figure 63: Summary of total AC losses power in CS (top) and PF (bottom) coils in the operation scenario S2 and in 4 control scenarios.

References

[1] L. Bottura, P. Bruzzone, J.B. Lister, C. Marinucci, A. Portone ″Computations of AC losses in the ITER magnets during fast field transients″, Submitted for publication in IEEE Trans. on Applied Superconductivity, 2007

[2] L. Bottura, C. Rosso ″AC loss calculation algorithm″, CryoSoft Report CRYO/97/001, 1997

[3] ″M'C. Magnetic field, inductance, vector potential, energy, forces and AC loss analysis in a 3-D superconducting coil system of arbitrary shape″, CryoSoft Manual, Version 2.7, June 2006

[4] ″ITER Design Description Document. Magnet Section 1: Engineering description″, N11 DDD 178 04-06-04 R 0.4, 2004.

[5] A. Portone (EFDA), Private communication, 2006.

[6] A. Kavin, ″Input for the AC losses study: Control actions of CS and PF coils″, ITER Rep. ITER–D–22JYAK v1.1, ? Courtesy of EFDA.

List of Tables

List of Figures

Appendix A

L. Bottura, P. Bruzzone, J.B. Lister, C. Marinucci, A. Portone, ″Computations of AC losses in the ITER magnets during fast field transients″, Submitted for publication in IEEE Trans. on Applied Superconductivity, 2007 (Presented at the ASC-2006 Conference in Seattle, USA).

Computations of AC Losses in the ITER Magnets During Fast Field Transients

Luca Bottura, Pierluigi Bruzzone, Jonathan B. Lister, Claudio Marinucci, Alfredo Portone

***Abstract*—The calculation of AC losses due to the control currents in ITER is a cumbersome task. The reason is that control transients require small field changes (0.1 T or less) at moderate frequency (up to 10 Hz), where effects of partial penetration of the filaments and shielding are important and need to be taken into account to produce sound AC loss estimates. In this paper we describe models developed for AC loss calculation, in particular hysteresis and coupling current losses, that are suitable for the above regime. Both hysteresis and coupling loss models are adapted to the conductor analyzed through few parameters (the effective filament diameter and time constants) that can be derived from measurement of loss on short samples. We report an example of calculations of AC loss in the ITER TF and PF coils for two vertical control scenarios (VS1 and VS2) during high beta operation at flattop.**

Index Terms—AC loss, Coupling currents, Hysteresis, Pulsed superconducting magnets

I. Introduction

AC loss in superconducting magnets is usually dominated by two contributions that originate within the superconducting strands and cables:

- hysteresis loss in the superconducting filaments;
- coupling loss within strands and among strands in a cable or composite.

The first component, hysteresis loss, is caused by persistent currents induced within the filament by field changes. Persistent currents produce a magnetization of hysteretic nature. Hysteresis loss involves thus the superconducting filaments only. The second component, coupling loss, is originated by electromagnetic coupling among filaments in a strand, and among strands in a cable. Coupling currents flow partially in the superconductor, partially in resistive contacts among them, and they dissipate power in the resistive transition. Coupling losses thus involve the cable as a whole unit. The next sections deal with each component separately, proposing a flexible calculation algorithm to cope with most practical situations in a superconducting magnet.

Manuscript received August 28, 2006.

L. Bottura is with CERN, Geneva, CH-1211 Switzerland (phone: +41-22-767-3729; fax: +41-22-767-6230; e-mail: Luca.Bottura@ cern.ch).

P. Bruzzone and C. Marinucci are with EPFL-CRPP, Fusion Technology Division, CH-5232 Villigen PSI, Switzerland.

J.B. Lister is with EPFL-CRPP, CH-1015 Lausanne Switzerland.

A. Portone is with EFDA-CSU, D-85748 Garching, Germany.

II. Hysteresis Loss Calculation

The calculation of hysteresis loss in a superconducting filament can be a complex task, especially when the magnetic field variation is arbitrary. The calculation method proposed below is based on tracking the magnetic and electric field profiles inside the filament. This allows, at each time, to compute the instantaneous, local heat density given by the product of electric field and current density. The average power and the total energy dissipation in the superconductor are then obtained by integrals in space and time of the local heating power density. As we wish to achieve reliable and fast calculation, we obviously aim at having analytic solutions for the field profiles inside the superconducting filament, which is a non-trivial task. Here we follow an approximate approach, based on the following assumptions:

- the filaments are round, and are not coupled;
- the change of the magnetic field components in each space direction k (k = 1…3) is treated separately, that is the effect of variation of each component is considered as independent from the variation of the other two components. The only coupling between field components arises through the value of the critical current density, which depends on the field module;
- the critical current density is uniform in the filament cross section;
- transport current effects are neglected.

Thanks to these simplifying assumptions, the magnetic and electric field profiles inside the filament can be computed in closed form for a cylindrical filament in parallel field [1]. In the case of a cylindrical filament in transverse field, however, only approximations are available [2],[3]. Therefore, in addition to the assumptions above, we choose to approximate a cylindrical filament in a transverse field with a slab of suitably scaled thickness (see later for the scaling), for which a closed form solution of the field profiles is available. In the

TABLE I
Normalization for Hysteresis Loss Calculation

scaled effective filament diameter	D
scaled space co-ordinate	$x = X$ / D/2
critical current density at zero field	$J_{c0}=J_c(0)$
virgin penetration field	$H_{p0}=J_{c0}\ D$ / 2
scaled critical current density	$j = J_c(B)$ / J_{c0}
scaled magnetic field	$h = H$ / H_{p0}
scaled electric field	$e = E$ / $\mu_0\ H_{p0}\ D$/2
scaled power	$p = P$ / $\mu_0\ H_{p0}^2$

sections below we report the expressions strictly necessary for the loss calculation in the case of an arbitrary field change. Throughout, we use the normalized quantities as defined in Tab. I. Note that the variable x spans the slab thickness and the cylinder radius, while the indexes of field and current density components are not indicated as all vectors have a single component, z for the magnetic field and y for the current density and electric field.

A. Slab solution

The field profile in a superconducting slab subjected to an external field change is piecewise linear, starting from the external value h_e at x=1 (the slab boundary in normalized coordinates). The outermost layer, being penetrated by the external field change, has a normalized field:

$$h = h_e \pm j(1-x) \tag{1}$$

where the sign of the current density on r.h.s. in Eq. (1) is determined by the direction of the field change. The depth at which the field profile penetrates inside the slab depends on the state of the superconductor, and two cases are possible: a virgin portion of the slab (no previous shielding current layer), or a portion of the slab with frozen field (a previously established shielding layer). The normalized penetration depth x_p in the two cases is:

$$x_p = \begin{cases} 1-\dfrac{|h_e|}{j} & virgin \\ 1-\dfrac{|h_e|}{2j} & non\ virgin \end{cases} \tag{2}.$$

The normalized electric field in the outermost layer, being penetrated (i.e. for $u_p \le x \le 1$) is given by:

$$e = \dot{h}_e(x-x_p) \tag{3}$$

and is zero elsewhere. The local value of the dissipated power density is the product of the electric field (given by Eq. (3)), and the current density in the penetration layer. The average normalized power density in the slab is then:

$$\bar{p} = \int_{x_p}^{1} \dot{h}_e j(x-x_p)dx = \dot{h}_e j\frac{(1-x_p)^2}{2} \tag{4}.$$

The above expressions are sufficient to solve the general case of arbitrary variation of the external field, keeping track of the shielding layers and their appearance/disappearance as the external field changes. To this aim, the magnetic field changes are subdivided in time in piecewise linear portions. The information needed by the tracking process consists, for each of the linear field swings, in the penetration depth x_p of a shielding current layer, the magnetic field h_e that caused it, and the direction of the shielding currents.

B. Scaling of the slab solution

The solution presented in the previous section for a slab can be scaled to represent the penetration of a cylinder in transverse field. The scaling is done so that the asymptotic behaviors of the equivalent slab and cylinder are the same for small and large field changes. To this aim we use the following known expressions [2] for the energy lost per cycle and per unit volume Q in the case of a slab in a parallel alternating field with total field swing B_m (peak to peak amplitude of the field change):

$$Q_s = \begin{cases} \dfrac{B_m^2}{2\mu_0}\dfrac{\beta}{3} & for \quad \beta \le 1 \\ \dfrac{B_m^2}{2\mu_0}\left(\dfrac{1}{\beta}-\dfrac{2}{3\beta^2}\right) & for \quad \beta > 1 \end{cases} \tag{5}$$

and for a cylinder in the same transverse alternating field:

$$Q_c = \begin{cases} \dfrac{B_m^2}{2\mu_0}\dfrac{2}{3}\left(2\beta-\beta^2\right) & for \quad \beta \le 1 \\ \dfrac{B_m^2}{2\mu_0}\dfrac{2}{3}\left(\dfrac{2}{\beta}-\dfrac{1}{\beta^2}\right) & for \quad \beta > 1 \end{cases} \tag{6}.$$

The parameter β above is the ratio of the field swing to the penetration field $2B_p$:

$$\beta = \frac{B_m}{2B_p} \tag{7}$$

where we recall that the (first) penetration field is given by:

slab: $$B_p = \mu_0 J_c \frac{D_s}{2} \tag{8}$$

cylinder: $$B_p = \mu_0 J_c \frac{D_c}{\pi} \tag{9}$$

with D_s and D_c respectively slab thickness and cylinder diameter. Inspecting Eqs. (5) and (6), we can obtain the same dissipated energy per cycle in the limits $\beta \to 0$, and $\beta \to \infty$ if we use a slab effective thickness $D_s = \dfrac{8}{3\pi F}D_c$, and scale the energy per cycle by a factor F=2.309.

C. Cylinder in parallel field

A cylinder in parallel field is described by equations that are very similar to those of a slab, treated previously. The magnetic field profile is indeed the same as in the case of the slab, so that Eqs. (1) and (2) hold in both cases. The electric field contains terms that are originated from the *rot* differential operator in cylindrical symmetry, and in the outermost layer, being penetrated, it is given by:

$$e = -\frac{\dot{h}_e}{2}\frac{x^2-x_p^2}{x} \tag{10}.$$

From Eq. (10) we compute the average power density in the cylinder:

$$\bar{p} = \frac{1}{\pi}\int_{x_p}^{1} \frac{j\dot{h}_e}{2}\frac{x^2 - x_p^2}{x} 2\pi x \, dx = \frac{\dot{h}_e j}{3}\left(1 - 3x_p^2 + 2x_p^3\right) \quad (11).$$

III. Coupling Loss Calculation

The calculation of coupling currents in the complex cabling geometry of a large size CICC can be just as daunting as an exact calculation of hysteresis in an arbitrary filament. Here, also, we make simplifying assumptions:

- the cable can be described macroscopically by three time constants τ_k and three demagnetization shape factors n_k [2]. Each time constant and demagnetization factor τ_k and n_k refer to a space direction k in the cable;
- as for hysteresis loss, we consider the three cable directions as completely independent, and solve for each direction independently from the other;
- the cable is not saturated, and coupling currents can flow unperturbed in the cable.

We stress that we do not consider parallel field losses separately, because there is a lack of recent experimental evidence that parallel field loss in a CICC has a significant impact.

The first step in the calculation of the coupling current loss is the integration of the equation governing the internal field in the cable [1]:

$$\dot{B}_i + \frac{B_i}{\tau} = \frac{B_e}{\tau} \quad (12)$$

where B_i is the field in the composite and B_e is the external, changing field. Note that, as we treat the three space direction in the same way, we drop indices from here on. To obtain an analytical solution, we assume that the external field changes piecewise linearly in time. During each time interval we can hence write that $B_e = B_e^0 + B_e^1 t$. If we indicate with B_i^0 the initial value of the internal field at the beginning of the time interval considered, we can solve Eq. (3.1), leading to the following integral:

$$B_i = B_e^0 + B_e^1(t - \tau) + \left[B_i^0 - \left(B_e^0 - B_e^1\tau\right)\right]e^{-\frac{t}{\tau}} \quad (13)$$

The last term in Eq. (13) is a decaying exponential with time constant τ that describes the shielding phase for fast field changes. Once the exponential has decayed, the contribution of the third term is negligible, and the internal field is equal to the external field delayed by τ.

Equation (13) provides the evolution of the field internal to the composite, once the initial condition is known (see later), and can be derived to give the internal field change rate:

$$\dot{B}_i = B_e^1 - \frac{\left[B_i^0 - \left(B_e^0 - B_e^1\tau\right)\right]}{\tau}e^{-\frac{t}{\tau}} \quad (14).$$

This is the desired result, used to calculate the instantaneous power dissipated as:

$$P = \frac{n\tau}{\mu_0}\dot{B}_i^2 \quad (15)$$

and finally the energy during a time interval (generically indicated below as $[0...T]$) with linear field swing:

$$E = \int_0^T P dt = \frac{n\tau}{\mu_0}B_e^{1\,2}T - \frac{n}{2\mu_0}\left[B_i^0 - \left(B_e^0 - B_e^1\tau\right)\right]^2\left(e^{-2\frac{T}{\tau}} - 1\right) + \frac{2n\tau}{\mu_0}B_e^1\left[B_i^0 - \left(B_e^0 - B_e^1\tau\right)\right]\left(e^{-\frac{T}{\tau}} - 1\right) \quad (16).$$

The coupling loss calculation algorithm uses the above equations for each field direction k, in turn. The internal field during a time interval with a linear field swing is tracked using Eq. (13), which gives in particular the value at the end of the swing to be used for the following time interval. Equations (15) and (16) are then used to compute instantaneous power and energy dissipated during the field swing. Following this logic, the calculation must keep track, for each cable, of the internal field at the end of the swing, that is used as initial condition for the following swing.

IV. Example of Application

As an example of the use of the above algorithms, we report the results of calculations of AC loss in the ITER TF and PF coils for two vertical plasma stabilization scenarios (VS1 and VS2) during high beta operation at start of burn (SOB). The magnetic model built to this aim includes all CS, PF and TF

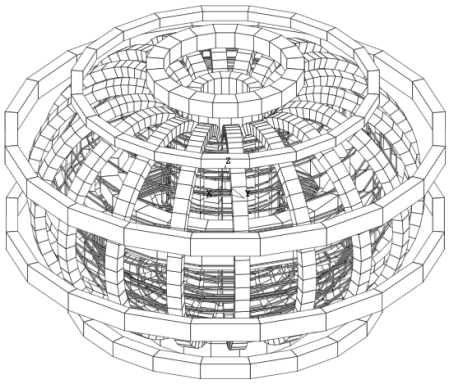

Figure 1. Model of the coil geometry of the ITER coils for the study of AC loss in vertical stabilization scenarios.

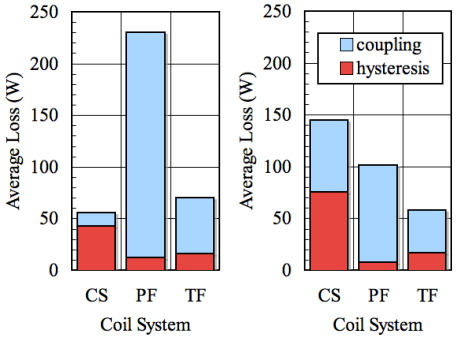

Figure 2. Average AC loss power computed for the vertical stabilization scenarios VS1 (left) and VS2 (right) at SOB.

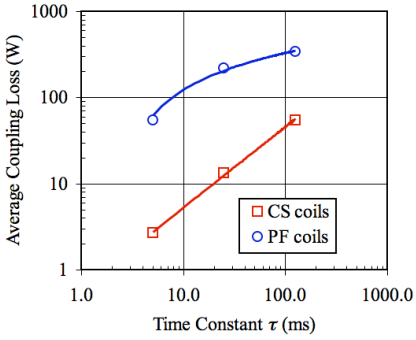

Figure 3. Sensitivity study: effect of time constant on coupling current loss in the CS and PF coil systems during the VS1 scenario.

coils, as well as some 60 axisymmetric passive circuits that represent the conductive wall of the vacuum vessel. A 3-D rendering of the model is shown in Fig. 1. The coil and conductor data have been taken from the reference design reported in [5]. In particular, for loss calculations, the effective filament diameter of Nb_3Sn is 30 μm, while for NbTi it is 6 μm. The coupling loss time constant is 25 ms in all space directions for all conductors. The current variation during the vertical control scenarios has a wide frequency spectrum (typically up to 10 Hz), and produces field changes of relatively small amplitudes (few 10's of mT on the PF coils, up to 0.1 T in the CS coils).

The AC loss calculation requires the knowledge of the three magnetic field components at each conductor location in the coil winding. This calculation has been done using standard linear magnetostatic techniques.

We report in Fig. 2 a summary of the overall results of these two simulations. The bars represent the total loss, split among each of the three main coil systems, and further subdivided in the different mechanism (coupling and hysteresis). Loads are reported as average power during the time simulated, 10 s. The calculation provides a quick means to qualify the controller scenarios in terms of the cryogenic load, as we see a clear distinction in the loss at the level of the CS and PF system. We note further that the contribution of the two loss mechanisms in the CS and PF coil systems is massively different in the two scenarios. This is due to the combined effect of the different current amplitudes as well as the different dynamic characteristics of the current waveforms in the CS and PF coils, affecting both hysteresis and coupling loss. Interestingly enough, the situation on the TF coil (close to the plasma) is essentially unaffected by the control scenario, as we should have expected.

To complete our example, we have performed sensitivity studies on the effect of a change in the loss parameters of the conductors. Figure 3 shows in particular the effect of a parametric change of τ by a factor 1/5 to 5 (i.e. from 5 ms to 125 ms) on the coupling loss in scenario VS1. As a side remark, this range of variation is representative for the spread measured on the large-scale ITER cables. The scaling of the coupling loss in the CS coil system is approximately linear, which indicates negligible shielding in the range of time constants explored for the specific scenario analyzed (low frequency regime). In the PF coil system, on the other hand, we clearly see the effect of shielding at high values of τ, which results in a coupling loss significantly smaller than would be expected by the low-frequency regime, linear extrapolation.

V. Conclusion

We have presented a calculation method for AC losses in pulsed superconducting magnets that is suitable over a wide regime of field changes (from partial to full penetration) and frequencies (from the low frequency limit to shielding). The example reported, vertical control scenarios in ITER, provides a measure of the flexibility in dealing with complex geometric and powering conditions. We believe that the model will be useful for other applications of similar nature, e.g. pulsed accelerator magnets requiring loss optimization.

Acknowledgment

The authors gratefully acknowledge the crucial contribution of Dr. C. Rosso (CryoSoft, France) in producing the solution of the coupling current loss. The slab-cylinder scaling is based on an idea of Dr. J. Minervini (MIT, USA).

References

[1] H. Brechna, Superconducting Magnet Systems, Springer-Verlag, 1973.
[2] M. Wilson, Superconducting Magnets, Clarendon Press Oxford, 1983.
[3] W.J. Carr, Jr., AC Loss and Macroscopic Theory of Superconductors, Gordon and Breach Science Publishers, 1983.
[4] A.M. Campbell, A General Treatment of Losses in Multifilamentary Superconductors, Cryogenics, **22**(1), pp. 3-16, 1982.
[5] ITER Design Description Document. Magnet Section 1: Engineering description, N11 DDD 178 04-06-04 R 0.4, 2004

Appendix B

Annotated M'C Input for case SOBVS1MP1x.

```
;;;;;;;;;;;;;;;;;;;;;;;;;;;;;;;;;;;;;;;;;;;;;;;;;;;;;;;;;;;;;;;;;;;;;;;;;;;
;;;;;;;;;;;;;;;;;;;;;;;;;;;;;;;;;;;;;;;;;;;;;;;;;;;;;;;;;;;;;;;;;;;;;;;;;;;
; THIS IS AN EXAMPLE OF INPUT TO M'C
;
; IT CONTAINS THREE PARTS:
; (1) PRE-PROCESSING
;     - Title
;     - Definition of the current tables (only one coil!!)
;     - Definition of the conductor data
;     - Definition of the coil data
; (2) PROCESSING
; (3) POST-PROCESSING
;;;;;;;;;;;;;;;;;;;;;;;;;;;;;;;;;;;;;;;;;;;;;;;;;;;;;;;;;;;;;;;;;;;;;;;;;;;
;;;;;;;;;;;;;;;;;;;;;;;;;;;;;;;;;;;;;;;;;;;;;;;;;;;;;;;;;;;;;;;;;;;;;;;;;;;
;-------------------------------------------------------------
; (1) PRE-PROCESSING
;     - Title
;-------------------------------------------------------------
;;;;;;;;;;;;;;;;;;;;;;;;;;;;;;;;;;;;;;;;;;;;;;;;;;;;;;;;;;;;;;;;;;;;;;;;;;;
;;;;;;;;;;;;;;;;;;;;;;;;;;;;;;;;;;;;;;;;;;;;;;;;;;;;;;;;;;;;;;;;;;;;;;;;;;;
;;;;;;;;;;;;;;;;;;;;;;;;;;;;;;;;;;;;;;;;;;;;;;;;;;;;;;;;;;;;;;;;;;;;;;;;;;;
; ITER (N11 DDD 177 04-05-12 W 0.2)
; PF coils + CS + TF coils segmented in 4 grades
;;;;;;;;;;;;;;;;;;;;;;;;;;;;;;;;;;;;;;;;;;;;;;;;;;;;;;;;;;;;;;;;;;;;;;;;;;;
ECHO OFF

TITL 'SOBVS1MP1x'
TITL 'N11 DDD 177 04-05-12 W 0.2'
;-------------------------------------------------------------
; (1) PRE-PROCESSING
;     - Definition of the current tables (only one coil!!)
;-------------------------------------------------------------
CURR name cupf1
   table  103
            0.0000    9.630000e+06
            1.6000    8.260000e+06
            4.6100    8.580000e+06
            7.8200    8.870000e+06
           11.3800    9.170000e+06
           15.2400    9.460000e+06
           19.5200    9.750000e+06
           24.1700    1.005000e+07
           29.3700    1.034000e+07
           35.2500    1.003000e+07
           42.1200    9.730000e+06
           49.2600    8.810000e+06
           56.2100    8.390000e+06
           63.2200    7.940000e+06
           72.5500    7.310000e+06
          100.0000    5.450000e+06
          105.0000    5.450000e+06
          110.0000    5.460000e+06
          115.0000    5.460000e+06
          120.0000    5.470000e+06
          125.0000    5.470000e+06
          130.0000    5.470000e+06
          130.1498    5.469697e+06
          130.2997    5.470373e+06
          130.4495    5.470578e+06
          130.5994    5.471056e+06
          130.7492    5.469675e+06
```



```
          130.8991    5.466989e+06
          131.0489    5.465866e+06
          131.1988    5.465094e+06
          131.3486    5.463274e+06
          131.4985    5.465602e+06
          131.6483    5.466005e+06
          131.7982    5.466978e+06
          131.9480    5.469902e+06
          132.0979    5.468714e+06
          132.2477    5.469840e+06
          132.3976    5.472454e+06
          132.5474    5.471922e+06
          132.6973    5.475002e+06
          132.8471    5.475260e+06
          132.9970    5.480008e+06
          133.1469    5.478165e+06
          133.2967    5.480769e+06
          133.4466    5.479417e+06
          133.5964    5.477885e+06
          133.7463    5.478129e+06
          133.8961    5.477570e+06
          134.0460    5.472938e+06
          134.1958    5.471974e+06
          134.3457    5.473360e+06
          134.4955    5.470872e+06
          134.6454    5.471391e+06
          134.7952    5.470260e+06
          134.9451    5.467703e+06
          135.0949    5.469619e+06
          135.2448    5.467689e+06
          135.3946    5.467625e+06
          135.5445    5.469119e+06
          135.6943    5.469984e+06
          135.8442    5.471533e+06
          135.9940    5.471218e+06
          136.1438    5.469962e+06
          136.2937    5.472119e+06
          136.4435    5.471107e+06
          136.5934    5.469364e+06
          136.7432    5.469478e+06
          136.8931    5.469512e+06
          137.0429    5.472891e+06
          137.1928    5.472201e+06
          137.3426    5.473632e+06
          137.4925    5.473939e+06
          137.6423    5.473346e+06
          137.7922    5.473402e+06
          137.9420    5.471076e+06
          138.0919    5.472152e+06
          138.2417    5.474276e+06
          138.3916    5.476006e+06
          138.5414    5.475924e+06
          138.6913    5.474947e+06
          138.8411    5.474235e+06
          138.9910    5.475190e+06
          139.1409    5.474038e+06
          139.2907    5.475969e+06
          139.4406    5.476677e+06
          139.5904    5.472456e+06
          139.7403    5.470750e+06
          139.8901    5.472220e+06
```



```
          530.0000    1.740000e+06
          546.0000    1.750000e+06
          564.0000    1.760000e+06
          580.0000    1.770000e+06
          590.0000    2.430000e+06
          616.1000    7.300000e+05
          647.4000   -1.310000e+06
          668.3000   -2.670000e+06
          689.1000   -4.030000e+06
          710.0000   -5.390000e+06
          720.0000   -6.000000e+06
          900.0000    0.000000e+00
         1490.0000    0.000000e+00
         1790.0000    9.630000e+06
         1800.0000    9.630000e+06
finish
;;;;;;;;;;;;;;;;;;;;;;;;;;;;;;;;;;;;;;;;;;;;;;;;;;;;;;;;;;;;;;;;;;;;;;;;;;;
;;;;;;;;;;;;;;;;;;;;;;;;;;;;;;;;;;;;;;;;;;;;;;;;;;;;;;;;;;;;;;;;;;;;;;;;;;;
;  currents of remaining 5  PF coils are missing
;  currents of           6  CS coils are missing
;  currents of           60 PA coils are missing
;  currents of           3  PL coils are missing
;;;;;;;;;;;;;;;;;;;;;;;;;;;;;;;;;;;;;;;;;;;;;;;;;;;;;;;;;;;;;;;;;;;;;;;;;;;


;-------------------------------------------------------------
; (1) PRE-PROCESSING
;     - Definition of the conductor data
;-------------------------------------------------------------
COND name coPF16
     Super  31
     asc    2.440e-4
     ast    3.904e-4
     deff   6.0e-6
     temp   4.7
     epsi   0.0
     lamb   1.0
     tau    0.025 0.025 0.025
     mfac   2.0 2.0 2.0
FINISH
COND name coPF234
     Super  31
     asc    4.819e-5
     ast    4.575e-4
     deff   6.0e-6
     temp   4.7
     epsi   0.0
     lamb   1.0
     tau    0.025 0.025 0.025
     mfac   2.0 2.0 2.0
FINISH
COND name coPF5
     Super  31
     asc    8.572e-5
     ast    4.491e-4
     deff   6.0e-6
     temp   4.7
     epsi   0.0
     lamb   1.0
     tau    0.025 0.025 0.025
     mfac   2.0 2.0 2.0
```



```
FINISH
COND name coCS
     Super  32
     asc    2.460e-4
     ast    2.460e-4
     deff   30.0e-6
     temp   4.7
     epsi   -0.0069
     lamb   0.3333
     tau    0.025 0.025 0.025
     mfac   2.0 2.0 2.0
FINISH
COND name coTF
     Super  32
     asc    2.501e-4
     ast    5.003e-4
     deff   30.0e-6
     temp   5.0
     epsi   -0.0077
     lamb   0.3333
     tau    0.025 0.025 0.025
     mfac   2.0 2.0 2.0
FINISH
;-------------------------------------------------------------
; (1) PRE-PROCESSING
;     - Definition of the coil data
;-------------------------------------------------------------
;;;;;;;;;;;;;;;;;;;;;;;;;;;;;;
;PF;;;;;;;;;;;;;;;;;;;;;;;;;;;
;;;;;;;;;;;;;;;;;;;;;;;;;;;;;;
COIL
   NAME   PF1
   CURR cupf1
   COND coPF16
   LOOP  0.000  0.000  7.557  0.000  0.000  3.943  0.968  0.976    20
   MESH  10  10
   WIND PANCAKE   16 TURNS   16    2 IN_HAND
FINISH
COIL
   NAME   PF2
   CURR cupf2
   COND coPF234
   LOOP  0.000  0.000  6.530  0.000  0.000  8.319  0.649  0.595    20
   MESH  10  10
   WIND PANCAKE   10 TURNS   11    2 IN_HAND
FINISH
COIL
   NAME   PF3
   CURR cupf3
   COND coPF234
   LOOP  0.000  0.000  3.265  0.000  0.000 11.997  0.708  1.125    20
   MESH  10  10
   WIND PANCAKE   16 TURNS   12    2 IN_HAND
FINISH
COIL
   NAME   PF4
   CURR cupf4
   COND coPF234
   LOOP  0.000  0.000 -2.243  0.000  0.000 11.967  0.649  1.125    20
   MESH  10  10
   WIND PANCAKE   16 TURNS   11    2 IN_HAND
```

```
FINISH
COIL
   NAME   PF5
   CURR cupf5
   COND coPF5
   LOOP  0.000  0.000 -6.730  0.000  0.000  8.395  0.820  0.945    20
   MESH  10  10
   WIND PANCAKE   16 TURNS   14    2 IN_HAND
FINISH
COIL
   NAME   PF6
   CURR cupf6
   COND coPF16
   LOOP  0.000  0.000 -7.557  0.000  0.000  4.263  1.633  0.976    20
   MESH  10  10
   WIND PANCAKE   16 TURNS   27    2 IN_HAND
FINISH
;;;;;;;;;;;;;;;;;;;;;;;;;;;;
;CS;;;;;;;;;;;;;;;;;;;;;;;;;
;;;;;;;;;;;;;;;;;;;;;;;;;;;;
COIL
   NAME   CS3U
   CURR cucs3u
   COND coCS
   LOOP  0.000  0.000  5.313  0.000  0.000  1.722  0.719  2.075    20
   MESH  10  10
   WIND PANCAKE   39 TURNS   14    1 IN_HAND
FINISH
COIL
   NAME   CS2U
   CURR cucs2u
   COND coCS
   LOOP  0.000  0.000  3.188  0.000  0.000  1.722  0.719  2.075    20
   MESH  10  10
   WIND PANCAKE   39 TURNS   14    1 IN_HAND
FINISH
COIL
   NAME   CS1U
   CURR cucs1u
   COND coCS
   LOOP  0.000  0.000  1.063  0.000  0.000  1.722  0.719  2.075    20
   MESH  10  10
   WIND PANCAKE   39 TURNS   14    1 IN_HAND
FINISH
COIL
   NAME   CS1L
   CURR cucs11
   COND coCS
   LOOP  0.000  0.000 -1.063  0.000  0.000  1.722  0.719  2.075    20
   MESH  10  10
   WIND PANCAKE   39 TURNS   14    1 IN_HAND
FINISH
COIL
   NAME   CS2L
   CURR cucs21
   COND coCS
   LOOP  0.000  0.000 -3.188  0.000  0.000  1.722  0.719  2.075    20
   MESH  10  10
   WIND PANCAKE   39 TURNS   14    1 IN_HAND
FINISH
COIL
```



```
   NAME   CS3L
   CURR cucs31
   COND coCS
   LOOP  0.000  0.000 -5.313  0.000  0.000  1.722  0.719  2.075    20
   MESH  10  10
   WIND PANCAKE   39 TURNS   14    1 IN_HAND
FINISH
;;;;;;;;;;;;;;;;;;;;;;;;;;;;;;;;
;Passive coils;;;;;;;;;;;;;;;;;;
;;;;;;;;;;;;;;;;;;;;;;;;;;;;;;;;
COIL
   NAME   PA01
   CURR cupa01
   LOOP  0.000  0.000 -2.727  0.000  0.000  7.416  0.060  0.060    20
FINISH
COIL
   NAME   PA02
   CURR cupa02
   LOOP  0.000  0.000 -2.838  0.000  0.000  7.271  0.060  0.060    20
FINISH
COIL
   NAME   PA03
   CURR cupa03
   LOOP  0.000  0.000 -2.950  0.000  0.000  7.127  0.060  0.060    20
FINISH
COIL
   NAME   PA04
   CURR cupa04
   LOOP  0.000  0.000 -3.062  0.000  0.000  6.982  0.060  0.060    20
FINISH
COIL
   NAME   PA05
   CURR cupa05
   LOOP  0.000  0.000 -3.174  0.000  0.000  6.838  0.060  0.060    20
FINISH
COIL
   NAME   PA06
   CURR cupa06
   LOOP  0.000  0.000 -2.751  0.000  0.000  7.435  0.060  0.060    20
FINISH
COIL
   NAME   PA07
   CURR cupa07
   LOOP  0.000  0.000 -2.863  0.000  0.000  7.290  0.060  0.060    20
FINISH
COIL
   NAME   PA08
   CURR cupa08
   LOOP  0.000  0.000 -2.974  0.000  0.000  7.146  0.060  0.060    20
FINISH
COIL
   NAME   PA09
   CURR cupa09
   LOOP  0.000  0.000 -3.086  0.000  0.000  7.001  0.060  0.060    20
FINISH
COIL
   NAME   PA10
   CURR cupa10
   LOOP  0.000  0.000 -3.198  0.000  0.000  6.856  0.060  0.060    20
FINISH
COIL
```



```
   NAME   PA11
   CURR cupa11
   LOOP  0.000  0.000  0.520  0.000  0.000  3.541  0.060  0.060    20
FINISH
COIL
   NAME   PA12
   CURR cupa12
   LOOP  0.000  0.000  1.560  0.000  0.000  3.541  0.060  0.060    20
FINISH
COIL
   NAME   PA13
   CURR cupa13
   LOOP  0.000  0.000  2.599  0.000  0.000  3.541  0.060  0.060    20
FINISH
COIL
   NAME   PA14
   CURR cupa14
   LOOP  0.000  0.000  3.638  0.000  0.000  3.548  0.060  0.060    20
FINISH
COIL
   NAME   PA15
   CURR cupa15
   LOOP  0.000  0.000  4.591  0.000  0.000  3.908  0.060  0.060    20
FINISH
COIL
   NAME   PA16
   CURR cupa16
   LOOP  0.000  0.000  5.149  0.000  0.000  4.759  0.060  0.060    20
FINISH
COIL
   NAME   PA17
   CURR cupa17
   LOOP  0.000  0.000  5.093  0.000  0.000  5.778  0.060  0.060    20
FINISH
COIL
   NAME   PA18
   CURR cupa18
   LOOP  0.000  0.000  4.514  0.000  0.000  6.639  0.060  0.060    20
FINISH
COIL
   NAME   PA19
   CURR cupa19
   LOOP  0.000  0.000  3.863  0.000  0.000  7.449  0.060  0.060    20
FINISH
COIL
   NAME   PA20
   CURR cupa20
   LOOP  0.000  0.000  3.074  0.000  0.000  8.124  0.060  0.060    20
FINISH
COIL
   NAME   PA21
   CURR cupa21
   LOOP  0.000  0.000  2.163  0.000  0.000  8.621  0.060  0.060    20
FINISH
COIL
   NAME   PA22
   CURR cupa22
   LOOP  0.000  0.000  1.171  0.000  0.000  8.921  0.060  0.060    20
FINISH
COIL
   NAME   PA23
```



```
   CURR cupa23
   LOOP  0.000  0.000  0.138  0.000  0.000  8.958  0.060  0.060    20
FINISH
COIL
   NAME   PA24
   CURR cupa24
   LOOP  0.000  0.000 -0.854  0.000  0.000  8.667  0.060  0.060    20
FINISH
COIL
   NAME   PA25
   CURR cupa25
   LOOP  0.000  0.000 -1.806  0.000  0.000  8.248  0.060  0.060    20
FINISH
COIL
   NAME   PA26
   CURR cupa26
   LOOP  0.000  0.000 -2.757  0.000  0.000  7.828  0.060  0.060    20
FINISH
COIL
   NAME   PA27
   CURR cupa27
   LOOP  0.000  0.000 -3.704  0.000  0.000  7.400  0.060  0.060    20
FINISH
COIL
   NAME   PA28
   CURR cupa28
   LOOP  0.000  0.000 -4.508  0.000  0.000  6.759  0.060  0.060    20
FINISH
COIL
   NAME   PA29
   CURR cupa29
   LOOP  0.000  0.000 -5.008  0.000  0.000  5.861  0.060  0.060    20
FINISH
COIL
   NAME   PA30
   CURR cupa30
   LOOP  0.000  0.000 -5.090  0.000  0.000  4.837  0.060  0.060    20
FINISH
COIL
   NAME   PA31
   CURR cupa31
   LOOP  0.000  0.000 -4.572  0.000  0.000  3.958  0.060  0.060    20
FINISH
COIL
   NAME   PA32
   CURR cupa32
   LOOP  0.000  0.000 -3.637  0.000  0.000  3.561  0.060  0.060    20
FINISH
COIL
   NAME   PA33
   CURR cupa33
   LOOP  0.000  0.000 -2.599  0.000  0.000  3.541  0.060  0.060    20
FINISH
COIL
   NAME   PA34
   CURR cupa34
   LOOP  0.000  0.000 -1.560  0.000  0.000  3.541  0.060  0.060    20
FINISH
COIL
   NAME   PA35
   CURR cupa35
```

```
   LOOP  0.000  0.000 -0.520  0.000  0.000  3.541  0.060  0.060    20
FINISH
COIL
   NAME   PA36
   CURR cupa36
   LOOP  0.000  0.000  0.584  0.000  0.000  3.264  0.060  0.060    20
FINISH
COIL
   NAME   PA37
   CURR cupa37
   LOOP  0.000  0.000  1.753  0.000  0.000  3.264  0.060  0.060    20
FINISH
COIL
   NAME   PA38
   CURR cupa38
   LOOP  0.000  0.000  2.922  0.000  0.000  3.264  0.060  0.060    20
FINISH
COIL
   NAME   PA39
   CURR cupa39
   LOOP  0.000  0.000  4.089  0.000  0.000  3.300  0.060  0.060    20
FINISH
COIL
   NAME   PA40
   CURR cupa40
   LOOP  0.000  0.000  5.112  0.000  0.000  3.814  0.060  0.060    20
FINISH
COIL
   NAME   PA41
   CURR cupa41
   LOOP  0.000  0.000  5.624  0.000  0.000  4.844  0.060  0.060    20
FINISH
COIL
   NAME   PA42
   CURR cupa42
   LOOP  0.000  0.000  5.552  0.000  0.000  5.997  0.060  0.060    20
FINISH
COIL
   NAME   PA43
   CURR cupa43
   LOOP  0.000  0.000  5.045  0.000  0.000  7.045  0.060  0.060    20
FINISH
COIL
   NAME   PA44
   CURR cupa44
   LOOP  0.000  0.000  4.327  0.000  0.000  7.965  0.060  0.060    20
FINISH
COIL
   NAME   PA45
   CURR cupa45
   LOOP  0.000  0.000  3.433  0.000  0.000  8.714  0.060  0.060    20
FINISH
COIL
   NAME   PA46
   CURR cupa46
   LOOP  0.000  0.000  2.407  0.000  0.000  9.269  0.060  0.060    20
FINISH
COIL
   NAME   PA47
   CURR cupa47
   LOOP  0.000  0.000  1.289  0.000  0.000  9.602  0.060  0.060    20
```



```
FINISH
COIL
   NAME   PA48
   CURR cupa48
   LOOP  0.000  0.000  0.127  0.000  0.000  9.656  0.060  0.060    20
FINISH
COIL
   NAME   PA49
   CURR cupa49
   LOOP  0.000  0.000 -0.997  0.000  0.000  9.360  0.060  0.060    20
FINISH
COIL
   NAME   PA50
   CURR cupa50
   LOOP  0.000  0.000 -2.067  0.000  0.000  8.888  0.060  0.060    20
FINISH
COIL
   NAME   PA51
   CURR cupa51
   LOOP  0.000  0.000 -3.136  0.000  0.000  8.416  0.060  0.060    20
FINISH
COIL
   NAME   PA52
   CURR cupa52
   LOOP  0.000  0.000 -4.177  0.000  0.000  7.889  0.060  0.060    20
FINISH
COIL
   NAME   PA53
   CURR cupa53
   LOOP  0.000  0.000 -5.027  0.000  0.000  7.100  0.060  0.060    20
FINISH
COIL
   NAME   PA54
   CURR cupa54
   LOOP  0.000  0.000 -5.518  0.000  0.000  6.046  0.060  0.060    20
FINISH
COIL
   NAME   PA55
   CURR cupa55
   LOOP  0.000  0.000 -5.593  0.000  0.000  4.889  0.060  0.060    20
FINISH
COIL
   NAME   PA56
   CURR cupa56
   LOOP  0.000  0.000 -5.094  0.000  0.000  3.855  0.060  0.060    20
FINISH
COIL
   NAME   PA57
   CURR cupa57
   LOOP  0.000  0.000 -4.088  0.000  0.000  3.308  0.060  0.060    20
FINISH
COIL
   NAME   PA58
   CURR cupa58
   LOOP  0.000  0.000 -2.922  0.000  0.000  3.264  0.060  0.060    20
FINISH
COIL
   NAME   PA59
   CURR cupa59
   LOOP  0.000  0.000 -1.753  0.000  0.000  3.264  0.060  0.060    20
FINISH
```



```
COIL
   NAME   PA60
   CURR cupa60
   LOOP  0.000  0.000 -0.584  0.000  0.000  3.264  0.060  0.060    20
FINISH
;;;;;;;;;;;;;;;;;;;;;;;;;;;;
;Moving Plasma ;;;;;;;;;;;;;;
;;;;;;;;;;;;;;;;;;;;;;;;;;;;
COIL
   NAME   PL1
   CURR cupl1
   LOOP  0.000  0.000 9.0000e-01  0.000  0.000 6.5000e+00  1.000  1.000    20
FINISH
COIL
   NAME   PL2
   CURR cupl2
   LOOP  0.000  0.000 0.0000e+00  0.000  0.000 7.8000e+00  1.000  1.000    20
FINISH
COIL
   NAME   PL3
   CURR cupl3
   LOOP  0.000  0.000 0.0000e+00  0.000  0.000 5.8000e+00  1.000  1.000    20
FINISH
;-----------------------------------------------------------------
; (2) PROCESSING
;-----------------------------------------------------------------
;;;;;;;;;;;;;;;;;;;;;;;;;;;;;;;;;;;;;;;;;;;;;;;;;;;;;;;;;;;;;;;;
;;;;;;;;;;;;;;;;;;;;;;;;;;;;;;;;;;;;;;;;;;;;;;;;;;;;;;;;;;;;;;;;
; COMPUTATION
;;;;;;;;;;;;;;;;;;;;;;;;;;;;;;;;;;;;;;;;;;;;;;;;;;;;;;;;;;;;;;;;
AXIS ON

AC_L TIME 0.0 710.0 COIL CS3U
AC_L TIME 0.0 710.0 COIL CS2U
AC_L TIME 0.0 710.0 COIL CS1U
AC_L TIME 0.0 710.0 COIL CS1L
AC_L TIME 0.0 710.0 COIL CS2L
AC_L TIME 0.0 710.0 COIL CS3L
AC_L TIME 0.0 710.0 COIL PF1
AC_L TIME 0.0 710.0 COIL PF2
AC_L TIME 0.0 710.0 COIL PF3
AC_L TIME 0.0 710.0 COIL PF4
AC_L TIME 0.0 710.0 COIL PF5
AC_L TIME 0.0 710.0 COIL PF6
;-----------------------------------------------------------------
; (3) POST-PROCESSING
;-----------------------------------------------------------------
;;;;;;;;;;;;;;;;;;;;;;;;;;;;;;;;;;;;;;;;;;;;;;;;;;;;;;;;;;;;;;;;
;;;;;;;;;;;;;;;;;;;;;;;;;;;;;;;;;;;;;;;;;;;;;;;;;;;;;;;;;;;;;;;;
; PLOT
;;;;;;;;;;;;;;;;;;;;;;;;;;;;;;;;;;;;;;;;;;;;;;;;;;;;;;;;;;;;;;;;
PLOT
NEW
COIL ALL
FINI
;
PLOT
 AC_L    aver COIL PF1  interval 130.0 140.0
 AC_L    aver COIL PF2  interval 130.0 140.0
 AC_L    aver COIL PF3  interval 130.0 140.0
 AC_L    aver COIL PF4  interval 130.0 140.0
```



```
 AC_L    aver COIL PF5  interval 130.0 140.0
 AC_L    aver COIL PF6  interval 130.0 140.0
 AC_L    aver COIL CS3U interval 130.0 140.0
 AC_L    aver COIL CS2U interval 130.0 140.0
 AC_L    aver COIL CS1U interval 130.0 140.0
 AC_L    aver COIL CS1L interval 130.0 140.0
 AC_L    aver COIL CS2L interval 130.0 140.0
 AC_L    aver COIL CS3L interval 130.0 140.0

FINI
;;;;;;;;;;;;;;;;;;;;;;;;;;;;;;;;;;;;;;;;;;;;;;;;;;;;;;;;;;;;;;;;
;;;;;;;;;;;;;;;;;;;;;;;;;;;;;;;;;;;;;;;;;;;;;;;;;;;;;;;;;;;;;;;;
; OUTPUT
;;;;;;;;;;;;;;;;;;;;;;;;;;;;;;;;;;;;;;;;;;;;;;;;;;;;;;;;;;;;;;;;
PRINT

 AC_L    aver COIL PF1  interval 130.0 140.0
 AC_L    aver COIL PF2  interval 130.0 140.0
 AC_L    aver COIL PF3  interval 130.0 140.0
 AC_L    aver COIL PF4  interval 130.0 140.0
 AC_L    aver COIL PF5  interval 130.0 140.0
 AC_L    aver COIL PF6  interval 130.0 140.0

 AC_L    aver COIL CS3U interval 130.0 140.0
 AC_L    aver COIL CS2U interval 130.0 140.0
 AC_L    aver COIL CS1U interval 130.0 140.0
 AC_L    aver COIL CS1L interval 130.0 140.0
 AC_L    aver COIL CS2L interval 130.0 140.0
 AC_L    aver COIL CS3L interval 130.0 140.0

FINI
;;;;;;;;;;;;;;;;;;;;;;;;;;;;;;;;;;;;;;;;;;;;;;;;;;;;;;;;;;;;;;;;
;;;;;;;;;;;;;;;;;;;;;;;;;;;;;;;;;;;;;;;;;;;;;;;;;;;;;;;;;;;;;;;;
STOP
```